NONCOHERENT RECEIVER DESIGNS FOR ULTRA-WIDEBAND SYSTEMS

A Thesis
Presented to
The Academic Faculty

by

Qi Zhou

In Partial Fulfillment
of the Requirements for the Degree
Doctor of Philosophy in the
School of Electrical and Computer Engineering

Georgia Institute of Technology
August 2013

NONCOHERENT RECEIVER DESIGNS FOR ULTRA-WIDEBAND SYSTEMS

Approved by:

Professor Xiaoli Ma, Advisor
School of Electrical and Computer Engineering
Georgia Institute of Technology

Professor Gisele Bennett
School of Electrical and Computer Engineering
Georgia Institute of Technology

Professor G. Tong Zhou
School of Electrical and Computer Engineering
Georgia Institute of Technology

Professor Jun Xu
College of Computing
Georgia Institute of Technology

Professor Gregory D. Durgin
School of Electrical and Computer Engineering
Georgia Institute of Technology

Date Approved: 23 May 2013

To myself, my family,

my advisor, and my friends.

ACKNOWLEDGEMENTS

First, I would like to express my sincerest gratitude to my advisor, Dr. Xiaoli Ma, for her complete support and persistent encouragement during my Ph.D. study. I benefit a lot from her unique training program that helps me develop critical thinking and presentation skills. As an excellent researcher, she influences me with good characteristics set by herself, including dedication, creativity, and diligence, and she continually and convincingly conveys a spirit of adventure in regard to research, which turns my Ph.D. journey into a joyful process. In addition, Dr. Ma is a great friend to me, and I am very grateful to her for sharing her wisdom and optimism in life. In all, I personally think I am extremely lucky to meet Dr. Ma in my life.

Second, I want to thank Dr. G. Tong Zhou for introducing the Georgia Tech Shanghai M.S. Program and the exciting areas of signal processing. Next, I would like to thank my committee members, Professor Gregory David Durgin, Professor Gisele Bennett, and Professor Jun Xu for serving on my committee and for providing me valuable comments to improve my dissertation. I would like to thank my group members and collaborators, Dr. Vincenzo Lottici, Dr. Robert J. Baxley, Dr. Wei Zhang, Dr. Qijia Liu, Dr. Benjamin Russell Hamilton, Dr. Sungeun Lee, Dr. Giwan Choi, Dr. Jiaxi Xiao, Dr. Yiyin Wang, Dr. Heng Liu, Zhenhua Yu, Hayang Kim, Marie Shinotsuka, Qingsong Wen, Malik Muhammad Usman Gul, Lingchen Zhu, Brian Beck, Andrew Harper, Marco Mondelli, and Hyunwoo Cho, for their friendly support and sharing the life at Georgia Tech. In

Third, I would like to thank the Georgia Tech Ultra Wideband Center of Excellence (http://www.uwbtech.gatech.edu/) for financial support and Dr. Rick Moore and Dr. Robert Rice for their encouragement and help during the past four years.

Finally, I am greatly indebted in my family and friends, especially my grandparents and parents for their love and support, and my fiancee, Wencen Wu, who makes my Ph.D. life more balanced and healthier.

TABLE OF CONTENTS

LIST OF TABLES

LIST OF FIGURES

SUMMARY

UWB communication is an attractive technology that has the potential to provide low-power, low-complexity, and high-speed communications in short range links. One of the main challenges of UWB communications is the highly frequency-selective channel, which induces hundreds of overlapped copies of the transmitted pulse with different delays and amplitudes. To collect the energy of these multipath components, coherent Rake receivers are proposed, but suffer from high implementation and computational costs on channel estimation. To avoid the stringent channel estimation, several noncoherent receivers, including energy detector (ED) and transmitted reference (TR), are proposed at the cost of degraded performance. In addition, when taking into account some practical issues of UWB communications, e.g., non-Gaussian impulsive noise, non-ideal antennas, and limited coverage, significant performance degradation may be introduced by noncoherent receivers.

In this dissertation, we present low-complexity, high-performance, noncoherent receiver designs for UWB communications that *i)* avoid the stringent channel estimation; *ii)* lower the computational complexity of the existing receivers with the aid of advanced digital signal processing techniques; and *iii)* improve the error performance of the noncoherent receivers by accommodating practical imperfections.

First, we propose three multi-symbol detectors (MSDs) for multi-symbol different detection (MSDD), which has recently caught attention in UWB communications because of its high performance without requiring explicit channel estimation. To alleviate the non-deterministic polynomial hardness (NP-hard) of MSDD, we analyze the statistical model of MSDD and propose an iterative MSD and two MSDs based on relaxation technique with near-optimal performance and low complexity. Moreover,

the error performance of MSDs is further enhanced by exploiting joint soft-input soft-output MSDD and forward error correction codes.

Next, we consider the non-Gaussian noise in the presence of multi-access interference, which is impulsive when the number of active users is small. To mitigate the impulsive noise effect, in this dissertation, we propose new differential UWB receivers based on the generalized Gaussian distribution and Laplace distribution and achieve better error performance.

Another main issue of UWB communications is the limited radio coverage. To extend the coverage and improve the performance of UWB systems, we focus on a novel differentially encoded decode-and-forward (DF) non-cooperative relaying scheme. Putting emphasis on the general case of multi-hop relaying, we illustrate a novel algorithm for the joint power allocation and path selection (JPAPS), minimizing an approximate of the overall bit error rate (BER). A simplified scheme is also presented, which reduces the complexity to $\mathcal{O}(N^2)$ and achieves a negligible performance loss.

Finally, we concentrate on code-multiplexing (CM) systems, which have recently drawn attention mainly because they enable noncoherent detection without requiring either a delay component, as in TR, or an analog carrier, as in frequency-shifted reference. In this dissertation, we propose a generalized code-multiplexing (GCM) system based on the formulation of a constrained mixed-integer optimization problem. The GCM extends the concept of existing CM while retaining their simple receiver structure, even offering better BER performance and a higher data rate in the sense that more data symbols can be embedded in each transmitted block. Moreover, the impacts of non-ideal antennas on the GCM systems are investigated given some practical antenna measurement data and IEEE 802.15.4a channel environments.

CHAPTER I

INTRODUCTION

1.1 Motivations

Ultra-wideband (UWB) transmission is a radio technology that utilizes a relatively large bandwidth (usually greater than 500 MHz). Because of its high resolution, low probability of intercept, resistance of jamming, and easy extraction of target features, UWB techniques have caught a great deal of attention in military radar applications at its early development stage from 1960s [80, 38]. However, those military-focused research activities were classified, and little development has been put into commercial area until recently [29, 63, 68, 2]. On the other side, UWB technique is promising for wireless communications, because the large bandwidth enables high channel capacity, which is proportional to the bandwidth as indicated by the famous Shannon theorem. In addition, by transmitting the signal at very low spectral density, UWB signal could coexist with current narrow-band services with limited mutual interference [89, 91, 64, 98, 93], avoiding the current overcrowded spectrum issue. The potential of UWB communications was further unleashed by the U.S. Federal Communications Commission (FCC), which allowed low-power UWB transmissions in a huge unlicensed band [23]. Because of these merits, UWB communications have recently gain wide interest as an enabling technique that provides low-power, low-complexity, and high-speed communications in short range links. For example, IEEE 802.15.4a [40] has regulated UWB communications with maximum 27.24 Mbps transmission within 10 meters in a single UWB channel (the maximum aggregate data rate is 653.76 Mbps with 24 non-overlapped channels). The WiMedia UWB [87] has the capability of 1,024 Mbps, and supports applications such as wireless USB,

DVI, and HDMI.

By transmitting ultra-short pulses at a very low-power spectral density, the impulse radio UWB (IR-UWB) is one of the most popular signaling in UWB communications and was adopted in IEEE 802.15.4a. However, one of the main challenges of the IR-UWB communication is the highly frequency-selective channel [90, 17, 92, 11], which induces hundreds of overlapped copies of the transmitted pulse with different delays and amplitudes into the received signal. To collect the energy of these multipath components (MPCs), the coherent Rake receivers [10, 16] are proposed, but require the high implementation cost on a large number of Rake fingers and the intensive computational cost for estimating the amplitudes and delays of the MPCs [49].

To cope with the multipath effect while considering the implementation cost, the sub-optimal noncoherent UWB receivers, including the energy detector (ED) [82, 20] and the transmitted-reference (TR) receivers [94, 15, 19], are proposed. The ED makes decisions on the information symbols by collecting the energy of the received signal over a desired time and frequency window, and the TR systems transmit a reference pulse prior to an information pulse and detect the information symbols by correlating the reference and information signals. Although the ED and the TR receivers do not require explicit channel estimation and enable simple receiver structures, they exhibit considerable error performance degradation compared to the ideal Rake receiver as a result of the high-order noise effect.

To mitigate the effect of the high-order noise, multi-symbol detectors (MSDs) [33, 50] are designed to jointly detect M consecutive information symbols for differential UWB systems. By increasing the block size M, the MSDs achieve significant performance improvements over the TR receivers. However, since the multi-symbol differential detection (MSDD) problem is generally non-deterministic polynomial-time hard (NP-hard), the existing MSDs require considerable computational efforts when

M is large. If high-performance MSD is of our interest with large M, the optimal MSD is prohibited for its exponential complexity, and thus near-optimal low-complexity MSDs are strongly desired for practical applications.

Meanwhile, most of existing differential UWB receivers are derived based on Gaussian approximation of correlation noise, which is well justified when the noise process is Gaussian distributed and the correlation-time-bandwidth product is long [66]. However, in the case of multiple user transmissions, recent studies for coherent Rake receivers show that the noise can be impulsive [5, 75, 56] when the number of active users is small. The non-Gaussian noise distribution could result in performance degradation without proper handling, and several methods in [5, 75, 56] have been proposed to mitigate the impulsive noise. However, for differential UWB systems, the statistics of correlation noise with few active users and the impacts to the differential receivers are not investigated.

One issue of UWB systems is that the communication range is limited due to the stringent emission power constraint imposed by the Federal Communications Commission (FCC). To extend the coverage of UWB communications, relaying systems are proposed for differential UWB systems. However, most of the existing relaying designs [3, 105, 86, 34, 58] employ equal power allocation and/or fixed path selection, which are simple but yield degraded performance, while the optimization of optimal power allocation and path selection is a high-dimensional combinatorial problem, which requires high complexity. Thus, the problem of finding a near-optimal low-complexity power allocation and path selection solution to the UWB relaying systems is of much interest.

Another main concern of the differential UWB receivers is the cost of accurate delay components on the order of nanoseconds. To overcome the implementation issue posed by the delay components, the frequency-shifted reference (FSR) system has been proposed to separate the reference and data-modulated signals in the frequency

domain at the price of requiring an analog carrier [30]. The FSR is further simplified by the code-multiplexed TR (CM-TR) [18] and code-shifted reference (CSR) [61] schemes based on orthogonal code sequence design. Both systems are promising schemes as they require neither delay elements nor analog carriers, while even exhibiting better bit error rate (BER) performance compared to the FSR solution. However, existing studies do not address the fundamental limits about the error performance of code-multiplexed systems and their corresponding code designs.

Finally, most of studies assume ideal antennas, which have perfect delta impulse response. However, the practical antennas could introduce linear and/or nonlinear distortions, which may degrade the performance. The performance impacts of the non-ideal antennas are not investigated.

1.2 Objectives

The objective of the proposed research is to design low-complexity, high-performance, noncoherent receivers for UWB communications. To be specific, the goals are given as follows:

1. Avoid the stringent channel estimation by exploiting noncoherent detection;
2. Maintain the simple hardware structure of the noncoherent receivers;
3. Lower the computational and hardware complexity of the existing detectors by employing advanced digital signal processing techniques; and
4. Improve the error performance of the noncoherent receivers by taking account of practical imperfections, e.g., impulsive noise, poor signal in long distance, and non-ideal antennas.

1.3 Outline

The rest of the dissertation is organized as follows:

Chapter 2 gives a brief introduction to UWB communications and presents the existing UWB receiver designs and their complexity-performance tradeoffs.

Chapter 3 proposes a fast iterative multi-symbol detector with low complexity and near-optimal performance.

Chapter 4 shows that the multi-symbol detection problem is "rank-one perturbation" problem and develops improved low-complexity near-optimal multi-symbol detectors using relaxation techniques.

Chapter 5 presents a soft-input soft-output multi-symbol detector to further enhance the error performance with error correction code.

Chapter 6 studies the distribution of correlation noise and proposes improved differential UWB receives in the presence of impulsive correlation noise.

Chapter 7 proposes joint power allocation and path selection for non-coherent UWB relaying systems.

Chapter 8 develops generalized code-multiplexing with delay components and analog carriers and discovers the fundamental limits of such systems.

Chapter 9 investigates the performance impacts of non-ideal antennas.

Chapter 10 concludes the dissertation and proposes some future research topics.

1.4 Notations

Notations. Matrices are in upper case bold while column vectors are in lower case bold, $(\cdot)^T$ denotes the transpose, $[\mathbf{A}]_{m,n}$ denotes the (m,n)th entry of the matrix $\mathbf{A}$, $\mathbf{a}^{(i)}$ denotes the ith row of matrix $\mathbf{A}$, $\odot$ denotes the Hadamard element-by-element vector multiplication, $\otimes$ denotes the Kronecker product, $\mathrm{diag}(\cdot)$ converts a sequence of size N into an $N \times N$ diagonal matrix, $*$ denotes linear convolution, $\lceil \cdot \rceil$ denotes the ceiling function, $\triangleq$ stands for definition, $\mathbf{A}_{N\times L}$ denotes an $N \times L$ matrix, $\mathbf{I}_N$ denotes the $N \times N$ identity matrix, $\mathbf{J}_N$ denotes an $N \times N$ matrix with 1 below the main diagonal and 0 elsewhere, $\mathbf{0}_{N\times L}$ is the $N \times L$ matrix with all entries zero, $\mathbf{1}_{N\times L}$ is

the $N \times L$ matrix with all entries one, and $\mathrm{sgn}(x)$ is the sign function, which takes values -1 and 1 depending on the polarity of the argument. $\mathrm{E}\{\cdot\}$ denotes statistical expectation, and $\mathrm{Var}\{\cdot\}$ denotes statistical variance. The Q-function is defined as $Q(x) \triangleq \frac{1}{\sqrt{2\pi}} \int_x^{+\infty} \mathrm{e}^{-t^2/2} dt$

CHAPTER II

BACKGROUND

The background information of UWB communications and the existing work on UWB receiver designs are presented in this chapter. Be specific, the first part describes the main characteristics of UWB communications, which have great impacts on UWB receiver designs, are presented in Section 2.1. A brief literature review of the existing receiver designs and their complexity-performance tradeoffs is given in Section 2.2.

2.1 Overview of UWB Communications

UWB communications use a very large bandwidth to transmit signals at a very low-power spectral density (PSD) [98]. According to the definition from the Federal Communications Commission (FCC) in the United States, the bandwidth of a UWB communication occupies at least 500 MHz or a fractional bandwidth exceeding 20% [23]. The huge signaling bandwidth reveals several attractive features of UWB communications, including the potential high-data-rate communications, the fine-resolution ranging, and the possibility of low-complexity devices.

However, as a result of the very large bandwidth of UWB communications, the spectrum of UWB systems inevitably overlays those of the existing narrowband or wideband signals, e.g., GSM, GPS, and WiFi, resulting in interference. To avoid the mutual interference with the existing signals, the transmission power of UWB communications has to be limited at a very low level (usually at the noise floor). Figure 1 illustrates the FCC spectral mask for indoor UWB commercial systems, which allows the operation of UWB systems over an up to 7.5 GHz bandwidth at the noise floor (-40 dBm).

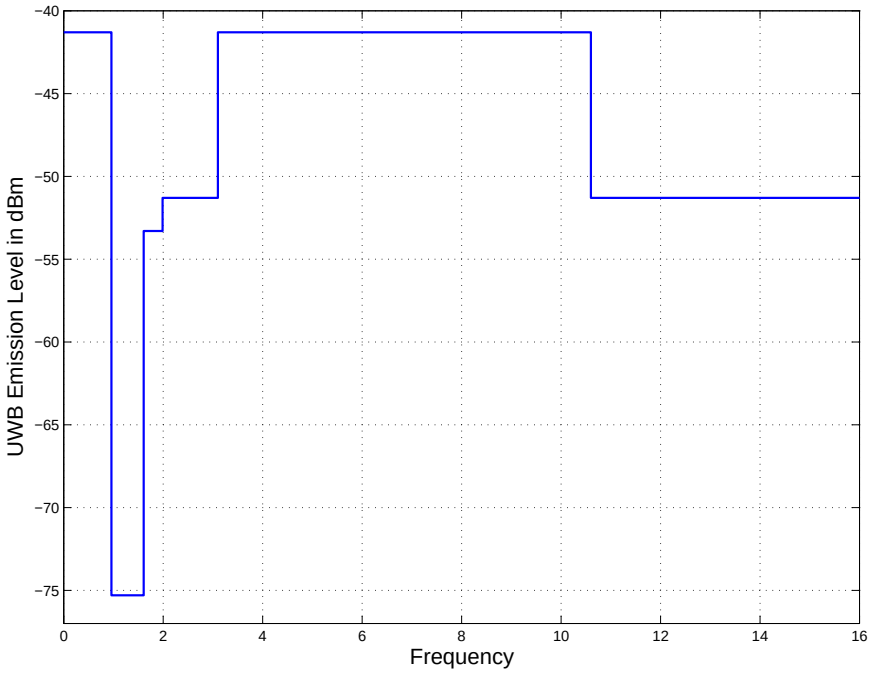

Figure 1: The FCC spectral mask for indoor UWB communications.

To exploit the large bandwidth of UWB communications with affordable complexity, the impulse-radio (IR) UWB [89], which is one of the most popular schemes of UWB communications, transmits the information symbols with low-power ultra-short pulses. Since the pulses are real, the IR-UWB signaling can be carrier-free, which greatly simplifies the transceiver structure. For the transmitted pulse, the IR-UWB adopts the Gaussian pulse or the high-order derivatives of the Gaussian pulse with duration T_p on the order of subnanoseconds (see Figure 2). The main benefits of the Gaussian pulses are *i)* their smallest possible time-bandwidth product of 0.5; *ii)* the well known analytical expression of the Fourier transform of the Gaussian pulses, which is useful for pulse shaping designs; and *iii)* the easy generation of the Gaussian pulses from antennas [70]. To match the FCC spectral mask using one of the Gaussian pulses as the basic pulse, the pulse shaper design in [51] can be used to generate the transmitted pulse based on the Parks-McClellan algorithm [62].

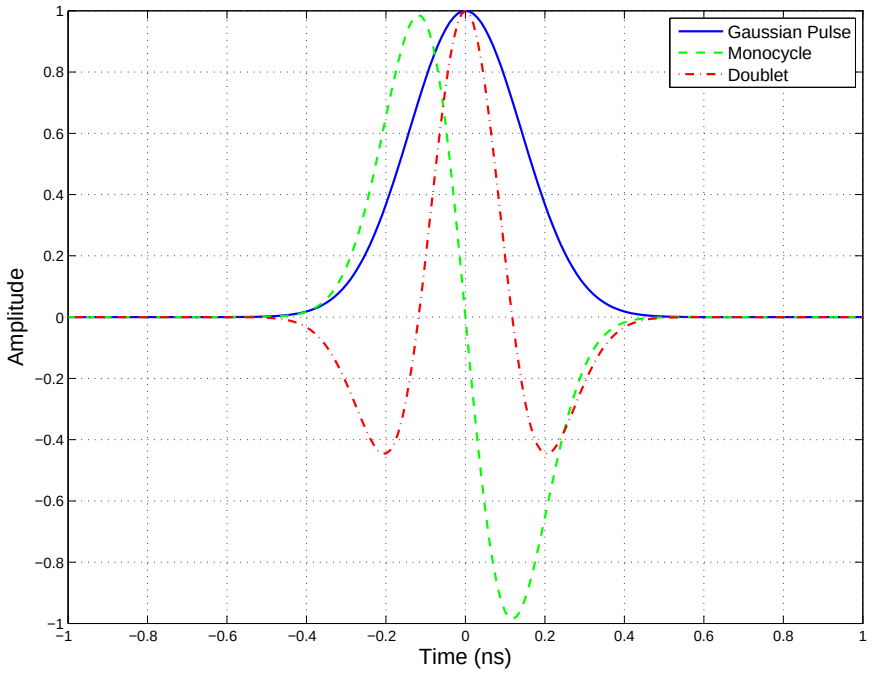

Figure 2: Transmitted pulses for IR-UWB systems with duration $T_p = 1.0$ ns.

Since the transmitted pulses are low power, each information symbol is conveyed over N_f pulses such that the receiver can collect enough energy. Each pulse is transmitted within a frame with duration $T_f \gg T_p$. A modulation (e.g., pulse position modulation (PPM), pulse amplitude modulation (PAM), or differential modulation) is applied for each pulse in each frame to carry the information of the desired symbol. For an IR-UWB transmission with a sequence of information symbols $\{a_i\}_{i=-\infty}^{\infty}, a_i \in \{\pm 1\}$, using PAM, the transmitted signal is

$$s(t) = \sum_{i=-\infty}^{\infty} \sum_{j=0}^{N_f-1} b_{iN_f+j} p(t - iT_s - jT_f - c_j T_c), \tag{1}$$

where b_{iN_f+j} is the modulated symbol for the jth frame of the ith information symbol, which equals a_i for coherent detection, $p(t)$ is the transmitted pulse, and $T_s = N_f T_f$ is the symbol duration. The time-hopping codes c_j are integers chosen from $0 \leq c_j \leq N_c - 1$ so that multiple users can access the channel concurrently, and the transmission time of the jth pulse is delayed with $c_j T_c$ seconds. To eliminate inter-frame interference (IFI), the frame duration is chosen such that $T_f > T_m + T_p + (N_c -$

1)T_c, where T_m is the maximum excess delay of the channel.

After the signal is transmitted, the receiver will obtain the signal that is mainly distorted by two effects: *i*) the highly frequency-selective UWB fading channel; and *ii*) the additive white Gaussian noise (AWGN). As a result of the large bandwidth of the transmitted pulse, the UWB channel is highly frequency selective, where the receiver can observe hundreds of overlapped copies of the transmitted pulse with different delays and amplitudes. The delays and amplitudes of these MPCs can be well characterized by the well-known Saleh-Valenzuela (S-V) channel model [69, 17, 92, 11, 25, 40], in which the channel impulse response is modeled as

$$h(t) = \sum_{l=0}^{\infty} \sum_{k=0}^{\infty} \beta_{kl} p_{kl} \delta(t - T_l - \tau_{kl}), \tag{2}$$

where $T_l + \tau_{kl}$ represents the delay of the kth ray of the lth cluster and $\beta_{kl} p_{kl}$ models the double-sided Rayleigh distributed amplitudes with exponentially decaying profile. Fig. 3 depicts a realization of the IEEE802.15.4Ga channel impulse response [40] based on the S-V channel model. From Fig. 3, we observe hundreds of MPCs and that the maximum excess delay T_m can be up to 300 ns.

2.2 Existing UWB Receiver Designs

This section gives a brief overview of the existing UWB receiver designs and their complexity-performance tradeoffs. Unless stated otherwise, we use the transmission model in Eq. (1), the channel model in Eq. (2), and the corresponding received signal model as

$$\begin{aligned} x(t) &= (s(t) * h(t) + n(t)) * f_{\text{rx}}(t) \\ &= \sum_{i=-\infty}^{\infty} \sum_{j=0}^{N_f - 1} b_{iN_f + j} g(t - iT_s - jT_f - c_j T_c) + w(t), \end{aligned} \tag{3}$$

where $f_{\text{rx}}(t)$ is an ideal bandpass filter with bandwidth B at the receiver, $g(t) = p(t) * h(t) * f_{\text{rx}}(t)$ is called channel template, and $n(t)$ stands for the noise including

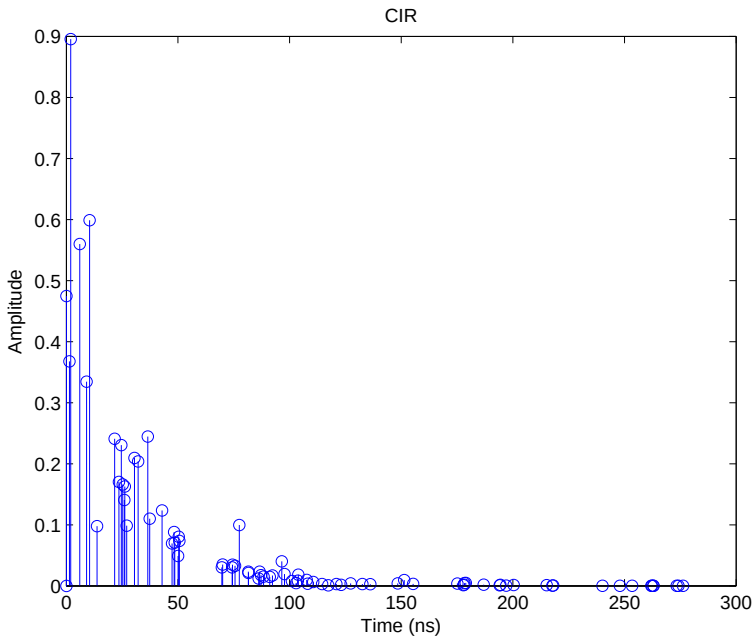

Figure 3: A realization of the channel impulse response of the IEEE802.15.4Ga CM1 channel model.

multiple access interference (MAI) and AWGN with zero mean and two-sided power spectral density $\frac{N_0}{2}$. The noiseless received signal energy in each frame is defined as $E_f = \int_0^{T_f} g^2(t)dt$.

To simplify the notations, $x_{iN_f+j}(t) = x(t + iT_s + jT_f + c_jT_c) = b_{iN_f+j}g(t) + w_{iN_f+j}(t), 0 \leq t \leq T_f$, represents the received signal of the jth frame ($0 \leq j \leq N_f - 1$) of the ith symbol, $w_{iN_f+j}(t) = w(t + iT_s + jT_f + c_jT_c)$ represents the corresponding noise in the frame, and the received signal-to-noise ratio (SNR) is defined as $\gamma = E_b/N_0 = E_fN_f/N_0$.

2.2.1 Coherent Rake Receiver

With coherent PAM, i.e., $b_{iN_f+j} = a_i, \forall j \in [0, N_f - 1]$, the ideal Rake receiver [10, 16, 88] applies a perfect match filter (channel template) $g(t)$ to collect all the energies of

the MPCs [90] and estimates the information symbols as

$$\hat{a}_i^{\text{RAKE}} = \text{sgn}\left(\frac{1}{N_f}\sum_{j=0}^{N_f}\int_0^{T_f} g(t)x_{iN_f+j}(t)dt\right) \tag{4}$$

$$= \text{sgn}\left(a_i E_f + \frac{1}{N_f}\sum_{j=0}^{N_f}\int_0^{T_f} g(t)w_{iN_f+j}(t)dt\right). \tag{5}$$

Note that in the absence of IFI, $w_{i,j}(t)$'s and $0 \le t \le T_f$ are identically independent distributed (i.i.d.) noise processes. Hence, the bit-error-rate (BER) performance of the ideal Rake receiver is

$$P_e^{\text{RAKE}} = Q(\sqrt{2\gamma}). \tag{6}$$

Although the ideal Rake receiver achieves the optimal error performance, the Rake receiver faces several challenges in practice: *i)* The Rake receiver requires perfect channel state information, which incurs the extremely high sampling rate and the intensive computational cost for estimating the amplitudes and delays of the MPCs [49]. *ii)* The Rake receiver may suffer from the error performance degradation as a consequence of the channel estimation error [49]. *iii)* The Rake receiver requires the high implementation cost on a large number of Rake fingers to construct $g(t)$.

2.2.2 Simple Transmitted-Reference Receiver

As an alternative of the Rake receiver, the simple TR (STR) method [37, 16, 14, 66, 97] sends a reference pulse along with the data-modulated pulse for each frame as

$$s(t) = \sum_{i=-\infty}^{\infty}\sum_{j=0}^{N_f-1} p(t - iT_s - jT_f - c_jT_c) + a_i p(t - iT_s - jT_f - c_jT_c - T_d), \tag{7}$$

where the first pulse is used to generate a noisy channel template and the second pulse is delayed with T_d. Similar to the transmitted signal model in Eq. (1), to avoid inter-pulse interference (IPI), $T_d \ge T_m + T_p + (N_c - 1)T_c$ and $T_f \ge T_d + T_m + T_p + (N_c - 1)T_c$ must hold. The corresponding received signal for a TR transmission is

$$x(t) = \sum_{i=-\infty}^{\infty}\sum_{j=0}^{N_f-1} g(t - iT_s - jT_f - c_jT_c) + a_i g(t - iT_s - jT_f - c_jT_c - T_d) + w(t). \tag{8}$$

At the receiver, the STR receiver is simply an autocorrelation receiver (AcR), which estimates the information symbols by correlating the reference signals with the data-modulated signals as

$$\begin{aligned}\hat{a}_i^{\mathrm{STR}} &= \mathrm{sgn}\left(\frac{1}{N_f}\sum_{j=0}^{N_f}\int_0^{T_r} x_{iN_f+j}(t)x_{iN_f+j}(t+T_d)dt\right)\\ &= \mathrm{sgn}\left(\frac{1}{N_f}\sum_{j=0}^{N_f}\int_0^{T_r}\left(g(t)+w_{iN_f+j}(t)\right)\left(a_i g(t)+w_{iN_f+j}(t+T_d)\right)dt\right)\\ &= \mathrm{sgn}\left(\frac{1}{2}a_i E_f\rho+\frac{1}{N_f}\sum_{j=0}^{N_f}\int_0^{T_r}\underbrace{\left(a_i g(t)w_{iN_f+j}(t)+g(t)w_{iN_f+j}(t+T_d)\right)}_{\text{First-order noise term}}+\right.\\ &\qquad\left.\underbrace{w_{iN_f+j}(t)w_{iN_f+j}(t+T_d)}_{\text{Second-order noise term}}\right)dt\Bigg), \end{aligned} \tag{9}$$

where $0 < T_r \leq T_f$ denotes integration interval, $\rho = \int_0^{T_r} g^2(t)dt / \int_0^{T_f} g^2(t)dt$ denotes the fraction of the frame of energy collected by the correlation, and the perfect channel template $g(t)$ for the ideal Rake receiver in Eq. (4) is replaced by the noisy channel template $g(t) + w_{iN_f+j}(t)$ for the TR transmission. Note that, since two pulses are transmitted in one frame, $E_f = 2\int_0^{T_f} g^2(t)dt$ at the STR receiver. Unless stated otherwise, we set $T_r = T_f$ for all integrations such that $\rho = 1$.

Assuming sufficiently large time-bandwidth product $T_r B$, we evaluate the BER of the STR receiver as [14, 66]

$$P_e^{\mathrm{STR}} = Q\left(\left[\frac{2}{\gamma}+\frac{N_f L}{\gamma^2}\right]^{-\frac{1}{2}}\right), \tag{10}$$

where $L = 2T_f B$ is the twice time-bandwidth product. Note that, the terms with $1/\gamma$ and $1/\gamma^2$ in Eq. (10) are caused by the first-order noise and the second-order noise, respectively.

Although the STR receiver does not require explicit channel estimation, compared to the ideal Rake receiver, the STR method exhibits several drawbacks: *i*) The STR method requires two pulses per frame, which increases transmission power and decreases data rate, yielding lower spectral efficiency. *ii)* The error performance of the

STR receiver is severely degraded by the second-order noise term in Eq. (9), especially when the twice time-bandwidth product L is large, which is usually satisfied in UWB communications[1].

2.2.3 Differential Transmitted-Reference Receiver

To save the transmission power of the reference signal, the differential TR (DTR) method transmits one pulse per frame as in Eq. (1) by employing the frame-by-frame differential encoding as

$$b_i = b_{i-1} a_{\lfloor i/N_f \rfloor}, \tag{11}$$

where $b_{-\infty} = \pm 1$ and $\lfloor \cdot \rfloor$ is a floor function.

After obtaining the signal in Eq. (3), the DTR receiver detects the information symbols by correlating the received signals in the adjacent frames as

$$\begin{aligned}
\hat{a}_i^{\mathrm{DTR}} &= \mathrm{sgn}\left(\frac{1}{N_f} \sum_{j=0}^{N_f} \int_0^{T_f} x_{iN_f+j-1}(t) x_{iN_f+j}(t) dt \right) \\
&= \mathrm{sgn}\left(\frac{1}{N_f} \sum_{j=0}^{N_f} z_{iN_f+j-1, iN_f+j} \right) \qquad (12) \\
&= \mathrm{sgn}\left(a_i E_f + \frac{1}{N_f} \sum_{j=0}^{N_f-1} \eta_{iN_f+j, iN_f+j-1} \right) \qquad (13)
\end{aligned}$$

where $z_{i,j}$ is the correlation between the ith and jth frame signals as

$$\begin{aligned}
z_{i,j} &= \int_0^{T_f} x_i(t) x_j(t) dt \\
&= b_i b_j E_f + \int_0^{T_r} \Bigg(\underbrace{b_i g(t) w_j(t) + b_j g(t) w_i(t)}_{\text{First-order noise term}} + \underbrace{w_i(t) w_j(t)}_{\text{Second-order noise term}} \Bigg) dt \\
&= b_i b_j E_f + \eta_{i,j} \qquad (14)
\end{aligned}$$

where $\eta_{i,j}$ is the correlation noise term, which can be well approximated as a Gaussian distributed variable when $w(t)$ is a white Gaussian process [14, 66].

[1] Taking as an example a system with bandwidth B of 2.5 GHz and a frame interval T_f of 80 ns, $L = 400$ can be obtained.

With $T_r = T_f$, i.e., $\rho = 1$, the BER performance of the DTR receiver is given as [14]

$$P_e^{\mathrm{DTR}} = Q\left(\left[\frac{2N_f - 1}{N_f\gamma} + \frac{N_f L}{4\gamma^2}\right]^{-\frac{1}{2}}\right). \tag{15}$$

Compared to the error performance of the STR in Eq. (10), since both effects of the first-order noise and the second-order noise are mitigated, the error performance of the DTR receiver is enhanced.

2.2.4 Differential Detection Receiver

To alleviate the noise effect in the DTR system, especially the second-order noise effect, the differential detection (DD) scheme utilizes the symbol-by-symbol differential encoding as

$$b_{iN_f} = b_{(i-1)N_f} a_i \qquad \text{and} \qquad b_{iN_f+j} = b_{iN_f}, \forall j \in [1, N_f - 1], \tag{16}$$

and detects the information symbol a_i using the averaged symbol signals instead of the frame signals of the DTR as [19]

$$\hat{a}_i^{\mathrm{DD}} = \mathrm{sgn}\left(Z_{i,i-1}\right), \tag{17}$$

where

$$\begin{aligned} Z_{i,j} &= \int_0^{T_r} \left(\frac{1}{N_f}\sum_{l=0}^{N_f-1} x_{iN_f+l}(t)\right)\left(\frac{1}{N_f}\sum_{n=0}^{N_f-1} x_{jN_f+n}(t)\right) dt \\ &= \int_0^{T_r} y_i(t) y_j(t) dt \\ &= \prod_{k=i+1}^{j} a_k E_f + \frac{1}{N_f^2}\sum_{l=0}^{N_f-1}\sum_{n=0}^{N_f-1} \eta_{iN_f+l,jN_f+n}, \end{aligned} \tag{18}$$

which is the symbol-by-symbol correlation between the ith and jth averaged symbol signals with $y_i(t)$ being the averaged symbol signal for the ith information symbol as

$$y_i(t) = \frac{1}{N_f}\sum_{l=0}^{N_f-1} x_{iN_f+l}(t). \tag{19}$$

With the symbol-by-symbol correlation and $T_r = T_f$, the BER of the DD receiver can be derived as [19]

$$P_{\mathrm{e}}^{\mathrm{DD}} = Q\left(\left[\frac{1}{\gamma} + \frac{L}{4\gamma^2}\right]^{-1/2}\right). \tag{20}$$

2.2.5 Multi-Symbol Differential Detectors

To further mitigate the noise-cross-noise effect of the DD receiver, the multi-symbol differential detection (MSDD) is proposed to perform joint estimation on M consecutive information symbols. Without loss of generality, we focus on the joint detection on information symbols $\mathbf{a} = [a_1, \cdots, a_M]^T$. Under the assumption that the noise process $n(t)$ is a white Gaussian process, by applying the generalized likelihood ratio test (GLRT), the MSDD receiver is in the form [33, 50]:

$$\hat{\mathbf{b}} = \arg \max_{\tilde{\mathbf{b}} \in \{\pm 1\}^{M+1}} \left(\sum_{i=0}^{M} \sum_{j=i+1}^{M} \tilde{b}_i \tilde{b}_j Z_{i,j} \right), \tag{21}$$

and

$$\hat{a}_i^{\mathrm{MSDD}} = \hat{b}_{i-1}\hat{b}_i, \qquad i \in [1, M], \tag{22}$$

where $Z_{i,j}$'s are the symbol-by-symbol correlations defined in Eq (18), and $\hat{\mathbf{b}} = [\hat{b}_0, \cdots, \hat{b}_M]^T$ and $\tilde{\mathbf{b}} = [\tilde{b}_0, \cdots, \tilde{b}_M]^T$ are the estimates and the candidates of the modulated symbols $[b_0, b_{N_f}, \cdots, b_{MN_f}]$, respectively. When $M = 1$, the MSDD receiver becomes the DD receiver in Eq. (17).

Written in matrix form, the MSDD receiver based on the GLRT rule can be reformulated as

$$\hat{\mathbf{b}} = \arg \max_{\tilde{\mathbf{b}} \in \{\pm 1\}^{M+1}} \left(\tilde{\mathbf{b}}^T \mathbf{Q} \tilde{\mathbf{b}} \right), \tag{23}$$

where $\mathbf{Q}$ is an $(M+1) \times (M+1)$ matrix, whose (i,j)th element is $Z_{i-1,j-1}$. It is worth noting that the diagonal elements of $\mathbf{Q}$ can be any finite constant because these diagonal elements do not affect the optimal solution to (23). Thus, we set $Z_{i,i} = 0$ in this proposal.

The main challenges of the MSDD are the implementation of M-branch AcRs and the design of reliable and computationally efficient MSDs. For the implementation of AcRs, accurate analog delay lines on the order of multiples of symbol intervals are still under investigation [4, 13, 24], and thus digital delay elements become a strong candidate for the TR-based UWB systems [13, 24, 26]. Based on the fast development of high-speed analog-to-digital converters, the digital delay element for UWB systems may be realizable in the near future (see [45, 13, 26, 47]).

For the computational complexity, the problem in Eq. (23) is generally NP-hard. To (approximately) solve this NP-hard problem in Eq. (23) in a reliable and computationally efficient manner, several MSDs have been proposed, including the exhaustive search method [33], the sphere decoding algorithm (SDA) [50, 74], the Viterbi algorithm (VA) [50], and the sorted block-wise decision-feedback differential detector (sbDF-DD). The exhaustive search method of [33] enumerates all 2^M possibilities of the candidate solutions to find the optimal one. This enumeration requires exponential complexity in block size M. The SDA proposed in [50, 74] reduces the complexity of the exhaustive search by searching the candidate solutions only within a specific radius, but the complexity remains exponential [42]. A sub-optimal MSD based on the VA is proposed in [50], which has polynomial complexity in M. However, the performance of the VA-based approach heavily depends on the memory length L and degrades significantly if the memory length is relatively small compared to M. The sbDF-DD is proposed in [72], which has low complexity, but the performance is inferior to the optimal performance.

2.3 Complexity-Performance Tradeoffs

The complexity-performance tradeoffs of the existing receivers discussed in the previous sections are summarized in Table 1. The complexity is measured in terms of hardware complexity and computational complexity.

Table 1: Complexity-performance comparisons of the existing UWB receivers (L is the memory length of the VA, and M is the block size of the MSD).

Receiver	Hardware cost	Computational cost	Error performance
Rake receiver	High	High	Optimal
TR	Low	Low	Low
DTR	Low	Low	Better than TR
DD	Mid	Low	Better than DTR
MSD with SDA	Mid	Exponential in M	Close to the Rake receiver when M is large
MSD with VA	Mid	Exponential in L	Degraded when L is small
MSD with sbDF-DD	Mid	Low	Inferior to the optimal one

To further illustrate the performance of the existing detectors, Fig. 4 depicts the error performance of the ideal Rake receiver, the STR receiver, the DTR receiver, the DD receiver, and the optimal MSD using the SDA in [50] with different block sizes M for UWB communications. We adopt the CM1 channel model described in [25], where $T_f = 80$ ns to exclude the ISI. The one-sided bandwidth of the baseband filter at the receiver is $B = 2.5$ GHz, and the twice time-bandwidth product $L = 2BT_f = 400$. The frame repetition factor is $N_f = 20$. From Fig. 4, the idea Rake receiver achieves the best error performance, which is 16 dB better than that of the STR receiver at BER $= 10^{-4}$. The STR receiver shows the worst error performance among all the receivers. The DTR receiver exhibits an about 2.5 dB gain over the STR receiver, and the DD receiver obtains an about 6 dB gain over the DTR receiver at BER $= 10^{-4}$. The performance of the noncoherent detection is further improved by the MSD, whose error performance approaches that of the ideal Rake receiver as M increases. When $M = 30$, the optimal MSD exhibits an about 2 dB loss to the ideal Rake one at BER $= 10^{-4}$.

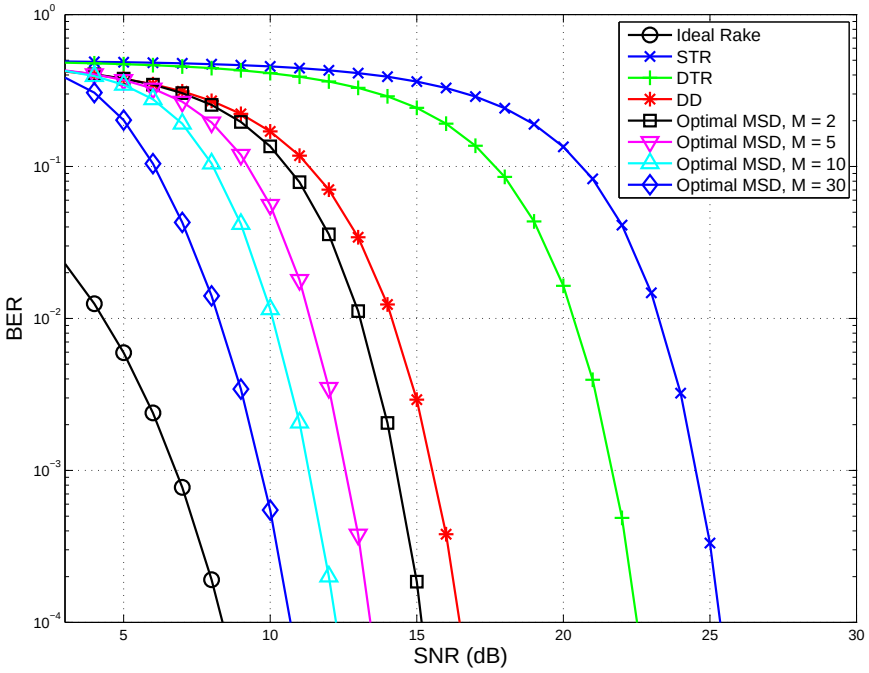

Figure 4: Performance of the UWB receivers with $L = 400$ and $N_f = 20$.

CHAPTER III

A FAST MULTI-SYMBOL BASED ITERATIVE DETECTOR

In this chapter, we develop an iterative MSDD algorithm that avoids the high computational complexity of the existing GLRT-based detectors (e.g., the exhaustive search [33]). As studied in Sec. 2, the MSDD based on the GLRT rule exhibits considerable error performance improvement over the STR, DTR, and DD methods while maintaining the simple AcR structure. However, the main concern of the MSDD is the computational complexity as a consequence of the NP-hardness of the GLRT problem in Eq. (23), especially when the block size M is large. To lower the complexity of the optimal MSD, this section presents iterative MSDs with low complexity and high performance.

Similar to the TR detection scheme, the proposed method first generates a reference template by using the initial symbol only, and then the method estimates the information symbols by correlating the reference template with the symbol waveforms. Furthermore, with the help of the information from the multiple transmitted symbols, our method manages to suppress the reference template noise. However, our method also generates additional noise-cross-signal and noise-cross-noise terms in TR BER analysis, which do not appear in the case of an ideal Rake receiver with perfect channel knowledge.

For the initialization, since the only known symbol is $b_0 = 1$, the best template at this stage is:

$$\tilde{g}^{(1)}(t) = b_0 y_0(t) = y_0(t), \tag{24}$$

where $y_0(t)$ can be found in Eq. (19).

The decision variables for the M information symbols are:

$$\begin{aligned} z_m^{(1)} &= \int_0^{T_f} \tilde{g}^{(1)}(t) y_m(t) dt \\ &= \int_0^{T_f} y_0(t) y_m(t) dt \\ &= Z_{0,m}, \qquad \forall m \in [1, M]. \end{aligned} \tag{25}$$

The estimated modulated symbols in this iteration are:

$$\tilde{b}_m^{(1)} = \text{sgn}(Z_{0,m}), \forall m \in [1, M]. \tag{26}$$

This means that at the first step the estimated symbols are obtained by correlating the waveform corresponding to b_0 with the mth symbol waveform. Hence, the BER performance is the same as that of the DD in Eq. (20).

For the nth iteration, the method firstly constructs a new reference template by weighting the products of each symbol waveform $y_i(t)$ and its corresponding detected symbol $\tilde{b}_i^{(n-1)}$ obtained from the previous iteration:

$$\tilde{g}^{(n)}(t) = w_0^{(n-1)} y_0(t) + \sum_{i=1}^{M} w_i^{(n-1)} \tilde{b}_i^{(n-1)} y_i(t). \tag{27}$$

Then, the decision variable for the mth symbol is evaluated in the same way as the one in Eq. (25):

$$\begin{aligned} z_m^{(n)} &= \int_0^{T_f} \tilde{g}_m^{(n)}(t) y_m(t) dt \\ &= w_0^{(n-1)} Z_{0,m} + \sum_{i=1, i\neq m}^{M} w_i^{(n-1)} \tilde{b}_i^{(n-1)} Z_{i,m}, \end{aligned} \tag{28}$$

where $\tilde{g}_m^{(n)}(t)$ is the reference template for the mth symbol by removing the mth waveform $y_m(t)$ from $\tilde{g}^{(n)}(t)$:

$$\tilde{g}_m^{(n)}(t) = w_0^{(n-1)} y_0(t) + \sum_{i=1, i\neq m}^{M} w_i^{(n-1)} \tilde{b}_i^{(n-1)} y_i(t). \tag{29}$$

At last, the iteration outputs the estimated symbols as:

$$\tilde{b}_m^{(n)} = \text{sgn}(z_m^{(n)}). \tag{30}$$

3.1 Weight Selections

A key factor that affects the performance of the method and the convergence is how to update the weights in each iteration. The ultimate goal of selecting the weights is to reduce BER while maintaining low computational complexity and requiring little extra knowledge (such as channel information). Here, we propose the hard-decision rule for the choice of the weights in each iteration.

The rule constructs the reference template as

$$\tilde{g}^{(n)}(t) = y_0(t) + \sum_{i=1}^{M} \tilde{b}_i^{(n-1)} y_i(t), \tag{31}$$

which indicates that $\mathbf{w}^{(n-1)} = [1, 1, \ldots, 1]$ in Eq. (27).

An interesting observation on the reference template in (31) is that the variance of the reference template is constant given the detected symbols $\tilde{b}_m^{(n-1)}$:

$$\begin{aligned} \mathrm{Var}\{\tilde{g}^{(n)}(t)\} &= \mathrm{Var}\{y_0(t)\} + \sum_{i=1}^{M} \mathrm{Var}\{\tilde{b}_i^{(n-1)} y_i(t)\} \\ &= (M+1)\mathrm{Var}\{y_0(t)\}. \end{aligned} \tag{32}$$

The conditional mean of the template is:

$$\begin{aligned} \mathrm{E}\{\tilde{g}^{(n)}(t)|\mathbf{b}\} &= g(t) + \sum_{m=1}^{M} \{\hat{b}_m^{(n-1)} b_{mN_f}\} g(t) \\ &= (1 + 2N_c^{(n-1)} - M) g(t), \end{aligned} \tag{33}$$

where $\mathbf{b} = [b_0, b_{N_f}, \cdots, b_{MN_f}]^T$ and $N_c^{(n-1)}$ is the number of correct symbols for the $(n-1)$st iteration. Hence, the mean and standard deviation ratio is

$$\frac{\mathrm{E}\{\tilde{g}^{(n)}(t)|\mathbf{b}\}}{\mathrm{Std}\{\tilde{g}^{(n)}(t)\}} = \frac{(1 + 2N_c^{(n-1)} - M) g(t)}{\sqrt{(M+1)}\mathrm{Std}\{y_0(t)\}}, \tag{34}$$

where $\mathrm{Std}\{\cdot\}$ is the standard deviation of the random variable. In general, the larger the mean-standard deviation ratio, the better the BER performance. Thus, in the case of the hard decision, if more correct symbols are detected for the current iteration, during the next iteration, the reference template is improved, and then the method

potentially results in better BER performance. The iterative procedure runs back and forth until no symbol is changed or the maximum number of iterations is reached. We call the iterative MSD using the hard-decision rule the "hard-decision-directed MSD (HDD-MSD)."

Now, we summarize the HDD-MSD in the following steps for one block symbol detection:

Table 2: Hard-decision-directed multi-symbol detector.

Input:	Correlation matrix $Z_{i,j}$ in Eq. (18) and the maximum number of iterations N.
Step 0	Initialize $\mathbf{w}^{(0)} = [1, 1, ..., 1]$, $\tilde{\mathbf{b}}^{(0)} = [1, 0, ..., 0]$, $n = 0$.
Step 1	$n = n + 1$.
Step 2	Obtain the decision variables by Eq. (28).
Step 3	Obtain the detected symbols by Eq. (30).
Step 4	Set $w^{(n)} = w^{(0)}$.
Step 5	If $n < N$ and $\tilde{\mathbf{b}}^{(n)} \neq \tilde{\mathbf{b}}^{(n-1)}$ goto Step 1, otherwise output $\tilde{\mathbf{b}}^{(n)}$ and exit.

3.2 Convergence and Discussions

- The convergence rate also affects the practical value of the method (e.g., a system with a tight constraint on decoding delay), and the number of iterations affects the performance. These will be verified by the numerical simulation, in which the proposed method converges to the stable performance curve within a few iterations (usually ≤ 5 iterations).

- Instead of evaluating the reference template of each iteration $\tilde{g}^{(n)}(t)$ explicitly, the method computes the decision variables by linear combining the correlation coefficients $Z_{i,j}$, which can be computed in the first iteration and reused later.

- For each iteration, Step 2 requires $2M(M-1)$ multiplications and M^2 additions to attain the decision variables for all M symbols. In Step 3, M sign operations are performed to obtain the detected symbols. No arithmetic is required for the HDD-MSD in Step 4, and then the computational complexity of the HDD-MSD for each iteration is $\mathcal{O}(M^2)$ where M is the block size. Note that the

complexity of the proposed method is independent of channel realizations whilst the computational complexity of the SDA relies on the specific realization of channels and SNR.

3.3 Numerical Results

This section compares the BER performance of the proposed HDD-MSD and the optimal MSD as benchmark. The channel scheme evaluated in this section is the same as the one in Sec. 2.3.

3.3.1 BER with Different Block Sizes

Fig. 5 illustrates the BER results for different M for the HDD-MSD. The proposed HDD-MSD can obtain an about 2 dB gain relative to the DD in the case of $M = 5$ and an about 3 dB gain if $M = 10$ at BER= 10^{-4}. With the increasing number of the symbols in one block, the performance of the proposed method grows monotonically but the improvement decelerates (a 5 dB gain for $M = 20$ and a 5.3 dB gain for $M = 30$ at BER= 10^{-4}). We also perform some simulations with very large M ($M = 100$), which is intractable for the optimal MSD. The system provides similar performance to that of the ideal Rake receiver, especially in high SNR range, where the difference is around 1 dB.

Compared to the HDD-MSD, the optimal MSD has an advantage when M is small (if $M = 2$, about 1.1 dB gain at BER= 10^{-4}) and the performance gap becomes smaller when M is larger. When $M = 10$, the gap reduces to around 0.5 dB for the HDD-MSD at BER= 10^{-4}. This shows that with the increasing value of M the difference between the optimal MSD method and our proposed HDD-MSD decreases rapidly and that the gap can be ignored for a sufficiently large M. Furthermore, the optimal MSD incurs much higher computational cost than our HDD-MSD.

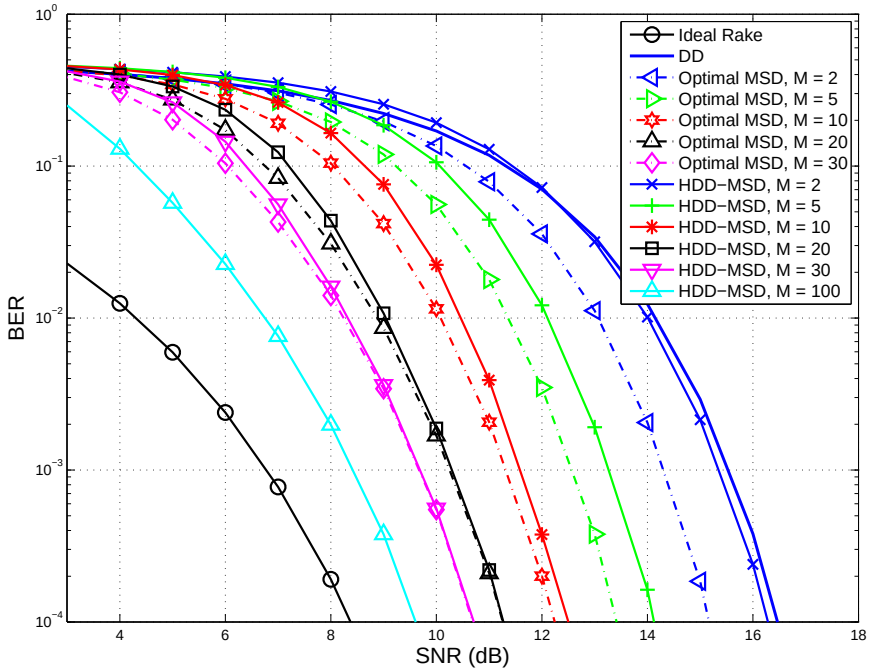

Figure 5: Performance of the HDD-MSD for different M and $L = 400$.

3.3.2 BER with Different Iterations

To answer the convergence question in Sec. 3.2, Fig. 6 depicts the BER values recorded in each iteration for $M = 5, 30$. When there is only one iteration, the system reduces to the DD system, and the BER result overlaps with that given by Eq. (20) (See Fig. 6). The BER is improved significantly in the second iteration and just after about 4 iterations, the algorithm reaches a stable BER performance curve with a small improvement in the 5th iteration at low SNRs. These show that our method converges fast, and thus it is practical for UWB systems.

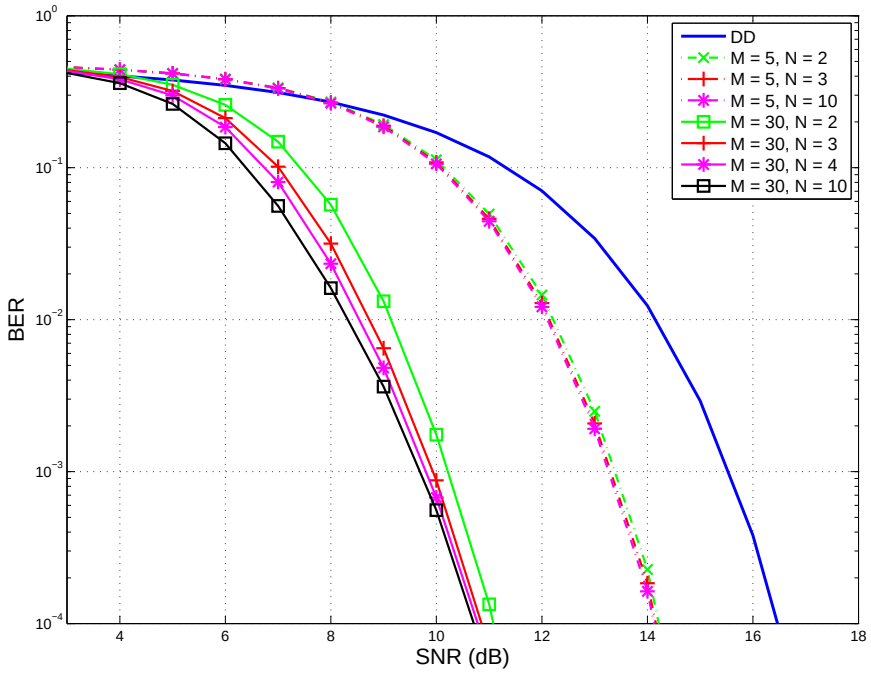

Figure 6: Performance of the HDD-MSD for different iterations, $M = 5, 30$, and $L = 400$.

CHAPTER IV

MULTI-SYMBOL DETECTORS BASED ON RELAXATION TECHNIQUES

4.1 Semi-Definite Programming Based Multi-Symbol Detector

In this section, we develop a near-optimal detector based on semi-definite programming (SDP) by performing semi-definite relaxation on the boolean constraints in (23).

The GLRT problem in (23) can be rewritten as

$$\begin{aligned} \max \quad & \mathcal{J}_{\text{GLRT}}(\mathbf{X}) = \text{Trace}(\mathbf{XQ}), \\ \text{s.t.} \quad & \mathbf{X} = \tilde{\mathbf{b}}\tilde{\mathbf{b}}^T, \\ & \tilde{b}_0 = +1, \\ & X_{i,i} = 1, \quad \text{for} \quad i = 1, \cdots, (M+1), \end{aligned} \tag{35}$$

where Trace$(\cdot)$ is the trace of a matrix, $\tilde{\mathbf{b}}^T\mathbf{Q}\tilde{\mathbf{b}} = \text{Trace}(\tilde{\mathbf{b}}\tilde{\mathbf{b}}^T\mathbf{Q})$, and matrix $\mathbf{X}$ is a rank-1 positive semi-definite (PSD) matrix because of the constraint $\mathbf{X} = \tilde{\mathbf{b}}\tilde{\mathbf{b}}^T$. To relax the non-convex optimization problem (35) to a convex one, which can be solved in polynomial time, the rank-1 constraint is omitted on matrix $\mathbf{X}$, giving the following SDP problem:

$$\begin{aligned} \max \quad & \mathcal{J}_{\text{SDP}}(\mathbf{X}) = \text{Trace}(\mathbf{XQ}), \\ \text{s.t.} \quad & \mathbf{X} \succeq 0, \\ & X_{i,i} = 1, \quad \text{for} \quad i = 1, \cdots, (M+1), \end{aligned} \tag{36}$$

where $\succeq 0$ denotes the PSD constraint on the left hand side matrix (matrix $\mathbf{X}$ in

(36)). Since the problem in (36) is a relaxation of (35), the optimal solution $\mathbf{X}^*$ of (36) can be a matrix with rank higher than one.

To convert the higher-rank solution matrix to an approximate rank-1 matrix solution, two methods can be employed: The first method uses the randomization method from [53, 31, 59], and the second method uses the sign of the principal eigenvector of $\mathbf{X}^*$, i.e.,

$$\hat{b}_{\text{SDP},i} = \text{sgn}(v_i/v_0), \quad \text{for} \quad i = 0, \cdots, M, \tag{37}$$

where $\mathbf{v} = [v_0, v_1, \cdots, v_M]^T$ is the eigenvector corresponding to the largest eigenvalue of the optimal solution $\mathbf{X}^*$ for problem (36). The randomization method generally provides better error performance, however, it lacks a closed form solution. Later by simulations, we show that the deterministic eigenvector method in (37) is sufficiently close in performance to the GLRT solution in (23). Thus, the deterministic eigenvector method is used for this work. The estimates of the information symbols for the SDP-MSD are:

$$\hat{a}_{\text{SDP},i} = \hat{b}_{\text{SDP},i-1}\hat{b}_{\text{SDP},i}, \qquad \text{for} \quad i = 1, \cdots, M.$$

The SDP-MSD in (36)-(37) has the following properties:

Property 1. *To solve* (36)*, we adopt the interior-point methods [67, 35], which can find an optimal solution to* (36) *in* $\mathcal{O}((M+1)^{3.5}) \simeq \mathcal{O}(M^{3.5})$ *for a given accuracy.*

Property 2. *For the SDP problem in* (36)*, the optimal solution is independent of the diagonal elements of matrix* $\mathbf{Q}$ *[53].*

Property 3. *If the optimal solution* $\mathbf{X}^*$ *to* (36) *is a rank-1 matrix, the solution to* $\hat{b}_{\text{SDP},i}$ *in* (37) *is also the optimal GLRT solution to* (23)*.*

Note that Property 3 also holds for randomization methods with probability 1 [53].

4.2 Performance Analysis of the SDP-MSD

In this section, we derive a discrete-time model for the GLRT problem by representing the transmitted and received signals in discrete form. The discrete-time model provides insights to the detection process and helps quantify the performance of the SDP-MSD.

4.2.1 Discrete-Time Model for Performance Analysis

Following the work in [82, 66], the continuous-time received waveform $y_m(t)$ is represented as a series of discrete samples based on the Sampling Theorem. Starting from a single user case with a low-pass filter, given the time interval $[0, T_f]$, the signal $y_m(t)$ in (19) can be well approximated using $L = 2BT_f$ samples [82, 66] as

$$\begin{aligned} y_m(t) &= b_{mN_f} g(t) + \sigma\omega_m(t) \\ &\approx \sum_{n=0}^{L-1} (b_{mN_f} g_n + \sigma\omega_{m,n})\sqrt{2B}\mathrm{sinc}(2Bt - n), \end{aligned} \tag{38}$$

where $\mathrm{sinc}(x) = \frac{\sin(\pi x)}{\pi x}$, $\omega_m(t)$ is a band-limited AWGN process with two-sided power spectrum 1, $g_n = \frac{1}{\sqrt{2B}} g(\frac{n}{2B})$, $\omega_{m,n} = \frac{1}{\sqrt{2B}} w_m(\frac{n}{2B})$, and $\sigma^2 = \frac{N_0}{2N_f}$. It is easy to verify that $\omega_{m,n}$'s are i.i.d. Gaussian variables with zero mean and unit variance. Note that, although we obtain Eq. (38) for a low-pass process, it is shown in [82, 66] that a band-pass process is equivalent with respect to the decision statistics.

The frame energy and the correlation can be approximated by the discrete samples as [66]

$$\begin{aligned} E_f &= \int_0^{T_f} g^2(t)dt \\ &\approx \int_0^{T_f} \left(\sum_{n=0}^{L-1} g_n \sqrt{2B}\mathrm{sinc}(2Bt - n) \right)^2 dt \approx \|\mathbf{g}\|_2^2, \end{aligned} \tag{39}$$

and

$$\begin{aligned} Z_{i,j} &= \int_0^{T_f} y_i(t) y_j(t) dt \\ &\approx \int_0^{T_f} \left(\sum_{n=0}^{L-1} y_{i,n} \sqrt{2B} \text{sinc}(2Bt - n) \right) \\ &\qquad \times \left(\sum_{n=0}^{L-1} y_{j,n} \sqrt{2B} \text{sinc}(2Bt - n) \right) dt, \\ &\approx \mathbf{y}_i^T \mathbf{y}_j, \end{aligned} \tag{40}$$

where $\mathbf{y}_m = [y_{m,0}, y_{m,1}, \cdots, y_{m,L-1}]^T$ with $y_{m,n} = \frac{1}{\sqrt{2B}} y_m(\frac{n}{2B}) = b_{mN_f} g_n + \sigma \omega_{m,n}$ are the samples of the mth received symbol, $\mathbf{g} = [g_0, g_1, \cdots, g_{L-1}]^T$ is the sampled channel template, and $\boldsymbol{\omega}_m = [\omega_{m,0}, \omega_{m,1}, \cdots, \omega_{m,L-1}]^T$ is the sampled noise in the mth received symbol signal. In vector form,

$$\mathbf{y}_m = b_{mN_f} \mathbf{g} + \sigma \boldsymbol{\omega}_m. \tag{41}$$

With the approximated correlation in Eq. (40), the correlation matrix $\mathbf{Q}$ is constructed using the discrete-time signals. Without loss of generality, one may choose $\|\mathbf{g}\|_2^2 = 1$, which can be done by normalizing the received signal $y_m(t)$. The received SNR then becomes

$$\gamma = \frac{E_b}{N_0} = \frac{N_f E_f}{N_0} = \frac{1}{2\sigma^2}. \tag{42}$$

By collecting all samples of the received symbol waveforms $y_m(t), m = 0, \cdots, M$, an $L \times (M+1)$ discrete-time signal matrix can be defined as

$$\mathbf{Y} = [\mathbf{y}_0, \mathbf{y}_1, \mathbf{y}_2, \cdots, \mathbf{y}_M] = [b_0 \mathbf{g}, b_{N_f} \mathbf{g}, \cdots, b_{MN_f} \mathbf{g}] + \sigma \mathbf{W}, \tag{43}$$

where $\mathbf{W} = [\boldsymbol{\omega}_0, \boldsymbol{\omega}_1, \cdots, \boldsymbol{\omega}_M]$.

Now, define $\mathbf{P} = \mathbf{Y}^T \mathbf{Y}$. Since the (i,j)th element of $\mathbf{P}$ is $P_{i,j} = \mathbf{y}_{i-1}^T \mathbf{y}_{j-1} \approx Z_{i-1,j-1}$ according to Eq. (40), it is clear that $\mathbf{P}$ is an approximation of $\mathbf{Q}$ using the discrete samples with the exception of the diagonal elements. We previously proved that the optimal solution of (23) does not depend on the diagonal elements

of $\mathbf{Q}$, and thus by replacing matrix $\mathbf{Q}$ with matrix $\mathbf{P}$ in Eq. (23), the discrete-time approximation of the detection problem is obtained in the following form:

$$\begin{aligned} \max \mathcal{J}(\tilde{\mathbf{b}}) &= \tilde{\mathbf{b}}^T \mathbf{P} \tilde{\mathbf{b}} \\ &= \|\mathbf{Y}\tilde{\mathbf{b}}\|_2^2, \\ \text{s.t.} \quad \tilde{b}_i &\in \{+1, -1\}, \qquad \text{for} \quad i = 1, \cdots, M, \\ \tilde{b}_0 &= +1. \end{aligned} \tag{44}$$

To further modify the formation of $\mathbf{P}$ in Eq. (44), we construct a unitary matrix $\mathbf{G}$ as

$$\mathbf{G} = \begin{bmatrix} \mathbf{g} & \mathbf{G}^{\perp}_{L\times(L-1)} \end{bmatrix}_{L\times L}, \tag{45}$$

where the columns of $\mathbf{G}^{\perp}_{L\times(L-1)}$ are $(L-1)$ vectors in an orthonormal basis for the complementary space of $\mathbf{g}$ so that $\mathbf{G}^T\mathbf{G} = \mathbf{I}$. Left multiplying the transpose of the unitary matrix $\mathbf{G}$ to $\mathbf{Y}$ in (43) gives

$$\mathbf{G}^T\mathbf{Y} = \begin{bmatrix} \mathbf{b}^T \\ \mathbf{0}_{(L-1)\times(M+1)} \end{bmatrix} + \sigma\mathbf{U} = \begin{bmatrix} \mathbf{b}^T + \sigma\mathbf{u}_1^T \\ \sigma\mathbf{u}_2^T \\ \vdots \\ \sigma\mathbf{u}_L^T \end{bmatrix}, \tag{46}$$

where $\mathbf{b} = [b_0, b_{N_f}, \cdots, b_{MN_f}]^T$, $\mathbf{U}_{L\times(M+1)} = \mathbf{G}^T\mathbf{W}$, whose elements are still i.i.d. standard normal variables, and $\mathbf{u}_i^T$ represents the ith row of matrix $\mathbf{U}$. Since $\mathbf{P} = (\mathbf{G}^T\mathbf{Y})^T(\mathbf{G}^T\mathbf{Y})$, and plugging (46) into (44), we obtain the following optimization problem

$$\begin{aligned} \max \mathcal{J}(\tilde{\mathbf{b}}) &= \tilde{\mathbf{b}}^T(\mathbf{G}^T\mathbf{Y})^T(\mathbf{G}^T\mathbf{Y})\tilde{\mathbf{b}} \\ &= \tilde{\mathbf{b}}^T \left((\mathbf{b} + \sigma\mathbf{u}_1)(\mathbf{b}^T + \sigma\mathbf{u}_1^T) + \sigma^2 \sum_{l=2}^{L} \mathbf{u}_l\mathbf{u}_l^T \right) \tilde{\mathbf{b}}, \\ \text{s.t.} \quad \tilde{b}_i &\in \{+1, -1\}, \qquad \text{for} \quad i = 1, \cdots, M, \\ \tilde{b}_0 &= +1. \end{aligned} \tag{47}$$

There are several interesting comments that can be drawn by observing (47):

- In the absence of noise, $\mathbf{P} = \mathbf{b}\mathbf{b}^T$ is a rank-1 matrix, hence the modulated symbols $\mathbf{b}$ are equal to the sign of the eigenvector associated with the non-zero (largest) eigenvalue of matrix $\mathbf{P}$.

- In the presence of noise and $L = 1$, matrix $\mathbf{P}$ is still rank-1, and the principal eigenvector of $\mathbf{P}$ is distorted by an additive noise $\mathbf{u}_1$. In this case, the optimal solution for the modulated symbols is the quantized value of the eigenvector corresponding to the non-zero (largest) eigenvalue of matrix $\mathbf{P}$. Note that increasing the block size M will not alleviate the additive noise effect.

- When $L > 1$, matrix $\mathbf{P}$ is a rank-1 matrix $(\mathbf{b} + \sigma\mathbf{u}_1)(\mathbf{b}^T + \sigma\mathbf{u}_1^T)$ perturbed by a Wishart random matrix $\sigma^2 \sum_{l=2}^{L} \mathbf{u}_l \mathbf{u}_l^T$. If SNR is sufficiently high, the effect of the Wishart perturbation matrix can be ignored. However, because $L = 2BT_f$ is usually a large number for IR-UWB systems, in the low to moderate SNR regime, the Wishart perturbation term plays an important role to the system performance. Intuitively, the approximation of $(\mathbf{b} + \sigma\mathbf{u}_1)$ is obtained using the eigenvector corresponding to the largest eigenvalue of matrix $\mathbf{P}$. This forms the motivation of the second detector in Section 4.3.

- If the block size $M = 1$, the MSDD receiver reduces to the DD receiver as

$$\hat{a}_1 = \mathrm{sgn}(Z_{1,0}).$$

  Using the discrete version of $Z_{i,j}$ in Eq. (40), $Z_{1,0}$ is given as

$$Z_{1,0} = a_1 + b_0 \sigma \mathbf{g}^T \boldsymbol{\omega}_1 + b_{N_f} \sigma \boldsymbol{\omega}_0^T \mathbf{g} + \sigma^2 \boldsymbol{\omega}_1^T \boldsymbol{\omega}_0, \tag{48}$$

  where the last term in Eq. (48) is the sum of the products of two normal random variables, which can be approximated as a Gaussian variable for large L by invoking central limit theorem. As a result, $Z_{1,0}$ is approximated as a

normal distributed random variable with mean a_1 and variance $2\sigma^2 + L\sigma^4$. The BER is given as

$$P_{\mathrm{e}}^{\mathrm{DD}} \approx Q\left(\left[2\sigma^2 + L\sigma^4\right]^{-1/2}\right) = Q\left(\left[\frac{1}{\gamma} + \frac{L}{4\gamma^2}\right]^{-1/2}\right),$$

which is identical to the one in Eq. (20).

4.2.1.1 Performance Analysis of the SDP-MSD Based on Discrete-Time Model

This subsection develops a necessary and sufficient condition for the SDP-MSD to produce a rank-1 solution. An $M = 2$ example demonstrates the tightness of the SDP-MSD.

Proposition 1. *Given* $\mathbf{b}$*, the proposed SDP-MSD produces the rank-1 error-free solution if and only if the noise vectors* $[\mathbf{u}_1, \mathbf{u}_2, \cdots, \mathbf{u}_L]$ *are in the following set*

$$\mathcal{U}_{\mathbf{b}} = \left\{ [\mathbf{u}_1, \mathbf{u}_2, \cdots, \mathbf{u}_L] | \lambda_{\mathbf{A},\max} \leq \frac{(M+1)}{\sigma} \right\}, \tag{49}$$

where

$$\begin{aligned} \mathbf{A} = \mathbf{u}_1\mathbf{b}^T + \mathbf{b}\mathbf{u}_1^T + \sigma\sum_{l=1}^{L} \mathbf{u}_l\mathbf{u}_l^T \\ - \mathrm{Diag}(\mathbf{b})\mathrm{Diag}\left(\left(\mathbf{u}_1\mathbf{b}^T + \mathbf{b}\mathbf{u}_1^T + \sigma\sum_{l=1}^{L} \mathbf{u}_l\mathbf{u}_l^T\right)\mathbf{b}\right), \end{aligned} \tag{50}$$

$\mathrm{Diag}(\mathbf{z})$ *returns a diagonal matrix with* $\mathbf{z}$ *on its main diagonal, and* $\lambda_{\mathbf{A},\max}$ *is the largest eigenvalue of matrix* $\mathbf{A}$*.*

Proof: See Appendix A.

To help clarify Proposition 1, the following remarks are provided.

- Based on Property 3 of SDP-MSD, if the proposed MSD produces a rank-1 solution, it is optimal. However, the eigenvector associated with the largest eigenvalue of the higher-rank solutions $\mathbf{X}^*$ from SDP-MSD may also yield the optimal GLRT solution with a high probability. Later, simulations confirm this claim.

- Note that matrix $\mathbf{A}$ can be rewritten as

$$\begin{aligned}\mathbf{A} &= \mathbf{u}_1\mathbf{b}^T + \mathbf{b}\mathbf{u}_1^T - \text{Diag}(\mathbf{b})\text{Diag}\left(\left(\mathbf{u}_1\mathbf{b}^T + \mathbf{b}\mathbf{u}_1^T\right)\mathbf{b}\right) \\ &\quad + \sigma\left(\sum_{l=1}^{L}\mathbf{u}_l\mathbf{u}_l^T - \text{Diag}(\mathbf{b})\text{Diag}\left(\left(\sum_{l=1}^{L}\mathbf{u}_l\mathbf{u}_l^T\right)\mathbf{b}\right)\right) \\ &= \mathbf{B} + \sigma\mathbf{C}. \end{aligned} \tag{51}$$

Because of the fact that $\sigma\lambda_{\mathbf{A},\max} \leq \sigma\lambda_{\mathbf{B},\max} + \sigma^2\lambda_{\mathbf{C},\max}$, there exists an upper bound of $\sigma\lambda_{\mathbf{A},\max}$, which is at least linearly decreasing as σ decreases and SNR > 0.5 for the given $\lambda_{\mathbf{B},\max}$ and $\lambda_{\mathbf{C},\max}$. Hence, the rank-1 condition holds with a high probability at high SNR. As SNR goes to infinity, we have

$$\lim_{\sigma\to 0^+} \text{P}\left\{\lambda_{\mathbf{A},\max} \leq \frac{(M+1)}{\sigma}\right\} = 1. \tag{52}$$

To illustrate that the condition in Proposition 1 is satisfied with a high probability at high SNR, Fig. 7 displays the histograms of the largest eigenvalues of $\frac{\sigma\mathbf{A}}{M+1}$ with block size $M = 5$ and SNR $= 5, 10, 15$ dB. When SNR is low (5 dB), the largest eigenvalue of $\frac{\sigma\mathbf{A}}{M+1}$ is usually a large number as a result of the high level of noise and the detector may give an error with a high probability. As the SNR increases, the largest eigenvalue of $\frac{\sigma\mathbf{A}}{M+1}$ decreases rapidly and when SNR $= 15$ dB, the condition defined in Proposition 1 holds with a high probability.

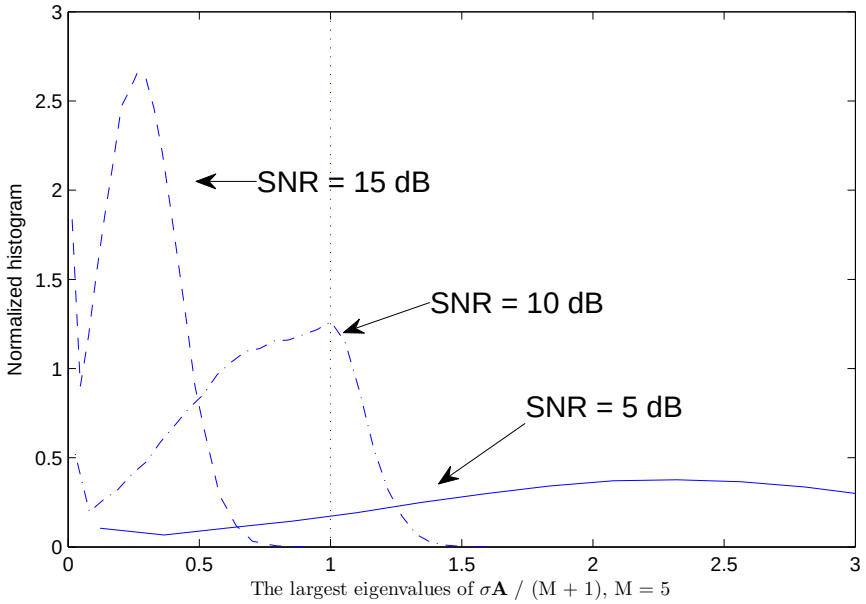

Figure 7: Histograms of the largest eigenvalues of $\sigma\mathbf{A}/(M+1)$ for $M = 5$ with SNR $= 5, 10, 15$ dB.

- The condition in (49) only relies on the distribution of the largest eigenvalue of the random matrix $\mathbf{A}$. As a result, in the case of MAI, the SDP-MSD can still obtain a rank-1 error-free solution if the noise space caused by MAI satisfies (49). The near-optimal performance of SDP-MSD in the presence of MAI will be verified via simulations in Section 4.4.3.

4.3 Modified Unconstrained Relaxation MSD

In this section, an alternative low-complexity MSD [104] is presented, which achieves near-optimal performance with a closed form. First of all, matrix $\mathbf{Q}$ has the following property:

Property 4. $\mathbf{Q}$ *is an indefinite matrix with probability one.*

Proof: See Appendix B.

To derive the modified unconstrained relaxation (MUR) MSD, we first modify the matrix $\mathbf{Q}$ to negative semi-definite and find the optimal solution without binary

constraints:

$$\begin{aligned} \max \quad & \mathcal{J}_{\mathrm{MUR}}(\mathbf{x}) = \mathbf{x}^T \mathbf{Q}' \mathbf{x} \\ \text{s.t.} \quad & x_0 = 1, \quad \mathbf{x} \in \mathbb{R}^{(M+1)}, \end{aligned} \tag{53}$$

where a constant is added to each of the diagonal elements of $\mathbf{Q}$ such that $\mathbf{Q}' = \mathbf{Q} - d\mathbf{I}$ by choosing $d = \lambda_{\mathbf{Q},\max}$, which is the largest eigenvalue of $\mathbf{Q}$. Since $\mathbf{Q}'$ is negative semi-definite, the solution to (53) is

$$\hat{x}_{\mathrm{MUR},i} = v_i / v_0, \qquad \text{for} \quad i = 0, \cdots, M. \tag{54}$$

where $\mathbf{v} = [v_0, v_1, \cdots, v_M]^T$ is the eigenvector corresponding to the largest eigenvalue of matrix $\mathbf{Q}$.

The estimates of the modulated symbol $\mathbf{b}$ and the information symbol $\mathbf{a}$ are given as

$$\hat{b}_{\mathrm{MUR},i} = \mathrm{sgn}(\hat{x}_{\mathrm{MUR},i}), \qquad \text{for} \quad i = 0, \cdots, M, \tag{55}$$

and

$$\hat{a}_{\mathrm{MUR},i} = \hat{b}_{\mathrm{MUR},i-1} \hat{b}_{\mathrm{MUR},i}, \qquad \text{for} \quad i = 1, \cdots, M. \tag{56}$$

Observations for MUR-MSD in (54)-(56) are given as follows.

- Unlike the GLRT problem in (23) and the SDP problem in (36), the optimal solution to the MUR problem in (53) generally relies on the diagonal elements of matrix $\mathbf{Q}$. Thus, the solution to (53) is not equivalent to the one for (23) or (36). As d gets smaller, the MUR problem in (53) becomes similar to the GLRT problem in (23). For simplicity, to make $\mathbf{Q}'$ negative semi-definite, in this proposal, we choose d as $\lambda_{\mathbf{Q},\max}$.

- For the computational complexity of the MUR-MSD, the modern eigendecomposition algorithm is used to evaluate the largest eigenvalue and its eigenvector of matrix $\mathbf{P}$ on the order of $\mathcal{O}((M+1)^3) \simeq \mathcal{O}(M^3)$. Hence, we would expect

that the MUR-MSD requires lower computational complexity than the SDP-MSD especially for large M.

- The unconstrained relaxation step is similar to the decorrelator adopted for code division multiple access (CDMA) and zero-forcing detectors for multi-input multi-output and/or orthogonal frequency division multiplexing (OFDM) systems [52, 65, 85]. By choosing $d = \lambda_{\mathbf{Q},\max}$, the MUR step is equivalent to the sphere constrained relaxation

$$\begin{aligned} \max \quad & \mathcal{J}_{\mathrm{MUR}}(\mathbf{x}) = \mathbf{x}^T\mathbf{Q}\mathbf{x} \\ \text{s.t.} \quad & \|\mathbf{x}\|_2^2 = M+1. \end{aligned} \tag{57}$$

  Since $\mathbf{Q}$ has at least one positive eigenvalue, the sphere constrained relaxation is also equivalent to the ball constrained relaxation adopted in [79, 99]

$$\begin{aligned} \max \quad & \mathcal{J}_{\mathrm{MUR}}(\mathbf{x}) = \mathbf{x}^T\mathbf{Q}\mathbf{x} \\ \text{s.t.} \quad & \|\mathbf{x}\|_2^2 \leq M+1. \end{aligned} \tag{58}$$

  However, our problem and approach are different from the existing approaches in two main aspects: *i*) Matrix $\mathbf{Q}$ in (23) is generally indefinite, and directly applying methods in [79, 99, 78, 52, 65, 85] yield non-convex optimization problems; and *ii*) matrix $\mathbf{Q}$ has a special structure – a rank-1 perturbed matrix as shown in Sec. 4.2. Since the eigenvector of the perturbed rank-1 matrix is still close to the one without perturbation with a high probability, our MUR approach reaches near-optimal performance while the detectors in [79, 99, 78, 52, 65, 85] can only achieve inferior performance relative to their optimal ones in CDMA or OFDM systems.

- The following proposition establishes the relation between the MUR-MSD and the SDP-MSD.

Proposition 2. *The MUR problem* (53) *is a relaxation of the SDP problem* (36).

Proof: See [53, Theorem 1].

Hence, the SDP-MSD yields a tighter approximation of the GLRT solution than the MUR-MSD, and thus we expect that the SDP-MSD performs favorably compared to the MUR-MSD in terms of BER. This claim is verified via simulations in Section 4.4.

4.4 Numerical Results

In this section, the performance of the proposed MUR-MSD and SDP-MSD, and the optimal MSD for UWB communications is demonstrated using Monte-Carlo simulations. The system is simulated based on continuous-time signals and subsequently validates discrete-time approximation by comparisons. BER performance for different detectors with different block sizes M is compared for the single user case. Next, the performance of the proposed detectors is considered in the presence of MAI. In the last sub-section, the complexity comparisons of the proposed detectors with the existing ones is conducted. In the simulation figures, SNR is defined as in Eq. (42).

4.4.1 Comparison of Continuous-Time and Discrete-Time Detection Models

For the continuous-time signal, the transmitted pulse $p(t)$ is the second derivative of a Gaussian pulse with duration $T_p = 1.0$ ns. We adopt the CM1 channel model described in [25] with $T_f = 80$ ns and $B = 2.5$ GHz. To simulate the continuous-time signal, we employ an 8 times oversampling, which equates to 3200 samples per frame. For the discrete-time model, there are 400 samples per symbol (Nyquist sampling rate). The single user case is considered, where $N_c = 1$.

Fig. 8 shows the performance comparisons of the discrete-time and continuous-time models with the optimal MSD. Clearly, the optimal MSD yields almost the same

performance for the continuous-time and discrete-time models. The comparison results of the SDP-MSD and the MUR-MSD have similar characteristics, which are not shown here. These results confirm that the discrete-time model is a close approximation to the continuous-time signal. Therefore, it is valid and convenient to analyze the performance based on the discrete-time model.

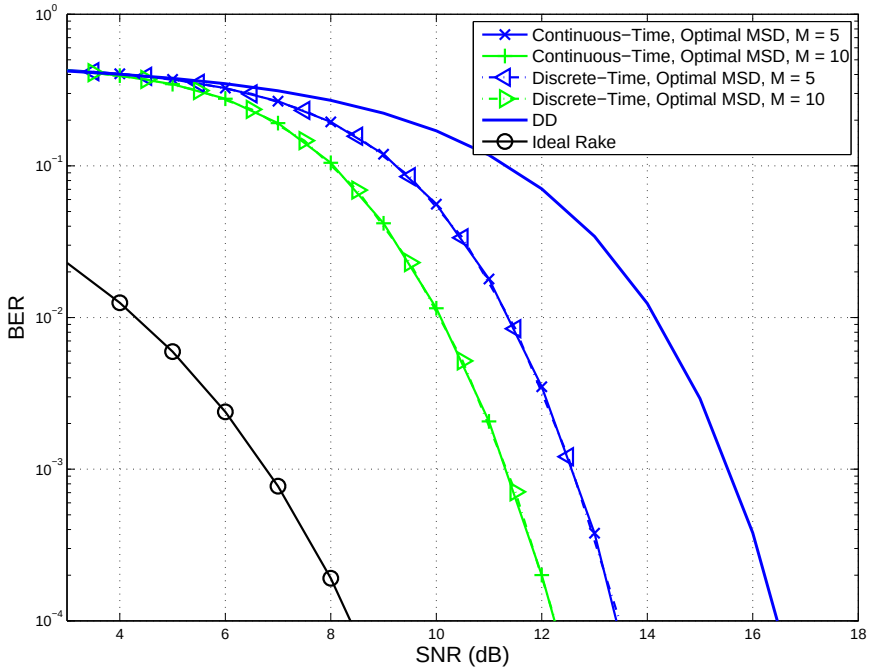

Figure 8: Performance of the optimal MSD for the continuous-time and discrete-time models with block sizes $M = 5, 10$.

4.4.2 BER Performance of Different Detectors

The BER performance for the optimal MSD (23), the SDP-MSD, and the MUR-MSD is compared over different block sizes M. The discrete-time detection model is used, where the twice time-bandwidth product $L = 400$.

Figs. 9 and 10 depict the BER results with different block sizes $M = 2, 5, 10, 20, 30, 100$ for the SDP-MSD and the MUR-MSD, respectively. Compared to the optimal performance obtained using the SDA in [50], the performance of the SDP-MSD is almost the same (with a negligible gap) for all SNR range when $M = 2, 5, 10, 20, 30$, respectively. Hence, the semi-definite relaxation on the GLRT problem can yield a very tight approximation. The MUR-MSD achieves a close result to that of the GLRT with an about 0.1 dB loss for $M = 5$ and a 0.2 dB loss for $M = 10, 20, 30$. Also as SNR increases, the gap between the MUR-MSD and the optimal GLRT detector decreases.

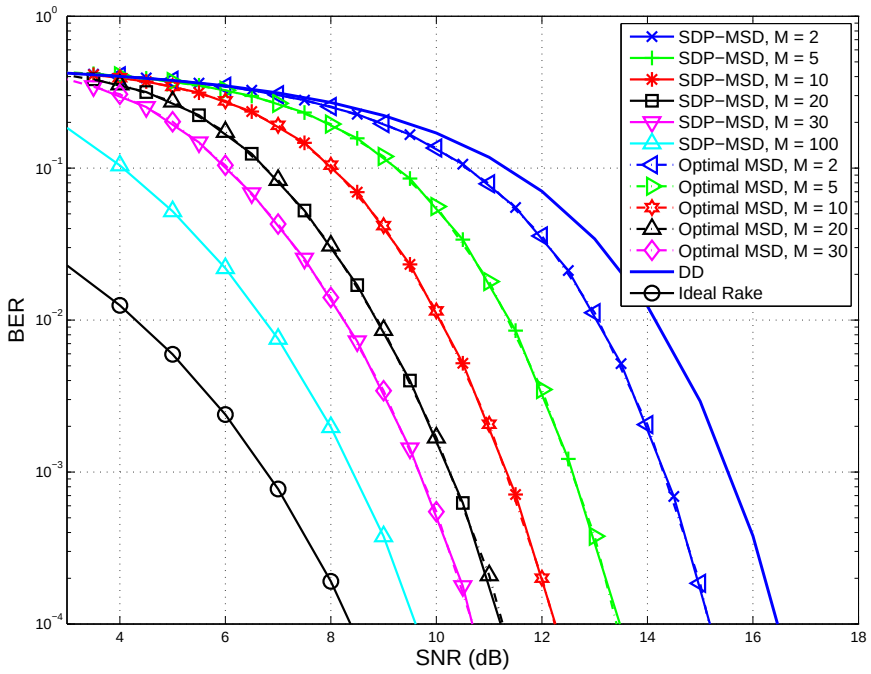

Figure 9: BER comparisons of the SDP-MSD and the optimal MSD for different block sizes M with $L = 400$.

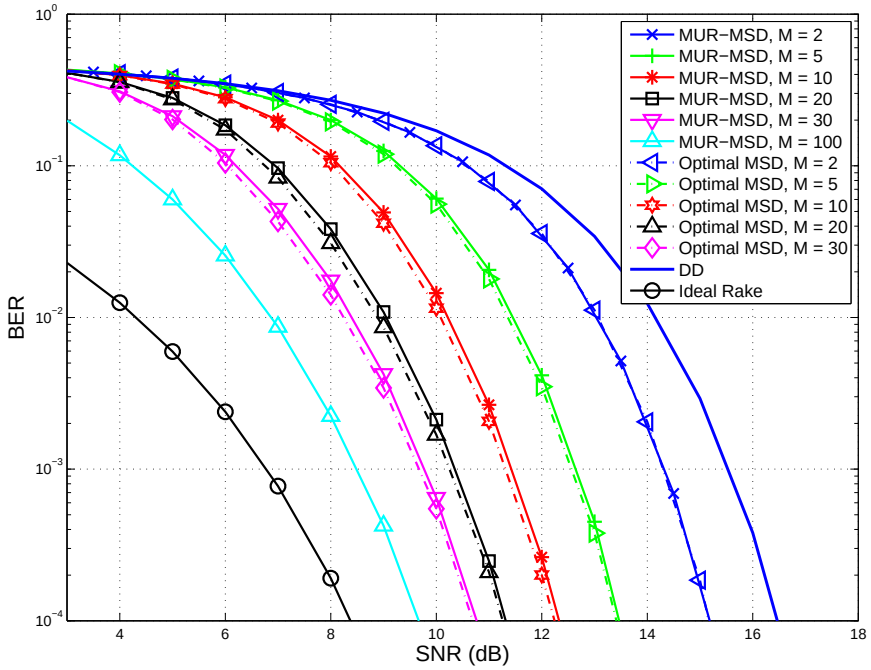

Figure 10: BER comparisons of the MUR-MSD and the optimal MSD for different block sizes M with $L = 400$.

The superior performance of the SDP-MSD to that of the MUR-MSD in Proposition 2 is also confirmed. However, both detectors (the MUR-MSD and the SDP-MSD) enjoy polynomial computational complexity, while the optimal MSD (through exhaustive search or SDA [50]) require exponential complexity in terms of block size [42].

Furthermore, compared to the performance of the DD [19], the proposed methods obtain an about 3 dB gain in the case of $M = 5$ and an about 4 dB gain if $M = 10$ at BER $= 10^{-4}$. The BER performance improves when the block size grows while the rate of improvement decelerates (an about 5.4 dB gain for $M = 30$). In addition, in the case of very large block size M ($M = 100$), where the SDA and the VA are infeasible, the proposed detectors are still practical. The performance closely approaches that of the ideal Rake receiver, especially in high SNR regime, where the gap is less than 1.5 dB.

4.4.3 BER Performance with MAI

In this sub-section, performance is evaluated for the proposed detectors in the presence of MAI with CM1 channel. The frame repetition factor is $N_f = 20$ and $T_f = 80$ ns. In the case of MAI, the chip interval is $T_c = 1.0$ ns, and the TH codes c_j are randomly selected from the range $[0, N_c - 1]$ where $N_c = 91$. For simplicity, we assume that the received energy for each interfering user is equal.

Fig. 11 illustrates the BER performance of the SDP-MSD, the MUR-MSD, the optimal MSD with the SDA, and the sbDF-DD [72] in the presence of MAI. When the number of users N_u is 50, both proposed detectors show significant robustness in the present of MAI. The SDP-MSD has an about 1.5 dB loss relative to the single user case but retains near-optimal performance compared to the optimal MSD. The MUR-MSD detector is slightly worse than SDP-MSD. This matches with our analysis since the MUR-MSD is a relaxation of the SDP-MSD, and the SDP-MSD should statistically perform better than that of the MUR-MSD. When $N_u = 150$, with the stringent MAI, the strong robustness of the proposed SDP-MSD and MUR-MSD is demonstrated, and the performance loss to the single user case is approximately 6.5 dB at BER = 10^{-5}. The sbDF-DD exhibits inferior performance to the SDP-MSD and the MUR-MSD. When $N_u = 50$, the gap between the sbDF-DD and the proposed detectors is about 1 dB at BER = 10^{-5}, and the gap increases as N_u increases, where the sbDF-DD has an approximately 2.5 dB performance degradation at BER = 10^{-5} when $N_u = 150$.

4.4.4 Complexity Comparisons of Different Detectors

Fig. 12 compares the average and the 1% upper percentile CPU computational time for the detectors. When the block size M is small (e.g., $M < 10$), the SDA, the MUR-MSD, and the sbDF-DD requires less complexity than that of the SDP-MSD. However, when the high performance MSD is of interest and the block size M is large,

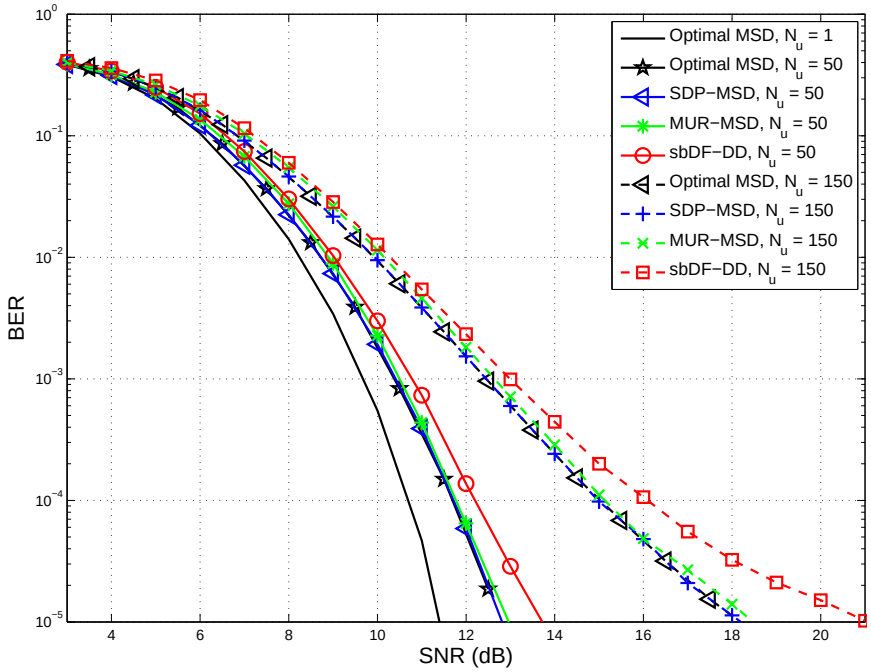

Figure 11: BER comparisons of the detectors with $M = 30$, $L = 400$, MAI, and CM1 channel.

the advantages of the SDP-MSD and the MUR-MSD in term of complexity are clear, and the exponential complexity of the SDA can be observed. In particular, the SDA with low SNR (SNR = 5 dB) requires much higher complexity than the SDA with high SNR (SNR = 10 dB), while the complexity of the MUR-MSD and the SDP-MSD generally does not rely on SNR. The sbDF-DD has the lowest complexity at the price of inferior error performance. We also conduct the comparisons of the 1% upper percentile complexity for all detectors except the sbDF-DD, which has fixed complexity given M. The results indicate that the worst-case complexity of the SDA is much higher than the average complexity, and there is no big difference between the worst-case complexity and the average complexity for the SDP-MSD and the MUR-MSD.

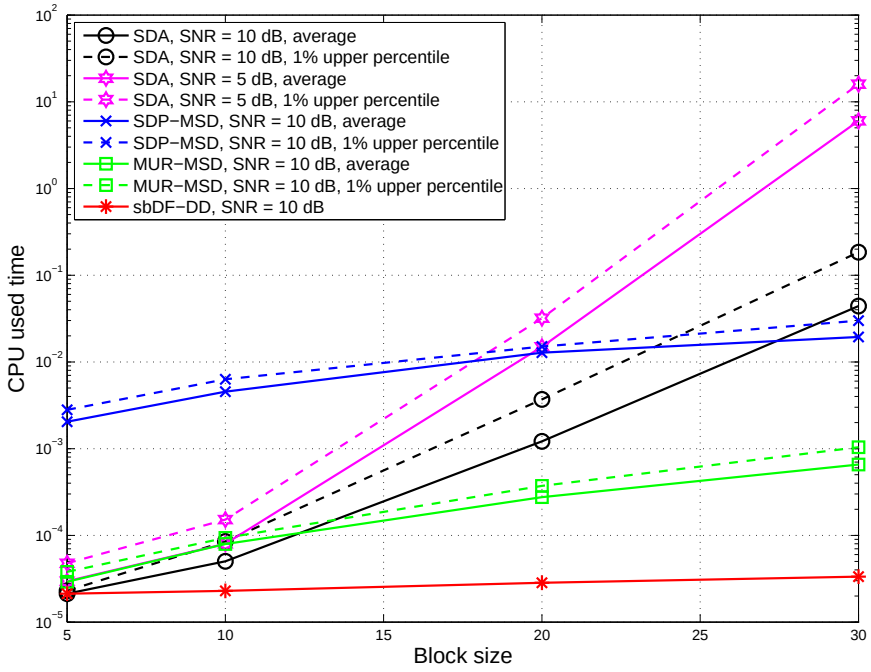

Figure 12: Complexity comparisons of the detectors.

CHAPTER V

SOFT-INPUT SOFT-OUTPUT MULTI-SYMBOL DIFFERENTIAL DETECTION FOR UWB COMMUNICATIONS

To further enhance the system performance, FEC codes, e.g. Turbo codes [7] and low-density parity check codes (LDPC) [28], are considered in most communication systems including UWB communications. However, most existing decoding schemes are combined with coherent detectors [40, 76], where a trellis-coded modulation scheme that is compatible for both coherent and TR receivers is proposed in [76], which uses a coherent receiver to resolve the extra parity information that is carried in the reference pulses of the TR signaling. Some soft-output MSDD methods are proposed in [71, 73], which combine FEC codes with MSDD noncoherent detector.

In this chapter, the performance of the MSD will be further improved by exploiting joint MSDD and FEC code decoding. The system diagram of a coded UWB transmission is depicted in Fig. 13. The soft-input soft-output (SISO) MSDD is developed to deliver *a posteriori* information, and a modified list sphere decoding (LSD) is used to generate a list of soft candidates and to alleviate the high complexity of evaluating exact soft information. Compared to the soft-output MSDD in [71, 73], the proposed SISO MSDD enables iterative processing between the SISO MSDD and the SISO channel decoder. Simulations are conducted to show that significant BER performance improvement can be achieved by the iterative processing.

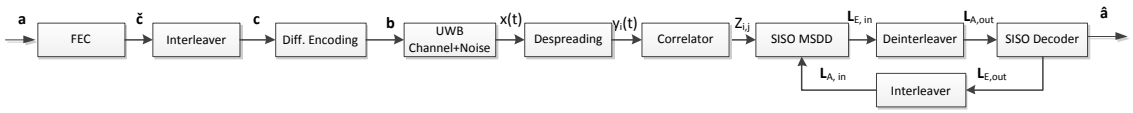

Figure 13: System diagram of the coded MSDD for UWB communications.

5.1 Log-Likelihood Metric for MSDD

As shown in [73, 66, 101], in the absence of IFI and with sufficiently large time-bandwidth product $T_rW = T_fW$, the correlations $Z_{i,j}$ in Eq. (18) can be well approximated as i.i.d. Gaussian variables with mean $\prod_{k=i+1}^{j} c_k E_f$ and variance $\sigma^2 = N_0E_f/N_f + WT_fN_0^2/(2N_f^2)$, where c_k's are the symbols after FEC code encoding and we assume $T_r = T_f$ in this chapterp. Therefore, the log-likelihood metric of the candidate symbols $\tilde{\mathbf{c}}$ given the correlations $Z_{i,j}$ is

$$\begin{aligned}\Gamma(\tilde{\mathbf{c}}) &= \ln p(\mathbf{Q}|\tilde{\mathbf{c}}) \\ &= C + \frac{E_f\Lambda(\tilde{\mathbf{c}})}{\sigma^2},\end{aligned} \tag{59}$$

where $\mathbf{Q}$ is an $(M+1)\times(M+1)$ matrix with the (i,j)th entry being $Z_{i-1,j-1}$ in (23), C is a constant that is irrelevant to the SISO detector, $p(\mathbf{Q}|\tilde{\mathbf{c}})$ is the likelihood metric of $\tilde{\mathbf{c}}$ given $\mathbf{Q}$, and

$$\Lambda(\tilde{\mathbf{c}}) = \sum_{i=0}^{M-1}\sum_{j=i+1}^{M} Z_{i,j}\prod_{k=i+1}^{j}\tilde{c}_k. \tag{60}$$

Thus, the hard-output MSDD becomes

$$\hat{\mathbf{c}} = \arg\max_{\tilde{\mathbf{c}}\in\{\pm1\}^M}\Gamma(\tilde{\mathbf{c}}) = \arg\max_{\tilde{\mathbf{c}}\in\{\pm1\}^M}\Lambda(\tilde{\mathbf{c}}), \tag{61}$$

which is identical to that based on GLRT rule in Eq. (23), where $b_{iN_f} = c_i b_{(i-1)N_f}$.

5.2 Soft-Input Soft-Output MSDD

Given the soft information (*a priori* information) $\mathbf{L}_{A,\text{in}}$ for the coded symbols $\mathbf{c}$, the extrinsic information of the ith coded symbol is (cf. [36, Eq. (7)])

$$L_{E,\text{in}}(c_i) = \ln\frac{\sum_{\tilde{\mathbf{c}}\in\mathbb{C}_{i,+1}} p(\mathbf{Q}|\tilde{\mathbf{c}})\exp\left(\frac{1}{2}(\tilde{\mathbf{c}}^T\mathbf{L}_{A,\text{in}} - L_{A,\text{in}}(c_i))\right)}{\sum_{\tilde{\mathbf{c}}\in\mathbb{C}_{i,-1}} p(\mathbf{Q}|\tilde{\mathbf{c}})\exp\left(\frac{1}{2}(\tilde{\mathbf{c}}^T\mathbf{L}_{A,\text{in}} + L_{A,\text{in}}(c_i))\right)}, \tag{62}$$

where $\mathbb{C}_{i,\pm 1} = \{\mathbf{c} | \forall \mathbf{c}, c_i = \pm 1\}$, containing all possible realizations of the coded symbols $\mathbf{c}$ with $c_i = +1$ or $c_i = -1$, respectively. The soft information $\mathbf{L}_{A,\text{in}}$ is initialized as a zero vector and is updated to the extrinsic information from the outer SISO decoder in each iteration [36].

With the max-log approximation, the extrinsic information can be simplified as (cf. [36, Eq. (12)])

$$\begin{aligned} L_{E,\text{in}}(c_i) \approx & \max_{\tilde{\mathbf{c}} \in \mathbb{C}_{i,+1}} \{\Gamma(\tilde{\mathbf{c}}) + \frac{1}{2}(\tilde{\mathbf{c}}^T \mathbf{L}_{A,\text{in}} - L_{A,\text{in}}(c_i))\} \\ & - \max_{\tilde{\mathbf{c}} \in \mathbb{C}_{i,-1}} \{\Gamma(\tilde{\mathbf{c}}) + \frac{1}{2}(\tilde{\mathbf{c}}^T \mathbf{L}_{A,\text{in}} + L_{A,\text{in}}(c_i))\}, \end{aligned} \tag{63}$$

where $\Gamma(\tilde{\mathbf{c}})$ is the log-likelihood metric defined in Eq. (59). Note that constant C in Eq. (59) is canceled in (63) while the information of E_f and σ^2 is still required. To further simplify the SISO detection without acquiring the information of E_f and σ^2, we ignore these scale terms and approximate Eq. (63) as

$$\begin{aligned} L_{E,\text{in}}(c_i) \approx & \max_{\tilde{\mathbf{c}} \in \mathbb{C}_{i,+1}} \{\Lambda(\tilde{\mathbf{c}}) + \frac{1}{2}(\tilde{\mathbf{c}}^T \mathbf{L}_{A,\text{in}} - L_{A,\text{in}}(c_i))\} \\ & - \max_{\tilde{\mathbf{c}} \in \mathbb{C}_{i,-1}} \{\Lambda(\tilde{\mathbf{c}}) + \frac{1}{2}(\tilde{\mathbf{c}}^T \mathbf{L}_{A,\text{in}} + L_{A,\text{in}}(c_i))\}. \end{aligned} \tag{64}$$

Although the approximation in Eq. (64) results in some performance degradation, studies in [96] show that the max-log turbo decoding without SNR information leads to a negligible performance loss compared to the exact log-MAP turbo decoding, especially for high SNR. Thus, the scale-invariant max-log turbo decoder that does not require the knowledge about signal-to-noise ratio (SNR) is then exploited as the SISO channel decoder in this section.

5.2.1 Modified List Sphere Decoding

One issue of evaluating Eq. (64) is that the cardinality of the candidate sets $\mathbb{C}_{i,\pm 1}$ grows exponentially when the MSDD block size M increases. Therefore, if M is large, it is computationally prohibited to evaluate the exact extrinsic metric in Eq. (64) over

all possible coded symbol candidates. To alleviate this issue, we employ a modified list sphere decoding (LSD) [36] that generates $N_c, N_c \ll 2^M$ candidates $\mathbb{L}$ with the top N_c highest metrics. The modified LSD reformulates the metric function to a cost function as

$$\Upsilon(\tilde{\mathbf{c}}) = \sum_{i=0}^{M-1} \sum_{j=i+1}^{M} \left(|Z_{i,j}| - Z_{i,j} \prod_{k=i+1}^{j} \tilde{c}_k \right). \tag{65}$$

Since the terms in the double summation in Eq. (65) are non-negative, the modified LSD performs depth-first search from $\tilde{c}_M$ to $\tilde{c}_1$ and finds all candidate symbols within a radius δ. Similar to the sphere decoding algorithm in [50], during the search, the modified LSD eliminates the paths with partial candidates $[\tilde{c}_l, \cdots, \tilde{c}_M]^T$ if the cost of the path exceeds the radius, i.e.,

$$\sum_{i=l-1}^{M-1} \sum_{j=i+1}^{M} \left(|Z_{i,j}| - Z_{i,j} \prod_{k=i+1}^{j} \tilde{c}_k \right) > \delta.$$

However, compared to the SDA in [50], the modified LSD here uses a different update rule for δ. When a candidate symbol vector $\tilde{\mathbf{c}}$ is found within the radius, $\tilde{\mathbf{c}}$ is added to the set $\mathbb{L}$. If the cardinality of $\mathbb{L}$ exceeds N_c, then the modified LSD removes the candidate symbol vector in $\mathbb{L}$ that has the largest cost. After $\mathbb{L}$ is updated, if the cardinality of $\mathbb{L}$ equals N_c, then the radius is changed to the largest cost for all candidate symbol vectors in $\mathbb{L}$.

Once the modified LSD obtains $\mathbb{L}$, the SISO MSDD evaluates the extrinsic metric over the subset $\mathbb{L}$ with reduced complexity.

5.3 Numerical Results

In this section, we demonstrate the BER performance of iterative decoding and detection with SISO MSDD. The transmitted pulse $p(t)$ is the normalized second derivative of a Gaussian function with $T_p = 1$ns. The number of frames is $N_f = 20$ and $T_f = 60$ns. We adopt CM1 channel in [25], and a 2.5 GHz baseband filter is employed at the receiver. SNR is defined as $E_f N_f/(RN_0)$. The block size of the information

bits is $N = 9000$. The FEC code encoder is a rate 1/2 parallel concatenated turbo encoder with feedback polynomial 7_8 and feedforward polynomial 6_8. For each MSDD block, our simulations show that 6 iterations within the outer SISO turbo decoder and 6 iterations between the inner SISO MSDD and the outer decoder are sufficient to generate converged performance, and thus are adopted.

Fig. 14 illustrates the performance comparisons of the uncoded MSDD and the coded MSDD with different block sizes M. It is clear to see that significant performance gain is achieved by using iterative processing with powerful codes. When $M = 2$ and 5, coded MSDD obtains about 3.5 dB gain over uncoded MSDD at BER $= 10^{-5}$. Simulation with $M = 20$ is performed, where the LSD with $N_c = 1024$ candidates is used to obtain a subset of coded symbol candidates. Performance gain becomes larger when the MSDD block size M increases, where for the case that $M = 20$, the coded MSDD outperforms the uncoded one with about 4.5 dB by using only $1024/2^{20} \approx 0.1\%$ candidates of the overall candidate set.

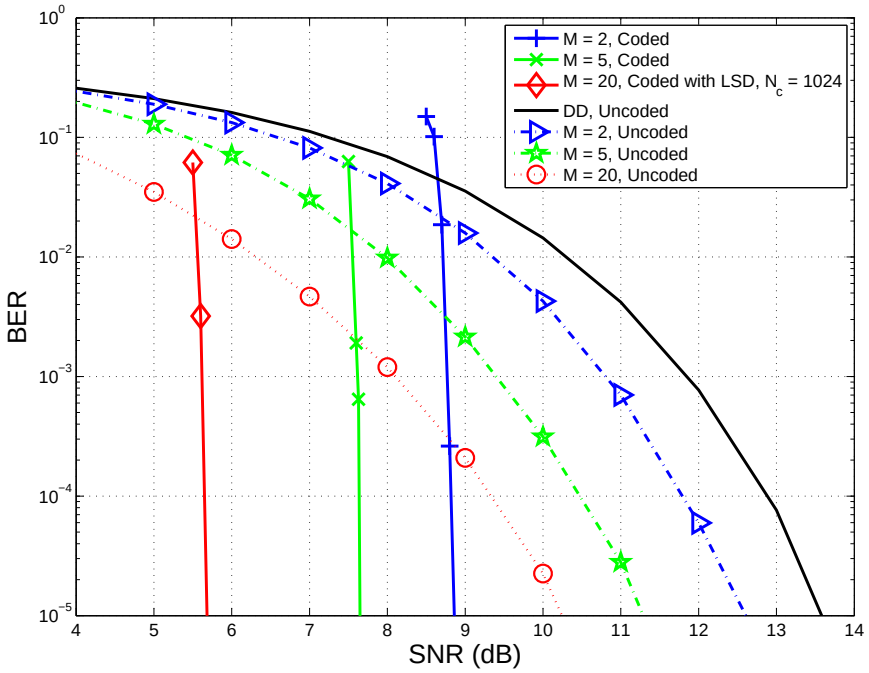

Figure 14: BER comparisons of coded MSDD and uncoded MSDD for different block sizes M.

Fig. 15 depicts the performance comparisons of coded MSDD with $M = 5$ and different numbers of inner iterations between detection and decoding. When the number of inner iteration is 1, the SISO MSDD degenerates to the soft-output MSDD since the SISO MSDD obtains no extrinsic information from the outer turbo decoder. In this case, the coded MSDD with 1 inner iteration exhibits about 0.6 dB loss relative to that with 6 inner iterations. In addition, one can observe that the performance of coded MSDD with 5 iterations is very close to that with 6 iterations, indicating that 6 iterations between the inner SISO MSDD and the outer SISO turbo decoder are sufficient to generate converged error performance.

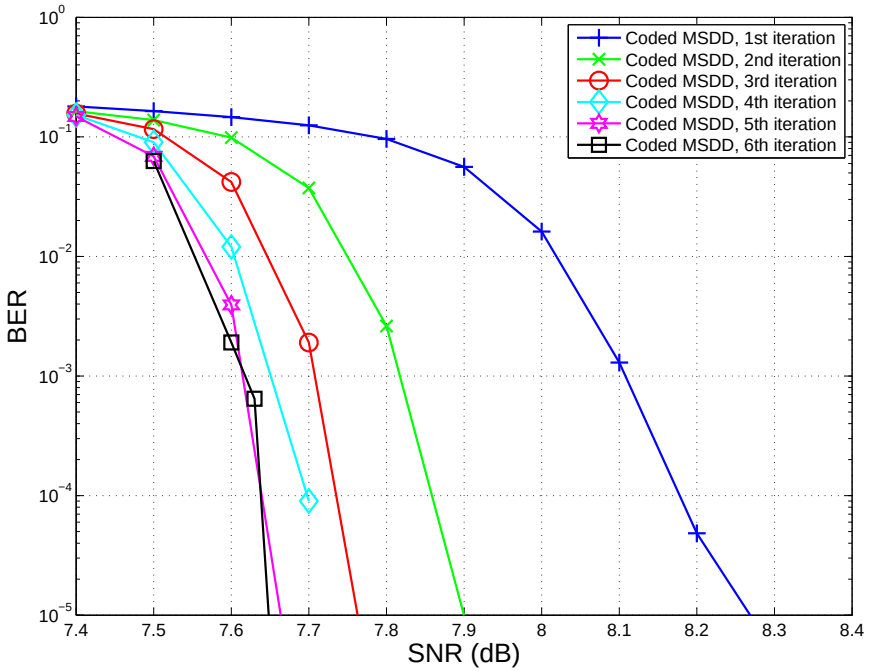

Figure 15: BER comparisons of coded MSDD with $M = 5$ and different numbers of iterations between detection and decoding.

Fig. 16 demonstrates the performance comparisons of the proposed SISO MSDD and the hard-output MSDD. First, compared to the results of the uncoded MSDD in Fig. 14, the coded hard-output MSDD using the powerful turbo decoding gains about 2 dB for $M = 2, 5$ and about 3 dB for $M = 20$ at BER $= 10^{-5}$. Next, the proposed SISO MSDD significantly improves the performance of the hard-output one, and the

gain is about 1.4 dB for different M at BER $= 10^{-5}$.

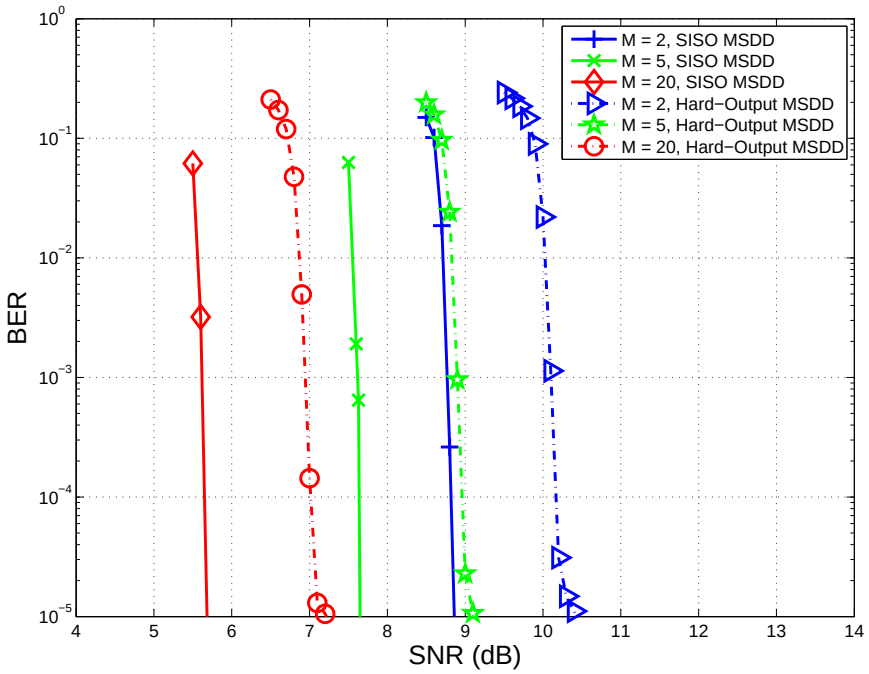

Figure 16: BER comparisons of SISO MSDD and hard-output MSDD for different block sizes M.

Fig. 17 compares the performance of the proposed SISO MSDD and the soft-output MSDD in [71]. Both schemes adopt a rate 1/2 convolution code (CC) with generator polynomial $(133_8, 171_8)$ and 3 iterations between CC decoder and inner SISO MSDD are performed for our proposed method. Compared to the results using turbo codes in Fig. 15, the gain of the proposed SISO MSDD over soft-output MSDD using CC is clearer. When $M = 2$, the SISO MSDD obtains about 0.8 dB gain over the soft output one, and when $M = 5, 20$, the gain of the SISO MSDD over the soft output one increases to about 1.5 dB.

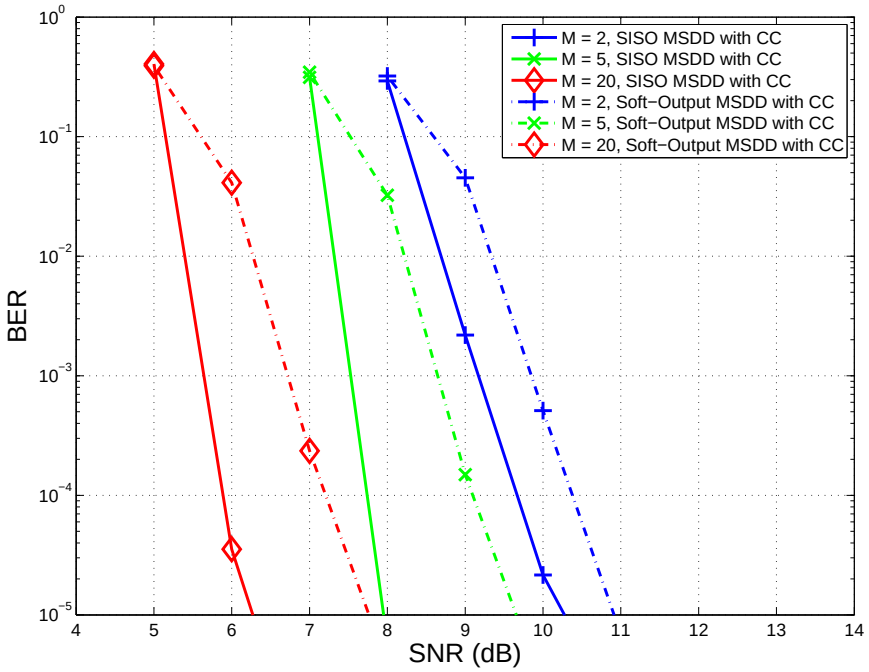

Figure 17: BER comparisons of SISO MSDD and soft-output MSDD for different block sizes M with convolution code.

CHAPTER VI

RECEIVER DESIGNS FOR DIFFERENTIAL UWB SYSTEMS WITH MULTIPLE ACCESS INTERFERENCE

6.1 Introduction

When considering TR systems in a multi-user environment, most of the existing differential UWB receivers (e.g., DTR, DD, and MSDD receivers) [94, 15, 19, 33, 50] employ Gaussian approximation to multiple access interference (MAI). However, in recent literature [6, 5, 75, 56], the results for time-hopping impulse-radio (TH-IR) UWB systems with Rake reception suggest the inaccuracy of Gaussian approximation to impulsive MAI when a small number of active users emit strong interference. In [5], the non-Gaussian distributed MAI is studied by simulations, and a soft-limiting (SL) receiver is proposed, which is optimal in the presence of Laplace noise. The SL receiver is extended in [6] by using generalized Gaussian (GG) distribution, which subsumes Gaussian distribution and Laplace distribution as special cases. The MAI for TH-IR UWB systems is further analyzed in [56], where a two-term (TT) detector and an α-detector are proposed. Since the studies in [6, 5, 75, 56] are conducted for Rake receivers (or matched filter receivers) only, they inherit the aforementioned drawbacks of Rake receivers as well. Our previous work in [100] developed an improved DTR receiver in the presence of impulsive MAI, but the general differential UWB receivers have not been studied.

In this chapter, we focus on designs for of the noncoherent differential UWB receivers in the presence of impulsive MAI. We employ numerical results on random channels [25] to study the distribution of the MAI in differential UWB systems. We find that the correlation noise in the presence of MAI can be well approximated by

the GG distribution. The differential UWB receivers based on the GG approximation are developed. Furthermore, soft-limiting (SL) differential UWB receivers are proposed by employing the Laplace approximation to the correlation noise. Different from the receivers in [6, 5], our GG receivers work on the frame-level correlations and thus circumvents the stringent channel estimation issue of Rake receivers. The SL receivers have slightly inferior performance to the GG receivers when the number of users is large. However, they require less parametric information to perform detection. In addition, we show that the MSDD problem using GG approximation can be formulated as the same form as the conventional MSDD problem and thus can be efficiently solved using existing low-complexity detectors. The number of training symbols required to estimate the parametric information is also studied. Extensive simulations are conducted to validate the improved error performance of our proposed receivers relative to the conventional differential UWB receivers.

6.2 System Model for Multiple User Transmissions

The transmitted signal of a differential UWB system at the kth transmitter is

$$s^{(k)}(t) = \sum_{i=-\infty}^{\infty} b_i^{(k)} d_i^{(k)} p(t - iT_f - c_i^{(k)} T_c - T_u^{(k)}), \tag{66}$$

where $b_i^{(k)} \in \{\pm 1\}$ is the modulated symbol, $d_i^{(k)} \in \{\pm 1\}$ is the polarity code, $p(t)$ is a Gaussian monocycle waveform with width T_p, T_f is the frame duration, $T_u^{(k)}, 0 \leq T_u^{(k)} \leq T_f$ determines the transmission time of the kth user (i.e., asynchronous users), T_c is the chip duration, and the $c_i^{(k)}$'s are the pseudo-random time-hopping (TH) codes for the kth user, which are integers uniformly distributed in $[0, N_c - 1]$. To eliminate inter-frame interference (IFI), the frame duration is chosen such that $T_f > T_m + T_p + (N_c - 1)T_c$, where T_m is the maximum excess delay of the channel.

Note that, compared to the transmitted signal in Eq. (1), the multiple user transmissions introduce polarity codes $d_i^{(k)}$'s to enhance multiple user capacity. In addition, for each transmitter k, the corresponding kth receiver is assumed to know the polarity

codes $d_i^{(k)}$'s and TH codes $c_i^{(k)}$'s, but it has no knowledge about the polarity codes and TH codes of other transmitters. In addition, perfect synchronization between the kth transmitter/receiver is assumed such that the kth receiver knows the transmission time $T_u^{(k)}$, but the users are asynchronous. Without loss of generality, in the following, we focus on the transmission from transmitter 1 to corresponding receiver 1.

The channel impulse response (CIR) of the UWB communication from transmitter k to receiver 1 is modeled with multipath propagation [25, 17]:

$$h^{(k)}(t) = \sum_{i=1}^{N_p^{(k)}} \alpha_i^{(k)} \delta(t - \tau_i^{(k)}), \tag{67}$$

where $N_p^{(k)}$ is the total number of MPCs with amplitude $\alpha_i^{(k)}$ and delay $\tau_i^{(k)}$. We assume a quasi-static channel model, which is time-invariant during the transmission.

At the receiver, the signal is obtained after processing with a bandpass filter to eliminate the out-of-band interference and noise as (see Eq. (3) for single user case)

$$\begin{aligned} x(t) &= \left(\sum_{k=1}^{N_u} s^{(k)}(t) * h^{(k)}(t) + n(t) \right) * f_{\text{rx}}(t) \\ &= \sum_{k=1}^{N_u} \sum_{i=-\infty}^{\infty} b_i^{(k)} g^{(k)}(t - iT_f - c_i^{(k)} T_c - T_u^{(k)}) + w(t), \end{aligned} \tag{68}$$

where N_u is the total number of concurrent transmissions, $g^{(k)}(t) = p(t) * h^{(k)}(t) * f_{\text{rx}}(t)$ is called channel template of the kth user, $f_{\text{rx}}(t)$ is the ideal bandpass filter at the receiver, $*$ denotes the linear convolution operation, $w(t)$ represents the AWGN with zero mean and two-sided power spectral density $\frac{N_0}{2}$, and $w(t) = n(t) * f_{\text{rx}}(t)$. The noise-free received signal energy in each frame from the kth transmitter is defined as $E_f^{(k)} = \int_0^{T_f} (g^{(k)}(t))^2 dt$ with the frame energy for the desired transmission denoting as $E_f = E_f^{(1)}$.

To separate the desired user signal and the MAI signal, we could further rewrite

Eq. (68) as

$$x(t) = \sum_{i=-\infty}^{\infty} b_i^{(1)} g^{(1)}(t - iT_f - c_i^{(1)} T_c - T_u^{(1)}) + n(t), \tag{69}$$

where

$$n(t) = \sum_{k=2}^{N_u} \sum_{i=-\infty}^{\infty} b_i^{(k)} g^{(k)}(t - iT_f - c_i^{(k)} T_c - T_u^{(k)}) + \eta(t),$$

which stands for the aggregated noise term including MAI and AWGN.

6.3 Analysis of Conventional Differential UWB Receivers

In this section, we derive the differential UWB receivers presented in Sec. 2.2 by employing Gaussian assumption. Although the Gaussian assumption results in the same receivers in Sec. 2.2, this sheds light on those receivers in the viewpoint of detection theory. To distinguish the proposed receivers in this chapter, we called them "convectional receivers."

First of all, we need to determine the way to encode the information symbols $a_i^{(k)}$ to modulated symbols $b_i^{(k)}$, which is critical to the demodulation structure at the receiver side for each differential UWB system. Similar to the single user case in Eqs. (11) and (16), we list two kinds of encoders:

- Frame-by-frame encoder for DTR with $b_i^{(k)} = b_{i-1}^{(k)} a_{\lfloor i/N_f \rfloor}^{(k)}$;
- Symbol-by-symbol encoder for DD and MSDD with $b_{iN_f}^{(k)} = b_{(i-1)N_f}^{(k)} a_i^{(k)}$ and $b_{iN_f+j}^{(k)} = b_{iN_f}^{(k)}, \forall j \in [1, N_f - 1]$;

where the modulated symbol is initialized as $b_{-\infty}^{(k)} \in \{\pm 1\}$, N_f is the number of frames per information symbol, and $\lfloor \cdot \rfloor$ denotes a floor function.

For both differential UWB systems, the detection is based on the correlation between the ith and jth frame signals as

$$z_{i,j} = \int_0^{T_r} y_i^{(1)}(t) y_j^{(1)}(t) dt, \tag{70}$$

where T_r is the integration interval and $y_l^{(k)}$ indicates the received signal of the lth frame of the kth user as

$$y_l^{(k)}(t) = d_l^{(k)} x\left(t + lT_f + c_l^{(k)} T_c + T_u^{(k)}\right). \tag{71}$$

By plugging Eq. (69) into Eqs. (70) and (71), we have (see Eq. (14) for single user case)

$$z_{i,j} = \rho E_f b_i^{(1)} b_j^{(1)} + \eta_{i,j}, \tag{72}$$

where ρ denotes the fraction of the desired frame energy collected at the receiver, and $\eta_{i,j}$ is the correlation noise term, which can be well approximated as a Gaussian distributed variable for UWB communications when MAI is a Gaussian process [14, 66].

6.3.1 DTR Receiver

The DTR receiver detects each information symbol $a_i = a_i^{(1)}$ based on the following N_f correlations between the reference and data-modulated frames:

$$z_{iN_f+j,iN_f+j-1} = \rho E_f a_i + \eta_{iN_f+j,iN_f+j-1}, \quad j \in [0, N_f - 1]. \tag{73}$$

Given the correlations $z_{iN_f+j,iN_f+j-1}, j \in [0, N_f-1]$, by approximating η_{iN_f+j,iN_f+j-1}'s as independent and identically distributed (i.i.d.) Gaussian variables and invoking maximum likelihood (ML) principle, the conventional DTR (C-DTR) receiver detects information symbols by averaging all frame correlations for each information symbol as [15]

$$\begin{aligned} \hat{a}_i^{\mathrm{C-DTR}} &= \mathrm{sgn}\left(\frac{1}{N_f}\sum_{j=0}^{N_f-1} z_{iN_f+j,iN_f+j-1}\right) \\ &= \mathrm{sgn}\left(\rho E_f a_i + \frac{1}{N_f}\sum_{j=0}^{N_f-1} \eta_{iN_f+j,iN_f+j-1}\right). \end{aligned} \tag{74}$$

6.3.2 DD Receiver

One of the main drawbacks of the C-DTR receiver is that the noise-cross-noise term in η_{iN_f+j,iN_f+j-1} degrades the system error performance significantly [15]. To alleviate the noise-cross-noise effect, the conventional differential detection (C-DD) receiver detects the information symbol a_i using the averaged symbol signals instead of the frame signals as [19]

$$\hat{a}_i^{\mathrm{C-DD}} = \mathrm{sgn}\left(Z_{i,i-1}\right), \tag{75}$$

where

$$\begin{aligned} Z_{i,j} &= \int_0^{T_r} \left(\frac{1}{N_f}\sum_{l=0}^{N_f-1} y_{iN_f+l}(t)\right)\left(\frac{1}{N_f}\sum_{n=0}^{N_f-1} y_{jN_f+n}(t)\right) dt \\ &= \rho E_f b_i b_j + \frac{1}{N_f^2}\sum_{l=0}^{N_f-1}\sum_{n=0}^{N_f-1} \eta_{iN_f+l,jN_f+n}, \end{aligned} \tag{76}$$

which is the symbol-by-symbol correlation between the ith and jth averaged symbol signals with $b_i = b_{iN_f}^{(1)}$ similar to Eq. (18). Note that similar to the C-DTR, the C-DD receiver in Eq. (75) is also optimal in terms of ML principle under the assumption that all frame-level correlations between the ith and the $(i-1)$st symbols, i.e., $z_{iN_f+l,(i-1)N_f+n}$'s, $\forall l, n \in [0, N_f-1]$, are i.i.d. Gaussian variables.

6.3.3 MSDD Receiver

To further mitigate the noise-cross-noise effect of the C-DD receiver, the conventional multiple-symbol differential detection (C-MSDD) is proposed to perform joint estimation on M consecutive information symbols. Without loss of generality, we focus on the joint detection on information symbols $\mathbf{a} = [a_1, \cdots, a_M]^T$. By approximating the noise process $n(t)$ as a white Gaussian process and applying generalized likelihood ratio test (GLRT), the C-MSDD receiver is of the form (See Eq. (23) for single user case)

$$\hat{\mathbf{b}} = \arg \max_{\tilde{\mathbf{b}} \in \{\pm 1\}^{M+1}} \left(\tilde{\mathbf{b}}^T \mathbf{Q} \tilde{\mathbf{b}}\right), \tag{77}$$

where $\hat{\mathbf{b}} = [\hat{b}_0, \cdots, \hat{b}_M]^T$ and $\tilde{\mathbf{b}} = [\tilde{b}_0, \cdots, \tilde{b}_M]^T$ are the estimates and candidates of modulated symbols $[b_0^{(1)}, b_{N_f}^{(1)}, \cdots, b_{MN_f}^{(1)}]$, respectively, $\mathbf{Q}$ is an $(M+1) \times (M+1)$ matrix, whose (i,j)th element is $Z_{i-1,j-1}$ defined in Eq. (76), and

$$\hat{a}_i^{\text{C-MSDD}} = \hat{b}_{i-1}\hat{b}_i, \qquad i \in [1, M]. \tag{78}$$

6.4 Improved Differential UWB Receivers with Impulsive MAI

In this section, we propose improved differential UWB receivers in the presence of impulsive MAI. First, we study the empirical distribution of the correlation noise $\eta_{i,j}$, which is impulsive when a few users emit strong interference. Second, to cope with this impulsive MAI, we study the generalized Gaussian (GG) distribution and Laplace distribution, which well match the distribution of the impulsive correlation noise. Third, by approximating the correlation noise as the GG distributed or Laplace distributed variables, we propose improved differential UWB receivers based on ML principle.

6.4.1 Examining the Distribution of the Correlation Noise

As shown in Sec. 6.3, the conventional differential receivers can be derived by employing Gaussian approximation on the correlations $z_{i,j}$. However, recent studies [6, 5, 75, 56] for TH-IR UWB system with Rake receivers show that the MAI is not Gaussian distributed given the strong interference caused by a small number of users N_u. The non-Gaussian distributed MAI also holds for differential UWB systems. Fig. 18 depicts the empirical probability density functions (PDFs) of the noise term $\eta_{i,j}$ with SNR= 30 dB, where the parameters of different distributions are estimated using ML principle. As depicted in Fig. 18, the empirical PDF differs from the Gaussian PDF significantly, especially when the total number of users is small (e.g., $N_u = 3$ in Fig. 18). This implies that the conventional differential receivers may suffer from performance degradation when N_u is small. This issue is alleviated for large N_u,

since $\eta_{i,j}$'s approach Gaussian variables as N_u increases (e.g., $N_u = 9$ in Fig. 18). In addition, we plot the Laplace PDF, which is applied in [5] to design the soft-limiting receiver. Although the Laplace PDF fits better to the empirical PDF than the Gaussian PDF when $N_u = 3$, Laplace PDF also faces the PDF mismatch problem when N_u is large. To address this issue, we adopt the GG distribution in [6] to approximate the empirical PDF, where the GG distribution subsumes the Gaussian and Laplace distributions as special cases. As shown in Fig. 18, a good approximation to the empirical PDF can be conducted using the GG distribution regardless the number of users N_u.

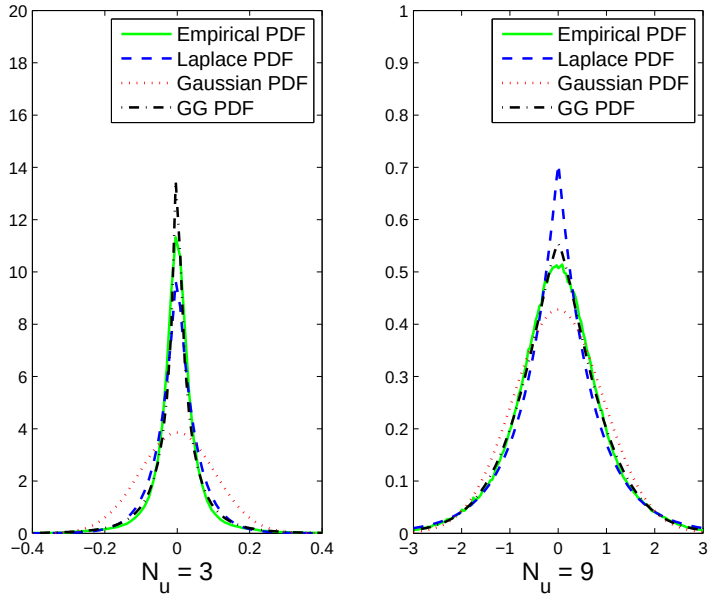

Figure 18: Empirical PDFs of noise term $\eta_{i,j}$ with SNR = 30 dB, $E_I = 32E_f$ (SIR $= -15$ dB), and different N_u's, which are generated using the configuration in Section 6.5 (left: $\alpha = 0.0179, \beta = 0.6315$; right: $\alpha = 0.9843, \beta = 1.3551$).

Based on the aforementioned observations, given moderate-to-high signal-to-Gaussian-noise ratio (SNR), we relax the Gaussian assumption of the MAI and model the noise term $\eta_{i,j}$'s in (72) to be i.i.d. GG distributed with zero mean, whose PDF is

$$f_\eta(x) = \frac{\beta}{2\alpha\Gamma(1/\beta)} \exp\left(-\left(\frac{|x|}{\alpha}\right)^\beta\right), \tag{79}$$

where α is the scale parameter, β is the shape parameter, and $\Gamma(z) = \int_0^\infty t^{z-1} \exp(-t)dt$ is the gamma function. Note that, when the parameter $\beta = 2$, the GG distribution becomes the Gaussian distribution, and when $\beta = 1$, the GG distribution becomes the Laplace distribution.

To further illustrate the transition of the correlation noise from impulsive to Gaussian-like, Figs. 19 and 20 display the histograms of the estimated β parameter given different N_u's and signal-to-interference ratios (SIRs) with 10^4 system realizations. From Fig. 19, we can observe that when $N_u = 3$, the estimated parameter β ranges from 0.6 and 0.9, implying that correlation noise is rather impulsive, while when $N_u = 9$, the estimated parameter β ranges from 1.1 to 1.8. As N_u increases, the estimated parameter β gradually centers at 1.9 (E.g., $N_u = 30$), indicating that correlation noise approaches Gaussian noise when N_u is large. In addition, the histograms of β with different SIRs are provided in Fig. 20, where we could observe that the correlation noise could be better approximated as Gaussian distributed when the interference is weaker.

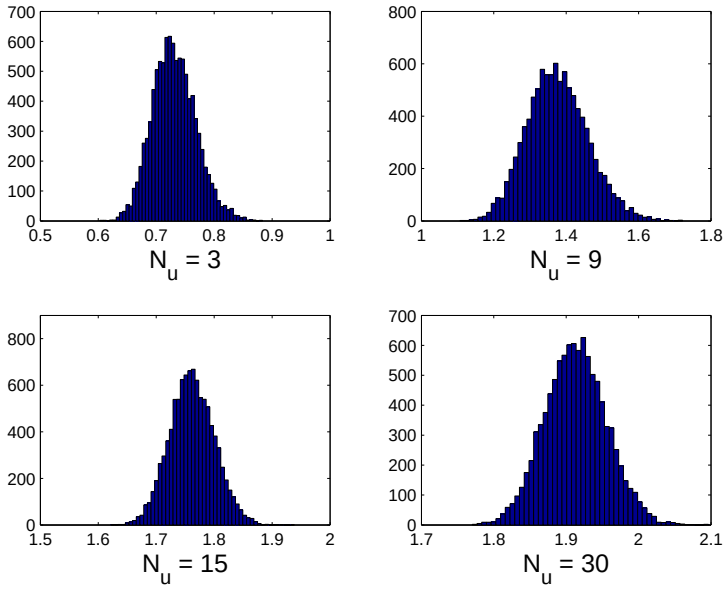

Figure 19: Histograms of estimated β with SNR = 30 dB, $E_I = 32E_f$ (SIR= -15 dB), and different N_u's.

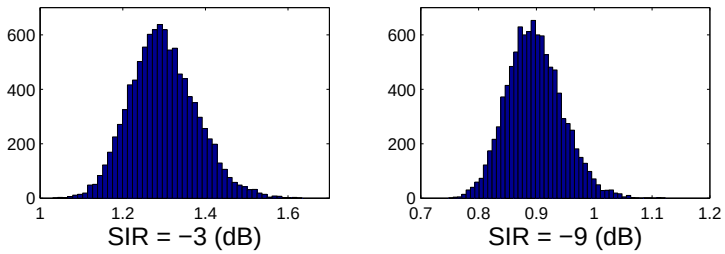

Figure 20: Histograms of estimated β with SNR = 30 dB, $N_u = 3$, and different SIRs.

6.4.2 Improved DTR Receiver

By assuming that the receiver has the knowledge of the GG parameters α and β, the proposed GG-DTR detector is derived as

$$\hat{a}_i^{\mathrm{GG-DTR}} = \mathrm{sgn}\left(\sum_{j=0}^{N_f-1}\left(|z_{iN_f+j,iN_f+j-1}+\rho E_f|^\beta - |z_{iN_f+j,iN_f+j-1}-\rho E_f|^\beta\right)\right). \quad (80)$$

Note that, although α is used to describe the GG distribution in Eq. (79), the GG-DTR receiver does not require the knowledge of α. From Eq. (80), it is ready to show that when $\beta = 2$, the GG-DTR receiver is equivalent to the C-DTR one, and when $\beta = 1$, the GG-DTR detector becomes an SL-DTR receiver as

$$\hat{a}_i^{\mathrm{SL-DTR}} = \mathrm{sgn}\left(\sum_{j=0}^{N_f-1}\Omega\left(z_{i,j},\rho E_f\right)\right), \quad (81)$$

where $\Omega(\cdot,\cdot)$ is a threshold function as

$$\Omega(x,y) = \begin{cases} |y|, & \text{if} \quad x > |y|; \\ x, & \text{if} \quad -|y| < x < |y|; \\ -|y|, & \text{if} \quad x < -|y|. \end{cases} \quad (82)$$

Note that the difference of this SL-DTR receiver with the one in [5] is that the SL-DTR receiver is based on the correlations among the frames such that the channel estimation issue of SL-Rake receivers is avoided.

6.4.3 Improved MSDD Receiver

Since DD is a special case of MSDD when $M = 1$, we only study the improved MSDD receiver in this subsection. First of all, by approximating η_{iN_f+l,jN_f+n}'s as i.i.d. GG distributed variables with zero mean, the PDF of z_{iN_f+l,jN_f+n} is

$$f_{z_{iN_f+l,jN_f+n}}(x) = \frac{\beta}{2\alpha\Gamma(1/\beta)} \exp\left(-\left(\frac{|x - b_i b_j \rho E_f|}{\alpha}\right)^{\beta}\right), \tag{83}$$

with $b_i = b^{(1)}_{iN_f+j}, \forall j \in [0, N_f - 1]$.

Given the correlations $z_{iN_f+l,jN_f+n}, \forall i, j \in [0, M], i \neq j, l, n \in [0, N_f - 1]$, the decision metric of the GG-MSDD is derived as

$$\Lambda(\tilde{\mathbf{b}}) = \sum_{i=0}^{M} \sum_{j=i+1}^{M} \sum_{l=0}^{N_f-1} \sum_{n=0}^{N_f-1} \Psi(z_{iN_f+l,jN_f+n}, \tilde{b}_i \tilde{b}_j), \tag{84}$$

where $\Psi(\cdot, \cdot)$ is the decision metric selection function as

$$\Psi(x, y) = \begin{cases} -\left(|x - \rho E_f|\right)^{\beta}, & \text{if} \quad y = +1; \\ -\left(|x + \rho E_f|\right)^{\beta}, & \text{if} \quad y = -1. \end{cases} \tag{85}$$

Therefore, the decision rule is of the form

$$\hat{\mathbf{b}} = \arg \max_{\tilde{\mathbf{b}} \in \{\pm 1\}^{M+1}} \left(\Lambda(\tilde{\mathbf{b}})\right), \tag{86}$$

and $\hat{a}_i^{\text{GG-MSDD}} = \hat{b}_i \hat{b}_{i-1}, \forall i \in [1, M]$. Compared to the C-MSDD problem in (77), the problem in (86) replaces the product of candidate symbols and symbol correlations, $\tilde{b}_i \tilde{b}_j Z_{i,j}$, in Eq. (77) with the summation of the decision metric selection functions in Eq. (85). However, the problem in (86) is generally not a BQP problem, which means that the state-of-the-art optimal or sub-optimal solvers (e.g., sphere decoding algorithms) cannot be directly applied to the problem in (86). To convert the problem into a BQP problem, we rewrite the decision metric selection function as

$$\Psi(x, y) = \frac{(\Psi(x, +1) - \Psi(x, -1))y}{2} + \frac{\Psi(x, +1) + \Psi(x, -1)}{2}, \tag{87}$$

where the first term is an odd function on y and the second term does not depend on y.

Therefore, by plugging Eq. (87) into Eq. (84), the decision metric becomes

$$\Lambda(\tilde{\mathbf{b}}) = \sum_{i=0}^{M}\sum_{j=i+1}^{M}\tilde{b}_i\tilde{b}_j\sum_{l=0}^{N_f-1}\sum_{n=0}^{N_f-1}\frac{(\Psi(z_{iN_f+l,jN_f+n},+1)-\Psi(z_{iN_f+l,jN_f+n},-1))}{2} + \sum_{i=0}^{M}\sum_{j=i+1}^{M}\sum_{l=0}^{N_f-1}\sum_{n=0}^{N_f-1}\frac{\Psi(z_{iN_f+l,jN_f+n},+1)+\Psi(z_{iN_f+l,jN_f+n},-1)}{2}. \quad (88)$$

Since the second term in Eq. (88) is constant regardless of candidate symbols $\tilde{\mathbf{b}}$, we drop the second term and finally arrive at the following GG-MSDD solution

$$\hat{\mathbf{b}} = \arg\max_{\tilde{\mathbf{b}}\in\{\pm1\}^{M+1}}\left(\sum_{i=0}^{M}\sum_{j=i+1}^{M}\tilde{b}_i\tilde{b}_jY_{i,j}\right), \quad (89)$$

with

$$Y_{i,j} = \sum_{l=0}^{N_f-1}\sum_{n=0}^{N_f-1}\left(\Psi(z_{iN_f+l,jN_f+n},+1)-\Psi(z_{iN_f+l,jN_f+n},-1)\right). \quad (90)$$

It is worth noting the special cases of GG-MSDD. When $\beta = 2$, i.e., $\eta_{i,j}$'s are approximated as Gaussian variables, Eq. (90) becomes (c.f. (18))

$$Y_{i,j} = 4\rho E_f\sum_{l=0}^{N_f-1}\sum_{n=0}^{N_f-1}z_{iN_f+l,jN_f+n} = 4\rho E_f N_f^2 Z_{i,j}, \quad (91)$$

and thus, the GG-MSDD receiver reduces to the C-MSDD receiver in (77).

When $\beta = 1$, Laplace-approximated $\eta_{i,j}$'s yield

$$Y_{i,j} = 2\sum_{l=0}^{N_f-1}\sum_{n=0}^{N_f-1}\Omega(z_{iN_f+l,jN_f+n},\rho E_f), \quad (92)$$

where $Y_{i,j}$ becomes the sum of the soft limiting functions on the N_f^2 correlations between the frame signals of the ith and jth symbols. Therefore, we refer to the GG-MSDD receiver as "the SL-MSDD receiver" when $\beta = 1$.

It is worthy noting the complexity of the proposed multiple-symbol receivers. Compared to the C-MSDD, the main extra complexity of the proposed multiple-symbol receivers is the computation of $Y_{i,j}$ in Eq. (90), where the complexity is

on the order of $\mathcal{O}(N_f^2 M^2)$ for GG-MSDD and SL-MSDD and $|x|^\beta$ Eq. (90) can be evaluated as $\exp(\beta \log(|x|))$, which can efficiently implemented using look-up table or CORDIC [55] for exp and log functions. In addition, similar to the C-MSDD, the proposed multiple-symbol receivers require an $N_f M$-branch autocorrelation receiver, which can be implemented in analog [4, 13, 24] or digital forms [45, 13, 26, 47]. Another complexity of the proposed multiple-symbol receivers is the computational complexity for the GG-MSDD problem in (89). Similar to the C-MSDD problem, we can resort to the SDA in [50], which has generally exponential complexity in terms of M, and the existing near-optimal polynomial-complexity detectors developed in the previous chapters. The performance of the existing multiple-symbol detectors for the GG-MSDD problem will be studied in Sec. 6.5.

6.4.4 Parameter Estimation for SL and GG Differential UWB Receivers

Since no MAI information is required for the conventional UWB receivers, while the SL differential receivers require ρE_f and the GG differential receivers generally require both ρE_f and β, we need to determine the parameters required for the proposed detectors when those parameters are unavailable or changed (e.g., N_u or the power of interference levels changes).

In this paper, we employ a data-aided parameter estimator with a random but known sequence of $N_{\rm tr}$ training symbols $[a_0^{(1)}, a_1^{(1)}, \cdots, a_{N_{\rm tr}-1}^{(1)}]$. After obtaining frame-level correlations at the receiver, the ML estimation is performed based on the training samples. Taking a DTR UWB system as an example, the received samples from the training symbols are

$$\begin{aligned} x_l &= a_{\lfloor l/N_f \rfloor}^{(1)} z_{l,l-1} \\ &= \rho E_f + \omega_l, \qquad 0 \le l \le N_f N_{\rm tr}, \end{aligned} \tag{93}$$

where $\omega_l = a_{\lfloor l/N_f \rfloor}^{(1)} \eta_{l,l-1}$ is treated as i.i.d. additive Laplace noise or i.i.d. additive GG noise for the SL-DTR or GG-DTR receivers, respectively. For an MSDD UWB

system, the training samples x_l's are $b^{(1)}_{iN_f+l} b^{(1)}_{jN_f+n} z_{iN_f+l,jN_f+n}, \forall i, j \in [0, N_{\rm tr}-1], i \neq j, |i-j| \leq M, \forall l, n \in [0, N_f-1]$.

For the SL differential receivers, the median of the training samples x_l is the ML estimate of ρE_f. When it comes to the GG differential receivers, the estimation is much more complicated since no closed form of the ML estimates is available to find the three parameters (mean, scale, and shape) of the GG distribution simultaneously [84, 21]. Here, we resort to the Newton-Raphson method in [21] to iteratively find the ML estimates of β and ρE_f.

For the complexity of parameter estimation for SL differential receivers, the complexity of finding the median of the training samples is linearly in terms of the size of the samples by using modern selection algorithms. For the complexity of parameter estimation for GG differential receivers, as discussed in [21], generally three iterations for the Newton-Raphson method can yield the ML estimates with accuracy 10^{-6}.

6.5 Numerical Results

In this section, we study the effectiveness of our proposed GG and SL differential UWB receivers via Monte-Carlo simulations. The transmitted pulse $p(t)$ is a second order derivative of the Gaussian function with duration $T_p = 1.0$ ns. We adopt the CM1 channel model described in [25] with T_m being about 60 ns. The parameters of the TH codes are $N_c = 19$ and $T_c = 1$ ns, $T_f = 80$ ns, $T_r = 40$ ns, and $N_f = 10$. The one-sided bandwidth of the received filter is $B = 2.5$ GHz. The bit energy is $E_b = E_f N_f$, and the overall frame energy from interfering users is defined as $E_I = \sum_{k=2}^{N_u} E_f^{(k)}$. The SIR is defined as SIR$= E_f/E_I$, and for simplicity, we employ equal frame energy for each interfering user $E_f^{(k)} = E_f^{(j)}, \forall k, j \in [2, N_u]$.

6.5.1 BER Comparisons with Different Numbers of Training Symbols

Fig. 21 displays the performance comparisons of the SL-DTR and GG-DTR receivers with different numbers of training symbols $N_{\rm tr}$. We find that with only $N_{\rm tr} = 10$

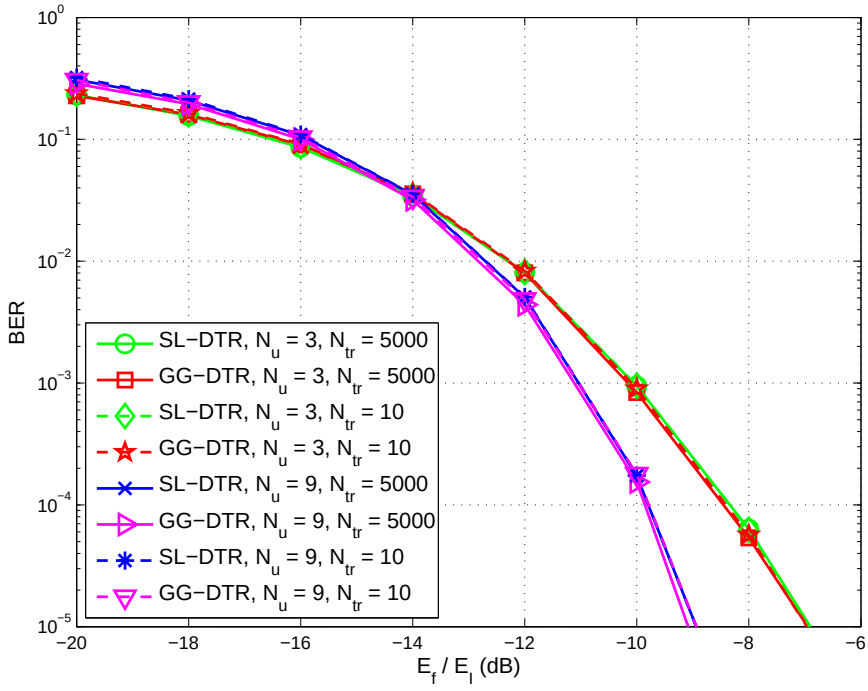

Figure 21: Performance comparisons of the GG-DTR and SL-DTR detectors with $N_{\rm tr} = 10$ or 5000, $N_u = 3$ or 9, and SNR= 30 dB.

training symbols, both SL-DTR and GG-DTR receivers can achieve close performance to the detectors with large number of training symbols ($N_{\rm tr} = 5000$). This shows that, with a few number of training symbols, our proposed detectors quickly adapt to the change of the environment (e.g., variant of channel, change of active number of users, etc), and thus, become practical for realistic UWB communications. Hence, we adopt $N_{\rm tr} = 10$ in the following simulations.

6.5.2 BER Comparisons of the DTR Receivers

Fig. 22 illustrates the performance comparisons among the C-DTR, SL-DTR, and GG-DTR receivers with different numbers of users N_u and SIR $= -9$ dB (i.e., $E_I = 8E_f$). First, when $N_u = 3$, compared to the C-DTR receiver, both the GG-DTR and SL-DTR receivers achieve significant error performance improvement at moderate-to-high SNR region (e.g., SNR $\geq$ 22 dB), where the error floor is reduced from around 2×10^{-3} for the C-DTR to 10^{-4} for the GG-DTR. Second, the GG-DTR receiver

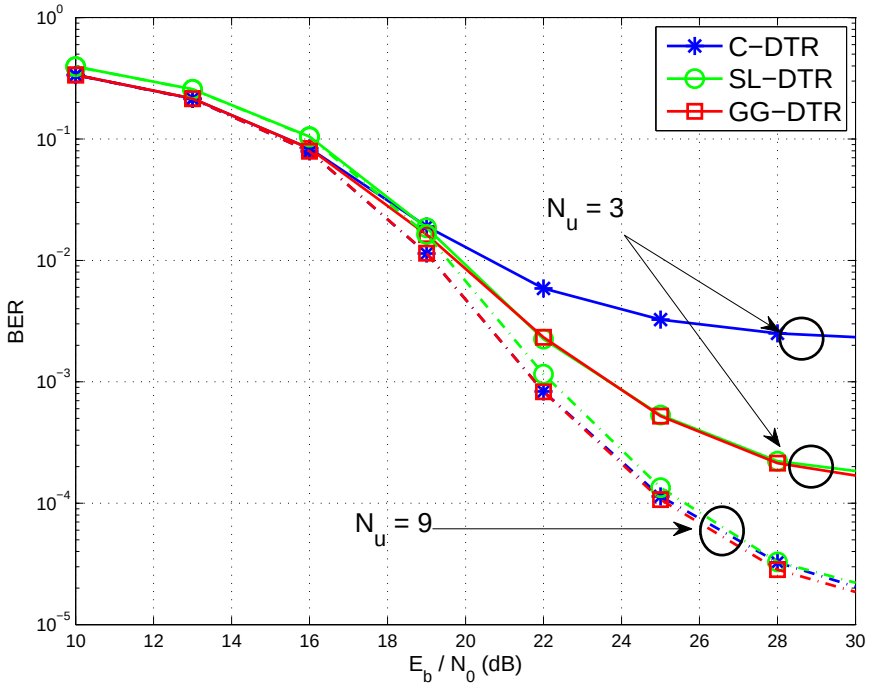

Figure 22: Performance comparisons of different DTR receivers with different numbers of users N_u and $E_I = 8E_f$.

performs slightly better than the SL-DTR one, especially for low SNR region. Third, as the number of users N_u increases, the performance gap between the C-DTR receiver and our proposed GG-DTR and SL-DTR receivers at moderate-to-high SNR region decreases. This is because the distribution of noise $\eta_{i,j}$ is better approximated by the Gaussian distribution as N_u increases. Finally, when the number of users increases, the performance becomes better (e.g. $N_u = 9$) at moderate-to-high SNR region (e.g., SNR$>$ 20 dB). The reason is that for a fixed interference power, when the number of users increases, the power of each interfering user is also lower, and thus the interference to the desired user is reduced when the TH sequence is long. However, when the number of users is further increased, the interference to the desired users gets saturated, and thus the performance curves get close.

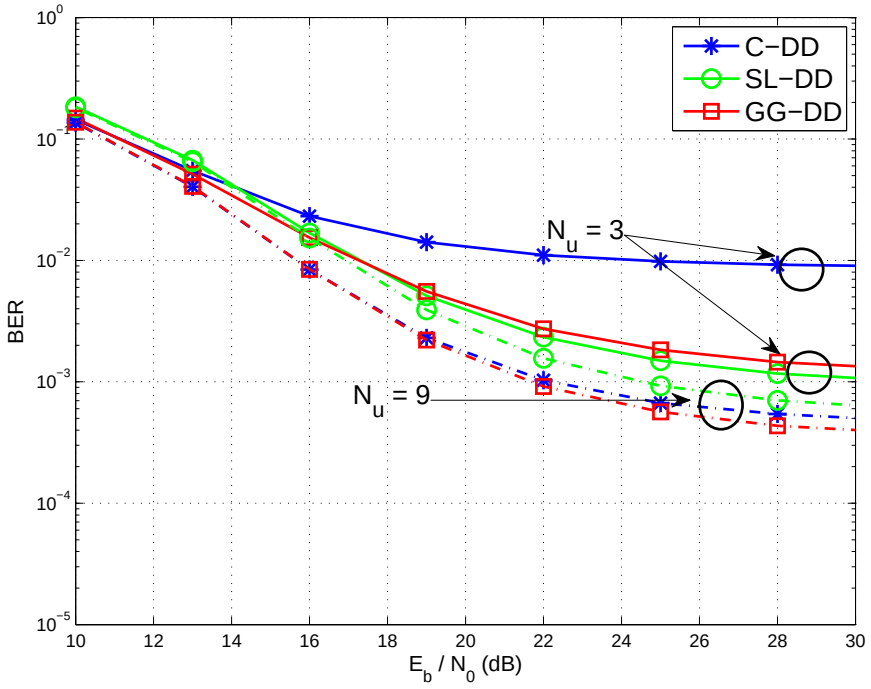

Figure 23: Performance comparisons of different DD receivers with different numbers of users N_u and $E_I = 32E_f$.

6.5.3 BER Comparisons of the MSDD Receivers

We first study the DD receivers with $M = 1$. Fig. 23 illustrates the performance comparisons among the C-DD, SL-DD, and GG-DD receivers with different numbers of users N_u and SIR $= -15$ dB. In this scenario, we have the following observations: *i*) Similar to the results of the DTR receivers, both the GG-DD and SL-GG receivers outperform the C-DD receiver remarkably at moderate-to-high SNR (e.g., SNR > 20 dB), and the error floor is reduced from around 9×10^{-3} for C-DD to 1×10^{-3}. *ii*) It is interesting to see that the performance of the GG-DD receiver is slightly worse than the SL-DD receiver at moderate-to-high SNR region. The reason may be that the GG parameter estimator is sensitive to the tail distribution of the correlation noise and thus may obtain sub-optimal parameters for detection. *iii*) When $N_u = 9$, the GG-DD receiver becomes the best one among the three receivers, especially for high SNR (e.g., SNR $= 30$), while the SL-DD exhibits worse performance than C-DD

receivers. *iv*) Compared to the results for the DTR receivers, the performance gap between $N_u = 3$ and $N_u = 9$ for the DD receivers is smaller (e.g., for the proposed SL-DD receiver, the error floor is around 1×10^{-3} when $N_u = 3$ and is around 6×10^{-4} when $N_u = 9$).

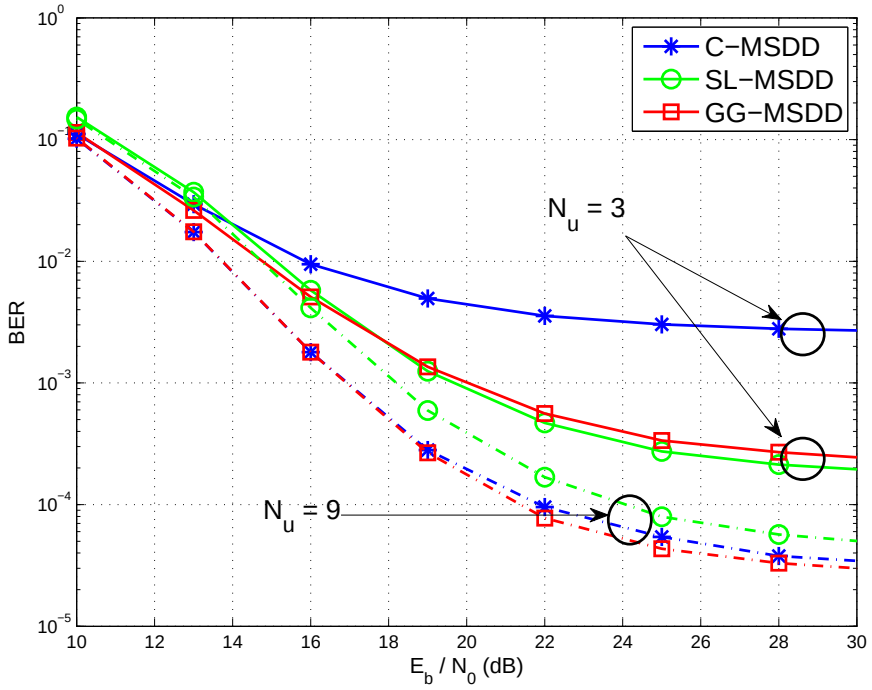

Figure 24: Performance comparisons of different MSDD receivers with $M = 2$, different numbers of users N_u, and $E_I = 32E_f$.

Fig. 24 depicts the performance of the C-MSDD, SL-MSDD, and GG-MSDD receivers with different numbers of users N_u, SIR $= -15$ dB, and $M = 2$. Unless stated otherwise, all the MSDD problems are optimally solved using the SDA in [50]. First, compared to the results in Fig. 22, MSDD receivers outperform DD receivers, especially at moderate-to-high SNR region. Second, similar to the results in Fig. 23, when $N_u = 3$, the SL-MSDD obtains significant gain over the C-MSDD, and it is slightly better than the GG-MSDD at moderate-to-high SNR (e..g, SNR > 20 dB). However, when $N_u = 9$, the SL-MSDD shows inferior performance to the GG-MSDD, and the the performance of GG-MSDD is slightly better than the C-MSDD at high SNR.

6.5.4 BER Comparisons with Different Levels of SIRs

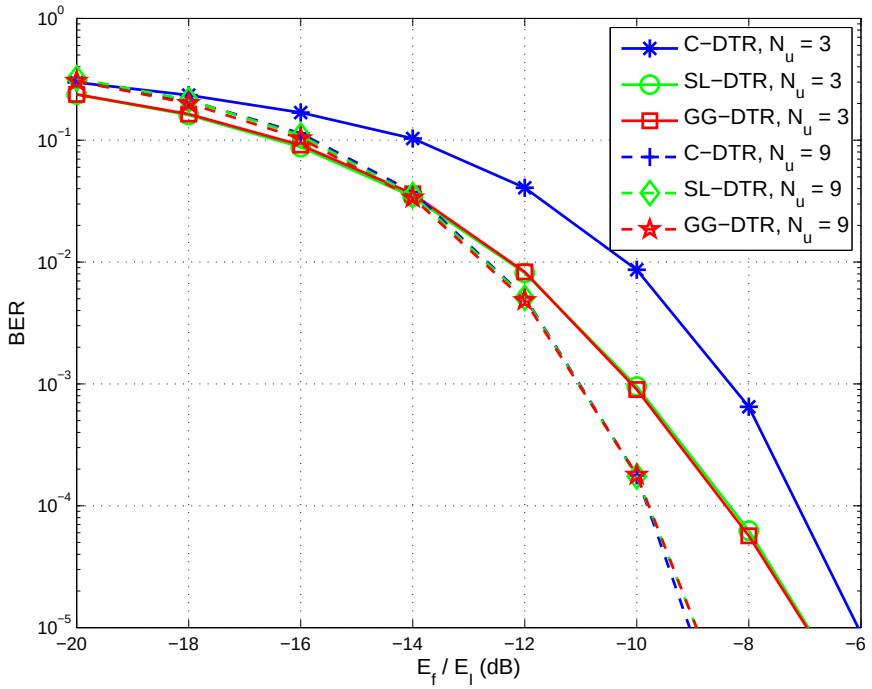

Figure 25: Performance comparisons of different DTR receivers with different levels of SIRs, $N_u = 3, 9$, and SNR= 30 dB.

Fig. 25 shows the performance comparisons of the C-DTR, SL-DTR, and GG-DTR receivers with different levels of SIRs. First of all, when $N_u = 3$, the GG-DTR receiver has significant gain over the C-DTR, where the gain is about 1.5 dB at BER $= 10^{-4}$. In this case, considerable improvement of the SL-DTR receiver over the C-DTR one is also observed, and the performance of the SL-DTR receiver is slightly worse than that of the GG-DTR. However, the gap between the C-DTR receiver and our proposed receivers is reduced to about 1.0 dB at BER $= 10^{-5}$, implying that the correlation noise becomes more Gaussian-like as SIR increases. When $N_u = 9$, all detectors have almost the same performance, and their error performance outperforms the ones when $N_u = 3$ when SIR ≥ -14 dB.

Fig. 26 demonstrates the performance comparisons between the SL differential UWB receivers and the conventional differential UWB receivers when $N_u = 3$. The

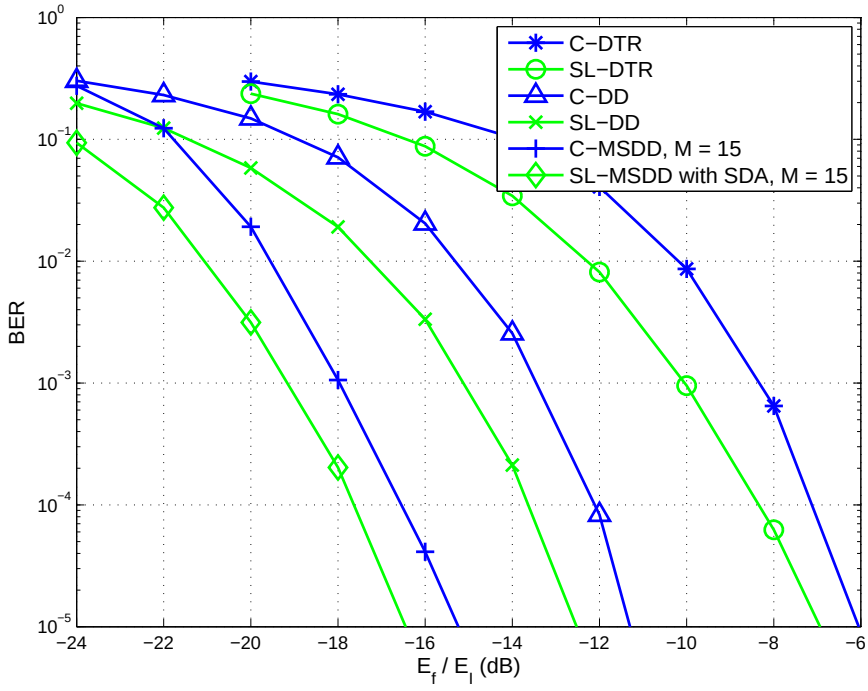

Figure 26: Performance comparisons of different detectors with different levels of SIRs, $N_u = 3$, and SNR= 30 dB.

performance of the GG differential UWB receivers is close to that of the SL differential UWB receivers, and is not presented. Again, the proposed SL differential UWB receivers achieve considerable error performance gain over the conventional ones. In addition, the SL-DD receiver has an about 5.5 dB SIR gain over the SL-DTR receiver, and the SL-MSDD receiver with $M = 15$ has an about 4 dB SIR gain over the SL-DD receiver at BER $= 10^{-5}$.

Fig. 27 illustrates the performance of different detectors for the SL-MSDD problem with different levels of SIRs, $N_u = 3$, and SNR= 30 dB. We adopt the SDA in [50], whose complexity is generally exponential in M at a fixed SNR [42], the SDP-MSD in Sec. 4.1, whose complexity is $\mathcal{O}(M^{3.5})$, and the modified unconstrained relaxation MUR-MSD in Sec. 4.3, whose complexity is $\mathcal{O}(M^3)$. As shown in Fig. 27, both SDP-MSD and MUR-MSD achieve almost the same performance as the SDA for different block size M and SIRs.

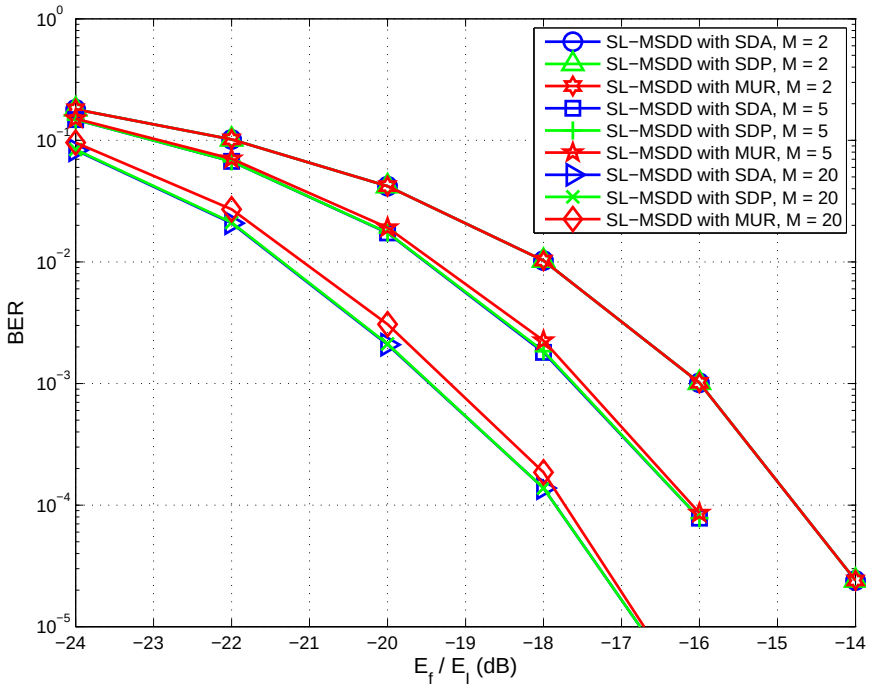

Figure 27: Performance comparisons of different detectors for the SL-MSDD problem with different levels of SIRs, $N_u = 3$, and SNR= 30 dB.

CHAPTER VII

JOINT POWER ALLOCATION AND PATH SELECTION FOR NONCOHERENT UWB SYSTEMS

7.1 Introduction

In view of the tight restrictions on the transmitted power spectral density (PSD) issued by the US Federal Communications Commission (FCC) to limit the interference to licensed wireless services [22], an additional key issue for UWB systems consists in the extension of the radio coverage. As a promising answer to this requirement, cooperative communications have been proposed in [44], where some different cooperating strategies are developed and analyzed in terms of outage probability. Henceforward, the cooperative communications concept has stimulated a lot of works: for instance, multi-hop relaying to enhance the capacity of cellular networks [46], relaying optimization based on the maximization of a network sum utility function [60], and opportunistic relaying based on relay selection through packet exchange at network level [8]. Even if the above references have been *de facto* proposed for narrowband systems, they have prompted the applications of cooperative communications to the UWB context as well. The BER performance analysis for a decode and forward (DF) UWB relaying network is tackled in [54]. Herein, the focus is put on relaying nodes which can adopt different configurations, either single or dual-antenna, and different detection schemes, either coherent or noncoherent, with an equal power allocation strategy. Further, both [3] and [105] consider a network where the nodes are equipped with coherent Rake receiver based on ideally-known channel response. In [3], the design of distributed algebraic space-time codes is addressed to achieve performance gain with the advantage of lower complexity decoding and lower peak-to-average-power-ratio.

Alternatively, the two-step approach in [105] is to first derive a cooperative routing strategy to select the highest quality two-hop route in the sense of the asymptotic outage probability (AOP), and then to propose a cooperative scheme, where the received signals from all the active two-hop links are equally weighted and combined together for source-to-destination data transfer.

Noncoherent receivers have been applied to the context of relaying networks as well [86], [34], [58]. In [86], a dual-hop two-way network is discussed wherein two devices exchange information through a single DF relay employing a code-multiplexing TR (CM-TR) signal structure. In [34], a non-cooperative relaying (NCR) strategy is suggested as a way to improve system coverage and performance of multi-hop networks. After multiple differential encoding, the source signal is forwarded to the destination node via a number of subsequent amplify and forward (AF) relays, each performing single differential demodulation. Numerical results indicate promising performance competing even with that offered by some DF schemes. However, a few limitations arise, namely: *i*) the relays have to be ordered before transmission starts; *ii*) in the specific dual-hop case, the performance is severely degraded when the link connecting either the source with the relay or the relay with the destination exhibits poor quality, and *iii*) the power allocation (PA) across the transmitting nodes is given in closed-form only for the dual-hop and through a sub-optimal recursive algorithm for the multi-hop, whereas the DF case (introduced for performance comparison) is solved through a demanding exhaustive search. In the scheme recently proposed in [58], the signals from both the relayed and direct paths are combined at the destination through a decision rule based on log-likelihood ratio (LLR) test. Significant performance gain is achieved with respect to both the direct transmission using single differential encoding and the NCR scheme of [34], even though the proposed semi-analytical PA strategy makes the extension to the multi-hop case unfeasible.

This chapter focuses on single differential encoded DF single-path NCR scheme,

in which the intermediate nodes re-encode and transmit again the hard-detected symbols, and proposes a novel relaying technique, referred to as *joint power allocation and path selection* (JPAPS). The presented algorithm optimizes the power allocation coefficients associated to the intermediate nodes and selects the path connecting source to destination capable of minimizing an approximate expression of the overall BER. Compared with the previous works the results here show the following distinctive features.

1. The power allocation over a path that crosses P relays is an optimization problem in $P+1$ dimensions. A closed-form power allocation strategy is developed which, according to simulation results, yields a BER close to the absolute minimum.

2. By performing the optimal path selection through a shortest path search on a connected graph, the computational load required by the JPAPS results to be polynomial in the number of relays of the network. In particular, it is possible to further lower the complexity $\mathcal{O}(N^3)$ of the exact JPAPS scheme by introducing an approximated path selection algorithm (AJPAPS) which runs in $\mathcal{O}(N^2)$ without showing a significant performance loss.

3. In contrast to the position-based routing techniques discussed in [77], the presented approach does not require information about the network topology and the coordinates of the source and destination.

4. A multi-hop CR strategy is also derived, which extends the AF approach in [58] to the DF setting. Herein, each relay forwards the symbols which are detected through first combining the signals received from the previous relays and then thresholding the LLR metrics. However, due to both its overall computational complexity and the significant amount of channel state information

(CSI) required, the DF CR scheme will be mainly employed as a performance benchmark.

The effectiveness of the JPAPS algorithm is corroborated by extensive simulation results over typical wireless propagation environments for various network setups. Although derived under a number of approximations, the JPAPS not only favorably compares to the AF and DF relaying techniques proposed in [34], [58], and [54], but also appears to be competitive with the more burdensome DF CR scheme.

7.2 System Model Overview

Consider a single-user relay-based UWB network made up by $N+2$ devices, namely the source S transmitting the sequence of information symbols, the destination D which collects them, and N DF relays R_i, $i = 1, \cdots, N$, acting as intermediate nodes to forward information toward the destination. For the ease of notation, let us denote with:

1. $\mathcal{P}(\mathrm{S}, \mathrm{R}_{i_1}, \cdots, \mathrm{R}_{i_P}, \mathrm{D})$ the path connecting S to D passing through the relays $\mathrm{R}_{i_1}, \cdots, \mathrm{R}_{i_P}$, with[1] $0 \leq P \leq N$, $i_1, \cdots, i_P \in \{1, \cdots, N\}$, with $i_j \neq i_k \, \forall j \neq k \in \{1, \cdots, P\}$;

2. $\mathcal{L}_{n,m}$ the link existing from node n to node m, with $n \neq m$, $n \in \mathcal{N}_P \triangleq \{\mathrm{S}, \mathrm{R}_{i_1}, \cdots, \mathrm{R}_{i_P}\}$ and $m \in \mathcal{M}_P \triangleq \{\mathrm{R}_{i_1}, \cdots, \mathrm{R}_{i_P}, \mathrm{D}\}$.

Two different DF strategies will be proposed:

- NCR adopting a single path across P relays, with $0 \leq P \leq N$, as described in Sec. 7.3;

- CR exploiting all the N relays of the network, as described in Sec. 7.4.

[1] If $P = 0$, the direct path $\mathcal{P}(\mathrm{S}, \mathrm{D})$ is considered.

It is worth emphasizing that in the former case the path $\mathcal{P}$ is chosen among *all the possible routes* according to the actual link propagation conditions, whereas in the CR scheme *all* the N relays play as intermediate steps on retransmitting the detected symbols.

7.2.1 Signal Model

At the device of index $n \in \mathcal{N}_P$, each symbol is transmitted as a block of N_f consecutive frames, with one pulse $g(t)$ per frame of sub-nanosecond width T_g and energy $E_g \triangleq \int_{-\infty}^{+\infty} g^2(t)dt$. Without loss of generality, let us adopt the following assumptions.

A1) P relays are active, with $0 \leq P \leq N$.

A2) The source and relays transmit in adjacent time slots, each having duration equal to the symbol interval $T_s = N_f T_f$, where T_f denotes the frame interval which is long enough to avoid the inter-symbol interference (ISI) effect. As a result, the time required to transmit from the source to the destination of the network one information symbol spans $(P+1)T_s$, thus ranging from T_s to $(N+1)T_s$.

A3) The index h_n, $n \in \mathcal{N}_P$, designates the slot number, with $h_{\mathrm{S}} = 0, h_{\mathrm{R}_1} = 1, \cdots, h_{\mathrm{R}_P} = P$.

Hence, the signal transmitted by node $n \in \mathcal{N}_P$ corresponding to a block of M information symbols can be written as

$$s_n(t) = \sqrt{p_n} \sum_{k=0}^{M-1} \sum_{j=0}^{N_f-1} b_k^{(n)} g[t - jT_f - k(P+1)T_s - h_n T_s], \tag{94}$$

where: *i*) p_n is the power allocation coefficient; *ii*) the channel symbol $b_k^{(n)}$ results from the differential encoding rule

$$b_k^{(n)} = \begin{cases} b_{k-1}^{(n)}\, a_k, & \text{if } n = \mathrm{S} \\ b_{k-1}^{(n)}\, \hat{a}_k^{(n)}, & \text{if } n \in \mathcal{N}_P \setminus \{\mathrm{S}\} \end{cases} \tag{95}$$

given $b_{-1}^{(n)}$ as initial value; *iii*) a_k, $0 \leq k \leq M-1$, is the sequence of the binary information-bearing symbols transmitted by the source, modeled as independent and identically distributed (i.i.d.) random variables (RVs) equiprobable in $\{\pm 1\}$, and *iv*) $\hat{a}_k^{(n)}$ is the hard decision taken at the relays having indices $n \in \mathcal{N}_P \setminus \{\mathrm{S}\}$.

The signal (94) travels through a slow-fading multipath channel connecting node $n \in \mathcal{N}_P$ with node $m \in \mathcal{M}_P$, $n \neq m$, which is assumed to be time-invariant within at least the transmission of two consecutive channel symbols and have $L_{n,m}$ paths, each with delay $\tau_i^{(n,m)}$ and uncorrelated normalized gain $\rho_i^{(n,m)}$, so that[2] $\sum_{i=0}^{L_{n,m}-1} \left[\rho_i^{(n,m)}\right]^2 = 1$. Under the assumptions A1)-A3), the signal at the output of the receiver bandpass filter $f_{\mathrm{rx}}(t)$ of bandwidth W at node m is

$$r_{n,m}(t) = \sqrt{p_n G_{n,m}} \sum_{k=0}^{M-1} \sum_{j=0}^{N_f-1} b_k^{(n)} q_{n,m}[t - jT_f - k(P+1)T_s - h_n T_s] + w_{n,m}(t), \quad (96)$$

with $G_{n,m}$ accounting for both the path loss and the log-normal fading component, where $G_{n,m}|_{\mathrm{dB}} \triangleq 10 \cdot \log_{10} G_{n,m} = -10\nu \cdot \log_{10} d_{n,m} + \vartheta_{n,m}$, ν being the path loss exponent depending on the operating scenario, $d_{n,m}$ the length of the link $\mathcal{L}_{n,m}$, and $\vartheta_{n,m}$ a zero-mean Gaussian RV with variance σ_{F}^2 [57]. The shadowing terms associated to different paths are supposed to be uncorrelated. Furthermore, the received frame-level waveform $q_{n,m}(t)$ in (96) is expressed as

$$q_{n,m}(t) = \left[\sum_{i=0}^{L_{n,m}-1} \rho_i^{(n,m)} g(t - \tau_i^{(n,m)}) \right] * f_{\mathrm{rx}}(t), \quad (97)$$

and $w_{n,m}(t)$ denotes filtered AWGN with PSD $\dfrac{N_0}{2}$ over the bandwidth W of $f_{\mathrm{rx}}(t)$.

7.2.2 Symbol Detection

Each receiving node $m \in \mathcal{M}_P$, which belongs to the path $\mathcal{P}$ connecting the source S with the destination D across P intermediate relays, in view of (95) performs

[2]The normalized gains are random variables given by the particular channel realization, but the sum of their squares is normalized to 1 at the receiver.

noncoherent differential detection without requiring the knowledge of the channel impulse response (CIR) of the link $\mathcal{L}_{n,m}$. Due to the time-slotted scheduling, first, the received signal (96) is collected over the non-adjacent slots $[(k-1)(P+1)T_s + h_nT_s, (k-1)(P+1)T_s + h_nT_s + T_s]$ and $[k(P+1)T_s + h_nT_s, k(P+1)T_s + h_nT_s + T_s]$, within which the channel symbols $b_{k-1}^{(n)}$ and $b_k^{(n)}$ have been transmitted, respectively. Then, the soft estimate for the information symbol a_k, i.e., the decision variable, is evaluated as

$$\lambda_{k,P}^{(n,m)} = \sum_{j=0}^{N_f-1} \int_{k(P+1)T_s+h_nT_s+jT_f}^{k(P+1)T_s+h_nT_s+jT_f+T_\varepsilon} r_{n,m}(t) r_{n,m}[t-(P+1)T_s]dt, \tag{98}$$

where T_ε is the integration interval depending on the CIR time span, which is assumed for simplicity to be the same for all the active links.

In order to design the DF relaying network based on either the NCR or CR strategy so that the BER performance at the destination node is maximized, some basic issues arise from the system model perspective.

About the NCR scheme using P relays out of the N available ones:

- how the power coefficients p_n, $n \in \mathcal{N}_P$, have to be chosen for the generic path $\mathcal{P}$ connecting S to D across P relays, according to the actual link conditions;
- how the optimal path can be identified.

About the CR strategy using all the N relays:

- how to decide the transmit sequence of all relays;
- how to combine the soft estimates $\lambda_{k,N}^{(n,m)}$ in (98), which are available at each receiving node.

The next Sec. 7.3 and Sec. 7.4 will address the above issues for the NCR and CR schemes, respectively, in the context of a DF multi-hop network. Significant effort will be put on keeping the required computational load at affordable levels to agree with the UWB philosophy that calls for as simple as possible processing schemes.

7.3 Joint Power Allocation and Path Selection for Non-Cooperative Relaying

In this section, we derive the JPAPS algorithm for a DF multi-hop single-path N-CR scheme. The steps we will take can be summarized as follows: *i*) definition of the transmission scheduling for the NCR network; *ii*) review of the statistics of the decision variables at the relay and the destination nodes; *iii*) formulation of the PA technique based on a sub-optimal yet efficient equal signal-to-noise ratio (SNR) s-trategy, given a path crossing P relays, with $0 \leq P \leq N$; and *iv*) choice of the path that minimizes a high-SNR approximation of the BER performance at the destination node.

7.3.1 Multi-Hop Single-Path Non-Cooperative Relaying Transmission Scheduling

Let us consider a generic path $\mathcal{P}(\mathrm{S}, \mathrm{R}_{i_1}, \cdots, \mathrm{R}_{i_P}, \mathrm{D})$ connecting S to D through P relays, composed of the links $\mathcal{L}_{n,m}$, with $n \in \mathcal{N}_P$ and $m \in \mathcal{M}_P$, $n \neq m$. The nodes transmit according to the following time-slot (TS) based scheduling:

- TS_1: S transmits to R_{i_1},
- TS_2: R_{i_1} transmits to R_{i_2},
- $\vdots$
- TS_{P+1}: R_{i_P} transmits to D.

At node m, the hard decision

$$\hat{a}_k^{(m)} = \mathrm{sgn}\left\{\lambda_{k,P}^{(n,m)}\right\} \tag{99}$$

is taken by thresholding the decision variable $\lambda_{k,P}^{(n,m)}$ given by (98). Then, if $m \neq \mathrm{D}$, i.e., the destination has not been reached yet, after differential encoding (95) we obtain the symbol $b_k^{(m)}$ to be retransmitted over the corresponding time slot. Otherwise, if

$m = \mathrm{D}$, $\hat{a}_k \triangleq \hat{a}_k^{(\mathrm{D})}$ is the final decision on the information symbol a_k made by the destination node.

7.3.2 Statistical Modeling of the Decision Variables

The decision variable $\lambda_{k,P}^{(n,m)}$ corresponding to the link $\mathcal{L}_{n,m}$ can be modeled as [93], [14]

$$\lambda_{k,P}^{(n,m)} = \begin{cases} \alpha_{n,m}\, a_k + \xi_k^{(n,m)}, & \text{if } n = \mathrm{S} \\ \alpha_{n,m}\, \hat{a}_k^{(n)} + \xi_k^{(n,m)}, & \text{if } n \neq \mathrm{S} \end{cases}, \tag{100}$$

where $\xi_k^{(n,m)}$ is a zero-mean Gaussian RV with variance $\sigma_{n,m}^2$, $\alpha_{n,m}$ is the scaling coefficient, and $\hat{a}_k^{(n)}$ is the hard decision at node n. Based on [34], it can be shown that the scaling coefficient $\alpha_{n,m}$ and the noise variance $\sigma_{n,m}^2$ are given by

$$\alpha_{n,m} = E_T\, \delta_{n,m}\, p_n, \tag{101}$$

$$\sigma_{n,m}^2 = \alpha_{n,m} N_0 + \frac{W N_f T_\varepsilon N_0^2}{2}. \tag{102}$$

Note that in (101) $E_T \triangleq N_f E_g$ is the energy transmitted when $p_n = 1$, and

$$\delta_{n,m} \triangleq G_{n,m} \int_0^{T_\varepsilon} q_{n,m}^2(t) dt \tag{103}$$

denotes the frame-level energy available at the output of the receiver bandpass filter over the interval $[0, T_\varepsilon]$.

7.3.3 Power Allocation for a Fixed Relaying Path

In order to formulate the PA rule, we fix a generic path $\bar{\mathcal{P}}(\mathrm{S}, \mathrm{R}_{i_1}, \cdots, \mathrm{R}_{i_P}, \mathrm{D})$ which crosses P of the N available relays, and we adopt the following assumptions.

A4) The available energy E_T is shared among the source, that transmits $p_{\mathrm{S}} E_T$, and the active relays $\mathrm{R}_{i_1}, \cdots, \mathrm{R}_{i_P}$, that transmit $p_{\mathrm{R}_{i_1}} E_T, \cdots, p_{\mathrm{R}_{i_P}} E_T$, respectively. After defining for simplicity $\mathrm{R}_{i_0} \triangleq \mathrm{S}$, this means that the constraint

$$\sum_{j=0}^{P} p_{\mathrm{R}_{i_j}} = 1 \tag{104}$$

must hold at network level.

A5) The SNR E_T/N_0 is thought to be sufficiently large so that (102) can be approximated as $\sigma^2_{n,m} \simeq \alpha_{n,m} N_0$.

Now, let us focus on the BER expression for a given path $\bar{\mathcal{P}}(\mathrm{S}, \mathrm{R}_{i_1}, \cdots, \mathrm{R}_{i_P}, \mathrm{D})$. Due to the DF-based processing performed by the intermediate nodes, an error is collected at the destination whenever there exists an odd number of errors along $\bar{\mathcal{P}}$. Upon neglecting the higher order terms given by the products of Q-functions in view of the assumption A5, we can obtain a high-SNR approximation of the BER metric as

$$\Phi_{\bar{\mathcal{P}}}(\mathbf{p}) = \sum_{\ell=0}^{P} Q\left(\sqrt{\gamma_{\mathrm{R}_{i_\ell},\mathrm{R}_{i_{\ell+1}}}}\right). \tag{105}$$

In plain words, $\Phi_{\bar{\mathcal{P}}}(\mathbf{p})$ is given by the sum of the BERs of the links which compose $\bar{\mathcal{P}}$, where for ease of notation $\mathrm{R}_{i_{P+1}} \triangleq \mathrm{D}$, and from (100)-(102) and assumption A5, the SNR at the output of the link $\mathcal{L}_{\mathrm{R}_{i_\ell},\mathrm{R}_{i_{\ell+1}}}$ can be written as

$$\gamma_{\mathrm{R}_{i_\ell},\mathrm{R}_{i_{\ell+1}}} \triangleq \frac{\alpha^2_{\mathrm{R}_{i_\ell},\mathrm{R}_{i_{\ell+1}}}}{\sigma^2_{\mathrm{R}_{i_\ell},\mathrm{R}_{i_{\ell+1}}}} \simeq \frac{E_T}{N_0} \delta_{\mathrm{R}_{i_\ell},\mathrm{R}_{i_{\ell+1}}} p_{\mathrm{R}_{i_\ell}}, \quad \ell = 0, \cdots, P, \tag{106}$$

with $\mathbf{p} \triangleq [p_{\mathrm{R}_{i_0}}, p_{\mathrm{R}_{i_1}}, \cdots, p_{\mathrm{R}_{i_{P+1}}}]^T$ denoting the vector of the power coefficients to be allocated on the transmitting nodes belonging to the path $\bar{\mathcal{P}}$.

Hence, the PA optimization problem (OP), or PA-OP for short, for a given path $\bar{\mathcal{P}}$ can be formally stated as follows,

$$\begin{cases} \mathbf{p}_{\mathrm{o}} = \arg\min\limits_{\mathbf{p}} \left\{\Phi_{\bar{\mathcal{P}}}(\mathbf{p})\right\} \\ \text{s.t.} \quad \mathbf{1}_P^T \, \mathbf{p} = 1 \end{cases}. \tag{107}$$

Notice that in the PA-OP (107) both the objective function and the constraint result to be continuous and convex. Thus, the PA-OP is convex as well, and as such, it admits a unique solution [9].

Unfortunately, applying the conventional method of Lagrange multipliers does not yield a closed-form solution, and, as a consequence, some alternatives are required. Due to the convex nature of the PA-OP, a possible numerical method relies on the

iterative sub-gradient algorithm [9]. Once the method converges, we are sure that the solution is the optimal one, although this is typically achieved with a slow convergence rate. As the PA-OP has to be solved for all the possible paths $\mathcal{P}$ of the network, it can be definitely concluded that the overall computational load required by this method is unaffordable.

Prompted by the above consideration, the idea behind the proposed strategy is *heuristically* based on the fact that the BER performance of a given path is well approximated by the BER of the link experiencing the worst channel conditions. Therefore, the PA-OP is (sub-optimally) solved according to the equal-SNR PA (ESPA) strategy, i.e., setting

$$\gamma_{\mathrm{R}_{i_0},\mathrm{R}_{i_1}} = \gamma_{\mathrm{R}_{i_1},\mathrm{R}_{i_2}} = \cdots = \gamma_{\mathrm{R}_{i_P},\mathrm{R}_{i_{P+1}}}, \tag{108}$$

so that all the links will experience the same BER level. Coming into details, after plugging the expression of the SNR (106) into condition (108) and exploiting the constraint (104) of assumption A4, the linear matrix equation

$$\mathbf{\Delta p} = \mathbf{b} \tag{109}$$

follows, where $\mathbf{\Delta}$ is the $(P+1) \times (P+1)$ matrix defined as

$$\mathbf{\Delta} \triangleq \begin{bmatrix} \delta_{\mathrm{R}_{i_0},\mathrm{R}_{i_1}} & -\delta_{\mathrm{R}_{i_1},\mathrm{R}_{i_2}} & 0 & \cdots & 0 & 0 \\ 0 & \delta_{\mathrm{R}_{i_1},\mathrm{R}_{i_2}} & -\delta_{\mathrm{R}_{i_2},\mathrm{R}_{i_3}} & \cdots & 0 & 0 \\ 0 & 0 & \delta_{\mathrm{R}_{i_2},\mathrm{R}_{i_3}} & \cdots & 0 & 0 \\ \vdots & \vdots & \vdots & \ddots & \vdots & \vdots \\ 0 & 0 & 0 & \cdots & \delta_{\mathrm{R}_{i_{P-1}},\mathrm{R}_{i_P}} & -\delta_{\mathrm{R}_{i_P},\mathrm{R}_{i_{P+1}}} \\ 1 & 1 & 1 & \cdots & 1 & 1 \end{bmatrix}, \tag{110}$$

and $\mathbf{b} \triangleq [0, \cdots, 0, 1]^T$ is a vector of size $P+1$. The solution of (109) leads us to the following proposition.

Proposition 3. *The closed-form sub-optimal ESPA solution for the path $\bar{\mathcal{P}}$ results as*

$$\mathbf{p}_{\text{ESPA}} = \frac{1}{\sum_{\ell=0}^{P} \delta^{-1}_{R_{i_\ell},R_{i_{\ell+1}}}} \cdot [\delta^{-1}_{R_{i_0},R_{i_1}}, \delta^{-1}_{R_{i_1},R_{i_2}}, \cdots, \delta^{-1}_{R_{i_P},R_{i_{P+1}}}]^T, \tag{111}$$

and accordingly, the minimum BER is approximately expressed by

$$\Phi_{\bar{\mathcal{P}}}(\mathbf{p}_{\text{ESPA}}) = (P+1) \cdot Q\left(\sqrt{\frac{E_T}{N_0} \cdot \left(\sum_{\ell=0}^{P} \delta^{-1}_{R_{i_\ell},R_{i_{\ell+1}}}\right)^{-1}}\right). \tag{112}$$

Proof. In view of the structure of the matrix $\mathbf{\Delta}$, it can be shown that its rows are linearly independent. Hence, $\det \mathbf{\Delta} > 0$, and the solution of the linear system is unique. Therefore, plugging (111) into (109) proves that the former is such a solution, from which the minimum BER $\Phi_{\bar{\mathcal{P}}}(\mathbf{p}_{\text{ESPA}})$ given by (112) follows. □

A few comments can help on grasping the meaning of Proposition 3.

1. Let us consider the dual-hop case ($N = 1$, and so $P = 0$ or $P = 1$), i.e., a relaying network composed of the source S, the relay R, and the destination D, where the possible paths are either the direct $\mathcal{P}(\text{S}, \text{D})$ ($P = 0$) or the relayed one $\mathcal{P}(\text{S}, \text{R}, \text{D})$ ($P = 1$). As for the path $\mathcal{P}(\text{S}, \text{R}, \text{D})$, let us assume $\delta_{\text{R,D}} > \delta_{\text{S,R}}$. If the power coefficients were chosen as $p_{\text{S}} = p_{\text{R}} = 1/2$, the received energy for the transmission over the link $\mathcal{L}_{\text{R,D}}$ would be greater than that for the transmission over $\mathcal{L}_{\text{S,R}}$, thus meaning that the BER of the overall path $\mathcal{P}(\text{S}, \text{R}, \text{D})$ would be dictated by the worst link $\mathcal{L}_{\text{S,R}}$. Applying the ESPA scheme, instead, the power coefficients have the form

$$\mathbf{p}_{\text{ESPA}} = [p_{\text{S}}, p_{\text{R}}]^T = \frac{1}{\delta_{\text{S,R}} + \delta_{\text{R,D}}} \cdot [\delta_{\text{R,D}}, \delta_{\text{S,R}}]^T, \tag{113}$$

and the received energies for the two transmissions are "equalized", so that the SNRs at the output of the bandpass filters at R and D result to be the same and equal to

$$\gamma_{\text{S,R}} = \gamma_{\text{R,D}} = \frac{E_T}{N_0} \cdot \left(\frac{1}{\delta_{\text{S,R}}} + \frac{1}{\delta_{\text{R,D}}}\right)^{-1}. \tag{114}$$

Consequently, the overall BER turns out to be

$$\Phi_{\mathcal{P}(\mathrm{S,R,D})}(\mathbf{p}_{\mathrm{ESPA}}) = Q\left(\sqrt{\gamma_{\mathrm{S,R}}}\right) + Q\left(\sqrt{\gamma_{\mathrm{R,D}}}\right) = 2Q\left(\sqrt{\frac{E_T}{N_0}\cdot\left(\frac{1}{\delta_{\mathrm{S,R}}}+\frac{1}{\delta_{\mathrm{R,D}}}\right)^{-1}}\right). \quad (115)$$

On the other hand, focusing on the direct path $\mathcal{P}(\mathrm{S},\mathrm{D})$, the ESPA solution (111) yields

$$\mathbf{p}_{\mathrm{ESPA}} = [1,0]^T, \quad (116)$$

i.e., all the available energy is assigned to the source S since the relay R is left unused. Therefore, the corresponding BER results as

$$\Phi_{\mathcal{P}(\mathrm{S,D})}(\mathbf{p}_{\mathrm{ESPA}}) = Q\left(\sqrt{\gamma_{\mathrm{S,D}}}\right) = Q\left(\sqrt{\frac{E_T}{N_0}\cdot\delta_{\mathrm{S,D}}}\right). \quad (117)$$

2. The ESPA (111) is a feasible solution for the PA-OP (107) since it satisfies the power constraint. However, due to its sub-optimal nature, it does not ensure to exactly hit the minimum of the objective function $\Phi_{\bar{\mathcal{P}}}(\mathbf{p})$ in (105). Nevertheless, the simulation results discussed in Sec. 7.5 will interestingly show that the proposed ESPA approach is *near-optimal*, in the sense that it achieves a BER value which is very close to the minimum obtainable through a numerical solution based on exhaustive search.

7.3.4 Optimal Path Selection

The JPAPS algorithm can be finalized by selecting the optimal path that minimizes the overall BER performance. Formally speaking, the optimal path selection problem can be formulated as

$$\mathcal{P}_{\mathrm{o}} = \arg\min_{\mathcal{P}\in\mathcal{G}} \{\eta(\mathcal{P})\}, \quad (118)$$

where $\mathcal{G}$ is the set of all possible paths connecting S with D and the objective function

$$\eta(\mathcal{P}) \triangleq (P+1)\cdot Q\left(\sqrt{\frac{E_T}{N_0}\cdot\left(\sum_{\ell=0}^{P}\delta^{-1}_{\mathrm{R}_{i_\ell},\mathrm{R}_{i_{\ell+1}}}\right)^{-1}}\right) \quad (119)$$

coincides with the (approximate) minimum BER given by (112) employing the ESPA strategy described in Sec. 7.3.3. Since there exist $N!/(N-P)!$ different routes to go from S to D passing through P relays, the cardinality of $\mathcal{G}$ amounts to $\sum_{\ell=0}^{N} N!/\ell!$. Therefore, solving (118) via a naive exhaustive search requires combinatorial complexity, which even for small N is clearly unfeasible. However, the specific structure of the metric $\eta(\mathcal{P})$ suggests a much more efficient path selection algorithm, whose rationale relies on: first, finding the set of *candidates* for the optimal path, i.e., one path for each value of P, with $0 \leq P \leq N$, and then, choosing the *global* optimal path in the candidate set as the one which minimizes the metric $\eta(\mathcal{P})$. The following proposition clarifies these concepts.

Proposition 4. *The solution to the minimization problem (118) can be obtained with polynomial complexity $\mathcal{O}(N^3)$ by means of a two-step procedure.*

S1) The $N+1$ sub-problems

$$\mathcal{P}_{\text{JPAPS}}^{(P)} = \underset{\mathcal{P}\in\mathcal{G}_P}{\arg\min} \left\{\mu(\mathcal{P})\right\}, \quad 0 \leq P \leq N, \tag{120}$$

are solved adopting the path metric

$$\mu(\mathcal{P}) \triangleq \sum_{\ell=0}^{P} \delta^{-1}_{R_{i_\ell}, R_{i_{\ell+1}}}, \tag{121}$$

where $\mathcal{G}_P \triangleq \{\mathcal{P} \,|\, \mathcal{P} \in \mathcal{G}$ and passes through P relays only$\}$.

The result is the set $\mathcal{C} \triangleq \left\{\mathcal{P}_{\text{JPAPS}}^{(P)}\right\}_{P=0}^{N}$, which includes the $N+1$ candidates for the optimal path.

S2) The optimal path follows from

$$\mathcal{P}_{\text{JPAPS}}^{(\text{opt})} = \underset{\mathcal{P}\in\mathcal{C}}{\arg\min} \left\{\eta(\mathcal{P})\right\}, \tag{122}$$

where $\eta(\mathcal{P})$ is the metric defined in (119).

Proof. Bearing in mind that: *i*) all the paths belonging to $\mathcal{G}_P$ have P relays only, and *ii*) the function $Q(\sqrt{x^{-1}})$ is increasing in x, then minimizing $\eta(\mathcal{P})$ for a given P and $\frac{E_T}{N_0}$ ratio is equivalent to minimize $\mu(\mathcal{P})$ in (121). Furthermore, $\mu(\mathcal{P})$ is an additive metric, i.e., it is the sum of the positive weights $\delta^{-1}_{\mathrm{R}_{i_\ell},\mathrm{R}_{i_{\ell+1}}}$, one for each link $\mathcal{L}_{\mathrm{R}_{i_\ell},\mathrm{R}_{i_{\ell+1}}}$ belonging to the path $\mathcal{P}$. Hence, each sub-problem (120) of step S1 turns into a *shortest path* problem constrained by P hops with non-negative link metric $\delta^{-1}_{\mathrm{R}_{i_\ell},\mathrm{R}_{i_{\ell+1}}}$, which can be efficiently solved with polynomial complexity by applying the modified Bellman-Ford (BF) algorithm [32]. More precisely, under the assumption that the relaying network is completely connected, the number of edges of the corresponding graph results to be $E = \dfrac{(N+1)(N+2)}{2}$, and therefore the complexity of step S1 is $\mathcal{O}(N \cdot E) = \mathcal{O}(N^3)$. The OP (122) of step S2 consists of selecting the path belonging to $\mathcal{C}$ that minimizes the original metric $\eta(\mathcal{P})$ in (119), i.e. of finding the minimum among $N+1$ elements, and as such, it can be performed in $\mathcal{O}(N)$. As a result, the overall complexity of the procedure is $\mathcal{O}(N^3)$. □

Just to exemplify the path selection algorithm, let us focus again on the dual-hop network considered in Sec. 7.3.3, wherein the possible paths are the direct $\mathcal{P}(\mathrm{S},\mathrm{D})$ ($P=0$) and the relayed one $\mathcal{P}(\mathrm{S},\mathrm{R},\mathrm{D})$ ($P=1$). From (115) and (117), the metric (119) evaluated for the relayed path amounts to

$$\eta[\mathcal{P}(\mathrm{S},\mathrm{R},\mathrm{D})] = 2Q\left(\sqrt{\frac{E_T}{N_0}\cdot\left(\frac{1}{\delta_{\mathrm{S,R}}}+\frac{1}{\delta_{\mathrm{R,D}}}\right)^{-1}}\right), \tag{123}$$

whereas that for the direct one is

$$\eta[\mathcal{P}(\mathrm{S},\mathrm{D})] = Q\left(\sqrt{\frac{E_T}{N_0}\cdot\delta_{\mathrm{S,D}}}\right). \tag{124}$$

Therefore, the JPAPS algorithm reduces to the binary testing

$$\mathcal{P}^{(\mathrm{opt})}_{\mathrm{JPAPS}} = \begin{cases} \mathcal{P}(\mathrm{S},\mathrm{R},\mathrm{D}), & \eta[\mathcal{P}(\mathrm{S},\mathrm{R},\mathrm{D})] < \eta[\mathcal{P}(\mathrm{S},\mathrm{D})] \\ \mathcal{P}(\mathrm{S},\mathrm{D}), & \text{otherwise} \end{cases}. \tag{125}$$

The meaning of (125) can be intuitively explained as follows. Let us assume that $\mathcal{P}(\mathrm{S},\mathrm{D})$ is not reliable, for example due to a large distance between S and D or to shadowing. This signifies that the BER of $\mathcal{P}(\mathrm{S},\mathrm{D})$ will be greater than that of $\mathcal{P}(\mathrm{S},\mathrm{R},\mathrm{D})$. As a result, the JPAPS algorithm according to the values of $\eta[\mathcal{P}(\mathrm{S},\mathrm{D})]$ and $\eta[\mathcal{P}(\mathrm{S},\mathrm{R},\mathrm{D})]$ will correctly choose the relayed path and use the intermediate relay R. Vice versa, whenever $\delta_{\mathrm{S,R}}$ or $\delta_{\mathrm{R,D}}$ is so small that the BER associated to $\mathcal{P}(\mathrm{S},\mathrm{R},\mathrm{D})$ is higher than that of $\mathcal{P}(\mathrm{S},\mathrm{D})$, the JPAPS algorithm will select the direct path $\mathcal{P}(\mathrm{S},\mathrm{D})$. In both cases, the path selection diversity is properly exploited, thus contributing to enhance the connectivity between source and destination.

7.3.5 Approximated Path Selection

In order to reduce the overall computational complexity, the path selection algorithm can be suitably approximated, as showed in the following corollary.

Corollary 1. *The approximated version of the JPAPS algorithm, or AJPAPS for short, finds an approximation to the minimization problem (118) via the OP*

$$\mathcal{P}_{\mathrm{AJPAPS}}^{(\mathrm{opt})} = \arg\min_{\mathcal{P}\in\mathcal{G}} \{\mu(\mathcal{P})\}, \tag{126}$$

which can be solved in $\mathcal{O}(N^2)$.

Proof. Since the metric $\mu(\mathcal{P})$ defined in (121) is additive on the links belonging to a given path $\mathcal{P}$, the OP (126) is equivalent to an unconstrained shortest path problem with non-negative link costs (see also Figure 28), which can be efficiently solved through the Fibonacci-heap-based Dijkstra algorithm with complexity $\mathcal{O}(N^2)$ [27].

□

A couple of comments about Corollary 1 can be of help.

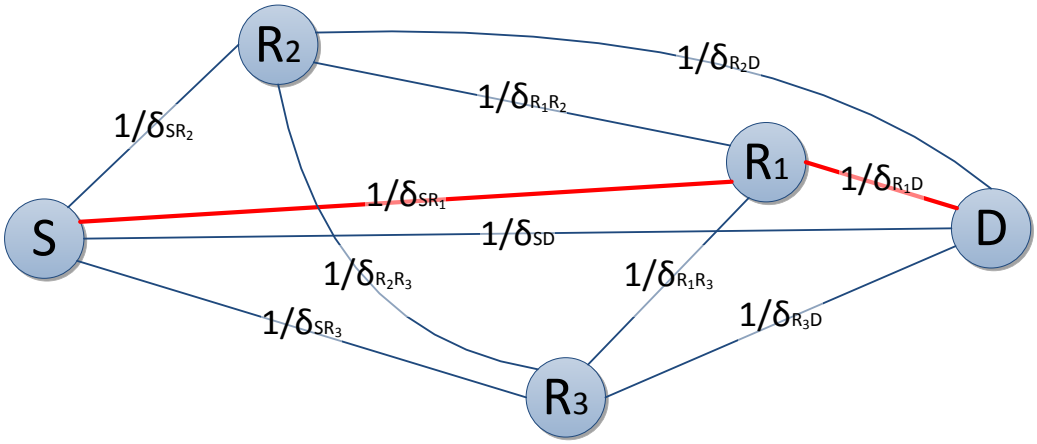

Figure 28: The AJPAPS algorithm reduces the path selection to an unconstrained shortest path problem with non-negative link costs.

1. In the case of dual-hop network ($N = 1$), the AJPAPS algorithm reduces to

$$\mathcal{P}_{\text{AJPAPS}}^{(\text{opt})} = \begin{cases} \mathcal{P}(\text{S},\text{R},\text{D}), & \text{if } \delta_{\text{S,R}}^{-1} + \delta_{\text{R,D}}^{-1} < \delta_{\text{S,D}}^{-1} \\ \mathcal{P}(\text{S},\text{D}), & \text{otherwise} \end{cases} . \tag{127}$$

2. The AJPAPS algorithm represents a good performance-versus-complexity trade-off. Indeed, as shown in Sec. 7.5, the BER performance offered by AJPAPS is very similar to that of the JPAPS algorithm, yet requiring a lower order of computational load.

7.4 Cooperative Relaying

We develop in this section a multi-hop CR scheme in which each relay of the network retransmits toward the destination the recovered symbol, obtained by first combining the received signals from the previously transmitting nodes and then thresholding the LLR corresponding to the soft estimates (98). The following points will be discussed: *i*) definition of the transmission scheduling for the CR network; *ii*) evaluation of the LLR for a given relay, and *iii*) choice of the power coefficients to be employed at the network devices to optimize the BER performance at the destination node.

7.4.1 Multi-Hop Cooperative Relaying Transmission Scheduling

Referring to Figure 29, let us consider the relaying network composed of the source S, N intermediate relays $\mathrm{R}_1, \cdots, \mathrm{R}_N$, and the destination D. Given an ordering of the N relays, transmissions take place according to the following TS-based scheduling:

- TS_1: S transmits to $\mathrm{R}_1, \cdots, \mathrm{R}_N$, D
- TS_2: R_1 transmits to $\mathrm{R}_2, \cdots, \mathrm{R}_N$, D
- $\vdots$
- TS_{N+1}: R_N transmits to D.

Defining for notational simplicity $\mathrm{R}_{N+1} \triangleq \mathrm{D}$, at the node of index $\mathrm{R}_j \in \mathcal{M}_N$, the k-th symbol is recovered by applying the optimal decision rule

$$\hat{a}_k^{(\mathrm{R}_j)} = \mathrm{sgn}\left\{\Lambda(\boldsymbol{\lambda}_{k,N}^{(\mathrm{R}_j)})\right\}, \quad 1 \leq j \leq N+1, \tag{128}$$

where $\boldsymbol{\lambda}_{k,N}^{(\mathrm{R}_j)} \triangleq [\lambda_{k,N}^{(\mathrm{S},\mathrm{R}_j)}, \lambda_{k,N}^{(\mathrm{R}_1,\mathrm{R}_j)}, \cdots, \lambda_{k,N}^{(\mathrm{R}_{j-1},\mathrm{R}_j)}]^T$ is the j-dimensional vector including the soft estimates collected in the time intervals TS_1, TS_2, $\cdots$, TS_j from the links $\mathcal{L}_{\mathrm{S},\mathrm{R}_j}, \mathcal{L}_{\mathrm{R}_1,\mathrm{R}_j}, \cdots, \mathcal{L}_{\mathrm{R}_{j-1},\mathrm{R}_j}$, and $\Lambda(\boldsymbol{\lambda}_{k,N}^{(\mathrm{R}_j)})$ is the LLR corresponding to $\boldsymbol{\lambda}_{k,N}^{(\mathrm{R}_j)}$, as evaluated in Sec. 7.4.2. After recovering the symbol $\hat{a}_k^{(\mathrm{R}_j)}$ from (128), if $j \neq N+1$ differential encoding (95) yields the channel symbol $b_k^{(\mathrm{R}_j)}$ to be retransmitted again. Otherwise, if $j = N+1$, $\hat{a}_k \triangleq \hat{a}_k^{(\mathrm{R}_{N+1})}$ is the final decision taken by the destination node on the information symbol a_k.

7.4.2 Evaluation of the LLR Metric

The LLR evaluated at the node R_j is defined as

$$\Lambda(\boldsymbol{\lambda}_{k,N}^{(\mathrm{R}_j)}) \triangleq \ln \frac{f_{\boldsymbol{\lambda}}(\boldsymbol{\lambda}_{k,N}^{(\mathrm{R}_j)}|a_k = 1)}{f_{\boldsymbol{\lambda}}(\boldsymbol{\lambda}_{k,N}^{(\mathrm{R}_j)}|a_k = -1)}, \tag{129}$$

where $f_{\boldsymbol{\lambda}}(\boldsymbol{\lambda}_{k,N}^{(\mathrm{R}_j)})$ is the joint probability density function (PDF) of $\boldsymbol{\lambda}_{k,N}^{(\mathrm{R}_j)}$. The metric (129) is computed in the following proposition.

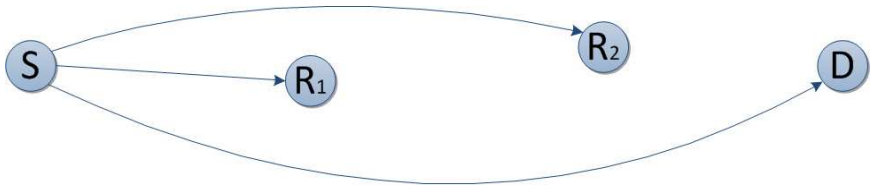

(a) S transmits during the first time slot.

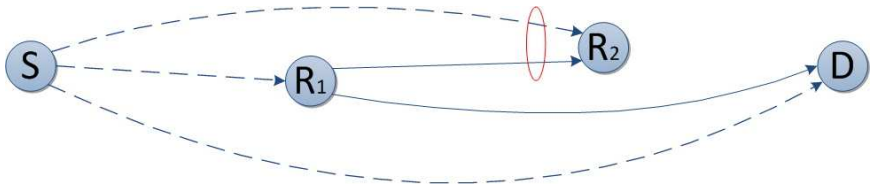

(b) R_1 transmits during the second time slot.

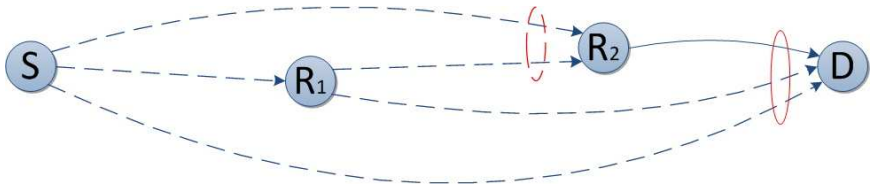

(c) R_2 transmits during the third time slot.

Figure 29: Multi-hop cooperative relaying ($N = 2$).

Proposition 5. *Under the assumptions A1 (with $P = N$) and A2, the LLR $\Lambda(\boldsymbol{\lambda}_{k,N}^{(R_j)})$, $1 \leq j \leq N+1$, can be written as*

$$\Lambda(\boldsymbol{\lambda}_{k,N}^{(R_j)}) = \frac{2\alpha_{S,R_j}}{\sigma^2_{S,R_j}} \lambda_{k,N}^{(S,R_j)} + \sum_{i=1}^{j-1} \Omega(\lambda_{k,N}^{(R_i,R_j)}), \tag{130}$$

with

$$\Omega(\lambda_{k,N}^{(R_i,R_j)}) \triangleq \ln \frac{\cosh\left(\dfrac{\alpha_{R_i,R_j}}{\sigma^2_{R_i,R_j}} \lambda_{k,N}^{(R_i,R_j)} + \varphi_{R_j}\right)}{\cosh\left(\dfrac{\alpha_{R_i,R_j}}{\sigma^2_{R_i,R_j}} \lambda_{k,N}^{(R_i,R_j)} - \varphi_{R_j}\right)}, \tag{131}$$

and approximated as

$$\Lambda(\boldsymbol{\lambda}_{k,N}^{(R_j)}) \simeq Z_{k,N}^{(j)} \triangleq \frac{2\alpha_{S,R_j}}{\sigma^2_{S,R_j}} \lambda_{k,N}^{(S,R_j)} + \sum_{i=1}^{j-1} \omega(\lambda_{k,N}^{(R_i,R_j)}), \tag{132}$$

with

$$\omega(\lambda_{k,N}^{(R_i,R_j)}) \triangleq \left| \frac{\alpha_{R_i,R_j}}{\sigma^2_{R_i,R_j}} \lambda_{k,N}^{(R_i,R_j)} + \varphi_{R_j} \right| - \left| \frac{\alpha_{R_i,R_j}}{\sigma^2_{R_i,R_j}} \lambda_{k,N}^{(R_i,R_j)} - \varphi_{R_j} \right|, \tag{133}$$

where $\varphi_{R_j} \triangleq \frac{1}{2} \ln \frac{1 - p_{e_{R_j}}}{p_{e_{R_j}}}$, $p_{e_{R_j}} \triangleq \Pr\{\hat{a}_k^{(R_j)} \neq a_k\}$ *being the BER at the node* R_j.

Proof. After setting $\mathrm{R}_0 \triangleq \mathrm{S}$ for simplicity of notation, since the soft estimates at node $\mathrm{R}_j \in \mathcal{M}_N$, i.e., $\lambda_{k,N}^{(\mathrm{R}_0,\mathrm{R}_j)}, \lambda_{k,N}^{(\mathrm{R}_1,\mathrm{R}_j)}, \cdots, \lambda_{k,N}^{(\mathrm{R}_{j-1},\mathrm{R}_j)}$, are independent from each other, the LLR in (129) turns out to be

$$\Lambda(\boldsymbol{\lambda}_{k,N}^{(\mathrm{R}_j)}) = \sum_{i=0}^{j-1} \ln f_\lambda(\lambda_{k,N}^{(\mathrm{R}_i,\mathrm{R}_j)} | a_k = 1) - \sum_{i=0}^{j-1} \ln f_\lambda(\lambda_{k,N}^{(\mathrm{R}_i,\mathrm{R}_j)} | a_k = -1). \tag{134}$$

Exploiting (100)-(102), the conditional marginal PDF $f_\lambda(\lambda_{k,N}^{(\mathrm{R}_i,\mathrm{R}_j)}|a_k)$ is given by

$$f_\lambda(\lambda_{k,N}^{(\mathrm{R}_i,\mathrm{R}_j)}|a_k) = \begin{cases} \dfrac{1}{\sigma_{\mathrm{R}_i,\mathrm{R}_j}\sqrt{2\pi}} \exp\left\{ -\dfrac{[\lambda_{k,N}^{(\mathrm{R}_i,\mathrm{R}_j)} - \alpha_{\mathrm{R}_i,\mathrm{R}_j} a_k]^2}{2\sigma^2_{\mathrm{R}_i,\mathrm{R}_j}} \right\}, & i = 0 \\ \dfrac{\Pr\{\hat{a}_k^{(\mathrm{R}_j)} \neq a_k\}}{\sigma_{\mathrm{R}_i,\mathrm{R}_j}\sqrt{2\pi}} \exp\left\{ -\dfrac{[\lambda_{k,N}^{(\mathrm{R}_i,\mathrm{R}_j)} + \alpha_{\mathrm{R}_i,\mathrm{R}_j} a_k]^2}{2\sigma^2_{\mathrm{R}_i,\mathrm{R}_j}} \right\} & \\ \quad + \dfrac{\Pr\{\hat{a}_k^{(\mathrm{R}_j)} = a_k\}}{\sigma_{\mathrm{R}_i,\mathrm{R}_j}\sqrt{2\pi}} \exp\left\{ -\dfrac{[\lambda_{k,N}^{(\mathrm{R}_i,\mathrm{R}_j)} - \alpha_{\mathrm{R}_i,\mathrm{R}_j} a_k]^2}{2\sigma^2_{\mathrm{R}_i,\mathrm{R}_j}} \right\}, & 1 \leq i \leq j-1 \end{cases} . \tag{135}$$

Upon replacing (135) into (134), the exact expression of the LLR (130)-(131) can thus be obtained. Furthermore, applying the Jacobi approximation, i.e., $\ln(\mathrm{e}^x + \mathrm{e}^y) \simeq \max\{x, y\}$, the approximations in (132)-(133) follow. □

Some remarks can be given about the multi-hop CR scheme.

1. The N available relays have to be pre-ordered so that transmissions comply with the TS-based scheduling procedure outlined in Sec. 7.4.1. Since there exist $N!$ different ways of sorting N relays, however, an exhaustive search looking for the ordering that enables the best performance appears unfeasible even for small N.

2. While the NCR JPAPS algorithm requires only partial CSI in the form of the frame-level energies $\delta_{n,m}$ defined in (103), with $n \in \mathcal{N}_N$ and $m \in \mathcal{M}_N$, $n \neq m$,

in the CR scheme the model parameters $\alpha_{\mathrm{R}_i,\mathrm{R}_j}$ and $\sigma^2_{\mathrm{R}_i,\mathrm{R}_j}$, with $0 \leq i \leq j-1$ and $1 \leq j \leq N+1$, have to be pre-computed together with an estimate of the BER level for all the nodes. As a result, the overall computational complexity of the CR is much higher than that of the JPAPS scheme.

7.4.3 Power Allocation for Multi-Hop Cooperative Relaying

The optimal power allocation strategy is far more demanding for the CR approach than for the NCR JPAPS scheme.

In analogy with the dual-hop AF CR technique proposed in [58], a possible option could be based on the solution of the OP

$$\begin{cases} \mathbf{p}_{\mathrm{o}} = \arg\min\limits_{\mathbf{p}} \{\mathrm{SNR}_{\mathrm{CR}}(\mathbf{p})\} \\ \text{s.t.} \quad \mathbf{1}_{N+1}^T \, \mathbf{p} = 1 \end{cases}, \tag{136}$$

where $\mathbf{p} \triangleq [p_{\mathrm{R}_0}, p_{\mathrm{R}_1}, \cdots, p_{\mathrm{R}_{N+1}}]^T$ and the objective function

$$\mathrm{SNR}_{\mathrm{CR}}(\mathbf{p}) \triangleq \frac{\mathrm{E}^2\{Z_{k,N}^{(N+1)}\}}{\mathrm{Var}\{Z_{k,N}^{(N+1)}\}} \tag{137}$$

is the effective SNR at the destination node, based on the RV $Z_{k,N}^{(N+1)}$ given by (132) with $j = N+1$. Unfortunately, differently from the AF CR scheme of [58], the PA strategy defined in (136)-(137) proves ineffective. Indeed, in the current DF CR scheme, the soft estimates included in $Z_{k,N}^{(N+1)}$, i.e., $\lambda_{k,N}^{(\mathrm{R}_j,\mathrm{R}_{N+1})}$ with $0 \leq j \leq N$, cannot be modeled as Gaussian RVs, but instead as mixtures of Gaussian RVs, because of the presence of the hard decisions $\hat{a}_k^{(\mathrm{R}_j)}$.

In order to find an alternative power allocation strategy, let us observe that, from a heuristic point of view, the best path coming into a given relay, say R_j, dominates its performance. Hence, it can be argued that a good approximation of the BER at the node R_j, i.e., $p_{e_{\mathrm{R}_j}}$, is just given by the minimum among all the BERs pertaining to the admissible paths, namely those going from S to R_j, R_1 to R_j, $\cdots$, R_{j-1} to R_j. Hence, after discarding the higher order terms given by the products of Q-functions

in line with the high-SNR assumption A5, the recursive equation

$$\begin{cases} p_{e_{\mathrm{R}_0}} = 0 \\ p_{e_{\mathrm{R}_j}} = \min_{i\in\{0,1,\cdots,j-1\}} \left\{ p_{e_{\mathrm{R}_i}} + Q\left(\sqrt{\gamma_{\mathrm{R}_i,\mathrm{R}_j}}\right) \right\}, \;\; j = 1,\cdots,N+1 \end{cases} \tag{138}$$

allows to evaluate the sequence $p_{e_{\mathrm{R}_j}}$, $1 \leq j \leq N$ of the BER at the relay nodes R_1, R_2, $\cdots$, R_N, together with the BER at the destination node $p_{e_{\mathrm{D}}} \triangleq p_{e_{\mathrm{R}_{N+1}}}$. Assuming as objective function $p_{e_{\mathrm{D}}}$ from (138), we are thus led to formulate the OP for the PA strategy in the CR scenario

$$\begin{cases} \mathbf{p}_{\mathrm{o}} = \arg\min\limits_{\mathbf{p}} \left\{ p_{e_{\mathrm{D}}}(\mathbf{p}) \right\} \\ \text{s.t.} \quad \mathbf{1}_{N+1}^T \, \mathbf{p} = 1 \end{cases} . \tag{139}$$

The analogy between the OP (107) and that in (139) suggests that a good approximated solution of the latter can be found by exploiting the ESPA strategy outlined in Sec. 7.3.3. Then, solving (139) yields the sequence $p_{e_{\mathrm{R}_j}}$, $1 \leq j \leq N$, which is eventually employed to evaluate the LLR metrics (130)-(131) or their approximate versions (132)-(133).

7.5 Simulation Results

In this section, the effectiveness of the JPAPS and AJPAPS schemes is verified through numerical simulations over realistic multipath wireless environments for various network configurations. The performance figure is quantified by the BER at the destination node as a function of the E_g/N_0 ratio with E_g and N_0 being defined in Sec. 7.2.

7.5.1 Benchmark Schemes

The following schemes will be taken as performance benchmarks:

1. source-destination direct transmission (DT) with single differential encoding;

2. DF NCR with single differential encoding and equal power allocation (DF-NCR-EP), as proposed in [54];

3. DF NCR with single differential encoding and the optimal power allocation (DF-NCR-OP) proposed in Sec. 7.3.3;

4. DF CR with single differential encoding and equal power allocation (DF-CR-EP), as discussed in Sec. 7.4.2;

5. DF CR with single differential encoding and optimal power distribution (DF-CR-OP), in which the power allocation coefficients are optimized numerically by making them vary in the interval $[0, 1]$ and choosing the values that yield the minimum BER;

6. AF CR with multiple differential encoding and the optimal power allocation strategy (AF-CR-OP) proposed in [58];

7. AF NCR with multiple differential encoding and the optimal power allocation strategy (AF-NCR-OP) proposed in [34];

8. DF NCR with single differential encoding and joint power allocation and path selection (JPAPS), as proposed in Sec. 7.3.3 and 7.3.4;

9. DF NCR with single differential encoding and approximate joint power allocation and path selection (AJPAPS), as proposed in Sec. 7.3.5.

Note that, if not otherwise specified, all the performance comparisons among the above benchmark schemes will be carried out taking as a reference the BER level of 10^{-3}.

7.5.2 Simulation Setup

In the setup considered for the numerical simulations, the source node transmits bursts of M binary information-bearing symbols, where the symbol interval is made up of $N_f = 2$ frames with an ultra-short pulse $g(t)$ per frame, the so-called monocycle,

defined as

$$g(t) = \left[1 - 4\pi \left(\frac{t-\vartheta}{\varphi}\right)^2\right] \mathrm{e}^{-2\pi[(t-\vartheta)/\varphi]^2}, \tag{140}$$

with $\vartheta = 0.35\,\mathrm{ns}$ and $\varphi = 0.2877\,\mathrm{ns}$. The pulse and frame durations are $T_g = 0.7\,\mathrm{ns}$ and $T_f = 70\,\mathrm{ns}$, respectively, and accordingly, the symbol interval equals $T_s = N_f T_f = 140\,\mathrm{ns}$. No time-hopping code is employed, the bandwidth of the receiver band-pass filter is set to $W = 5\,\mathrm{GHz}$, and the integration interval is $T_\varepsilon = 5.25\,\mathrm{ns}$ [34].

The channel model is assumed to be time-invariant within each burst, but randomly varying from burst to burst according to the CM1 model [57]. The path loss exponent is $\nu = 3$, and the deviation of the log-normal fading component is $\sigma_\mathrm{F} = 2.5$. Thus, according to the time-spread of the channel model and the value of the frame interval T_f, the ISI effect can be considered negligible.

We focus on five network configurations (NCs), as depicted in Figure 30, differing for both the number of relays and their disposition.

NC1: line configuration with $N = 1$ relay between the source S and the destination D;

NC2: isosceles triangle configuration with $N = 1$ relay;

NC3: line configuration with $N = 2$ relays between the source S and the destination D;

NC4: square configuration with $N = 2$ relays positioned on the vertices;

NC5: generic configuration formed by a square room of side 4 meters, with the source S and the destination D placed on a couple of diagonal vertices, and $N = 10$ relays, one of which is placed in the middle and the other ones are uniformly and randomly distributed inside.

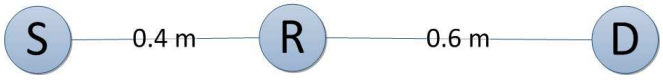

(a) Line configuration with $N = 1$ relay (NC1).

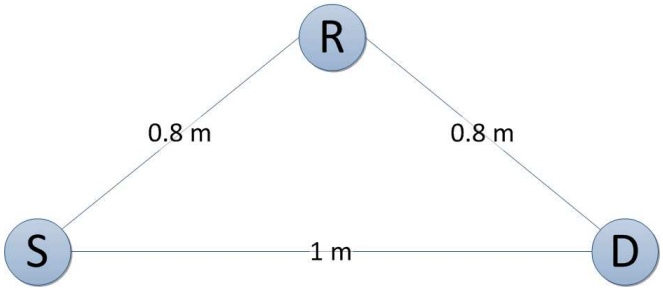

(b) Triangle configuration with $N = 1$ relay (NC2).

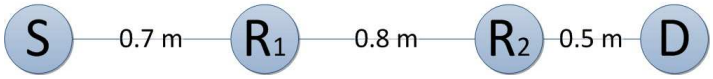

(c) Line configuration with $N = 2$ relays (NC3).

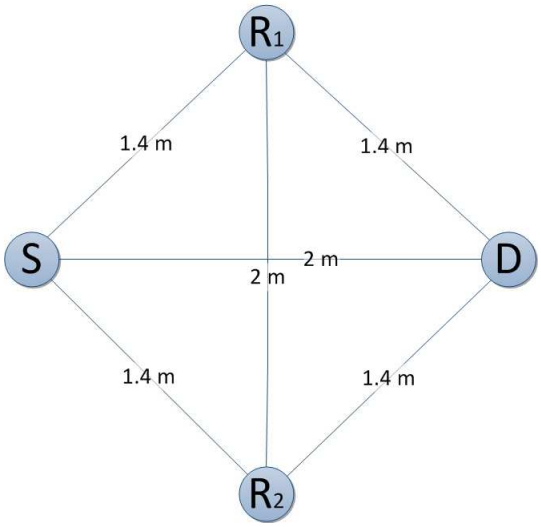

(d) Square configuration with $N = 2$ relays (NC4).

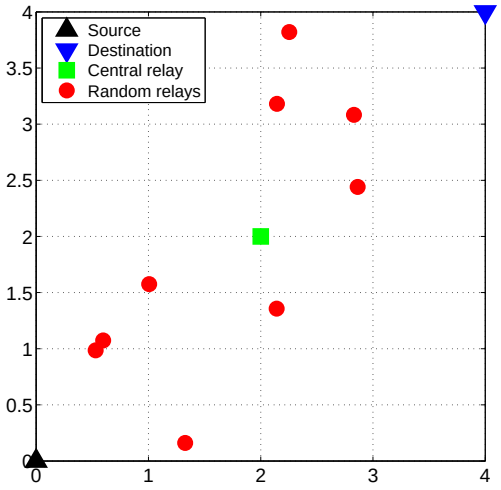

(e) Generic configuration with $N = 10$ relays (NC5).

Figure 30: Network configurations.

7.5.3 Check for the Power Allocation Adopted for the JPAPS Algorithm

Figs. 31-32 deal with the transmission of a single burst of M consecutive information symbols over a given realization of the CIRs and channel gains, adopting the configurations NC1, NC2 ($N = 1$) and NC3 ($N = 2$). In both figures, the BER is plotted against the N power allocation coefficients[3] by making them vary in the interval $[0, 1]$ with the step-size of 10^{-2}. For the single relay system analyzed in Figure 31, $M = 10^6$, and two values of E_g/N_0 are chosen for each of the two dual-hop scenarios, in order to obtain a minimum BER close to 10^{-2} and 10^{-4}. For the configuration with two relays in Figure 32, $M = 10^5$ and $E_g/N_0 = 12$ dB, so that the minimum BER is close to 10^{-3}. In all the cases, the BER performance achieved using the PA coefficients given by (114) and (111) for the case $N = 1$ and $N = 2$ respectively, is very close to that obtained through exhaustive search.

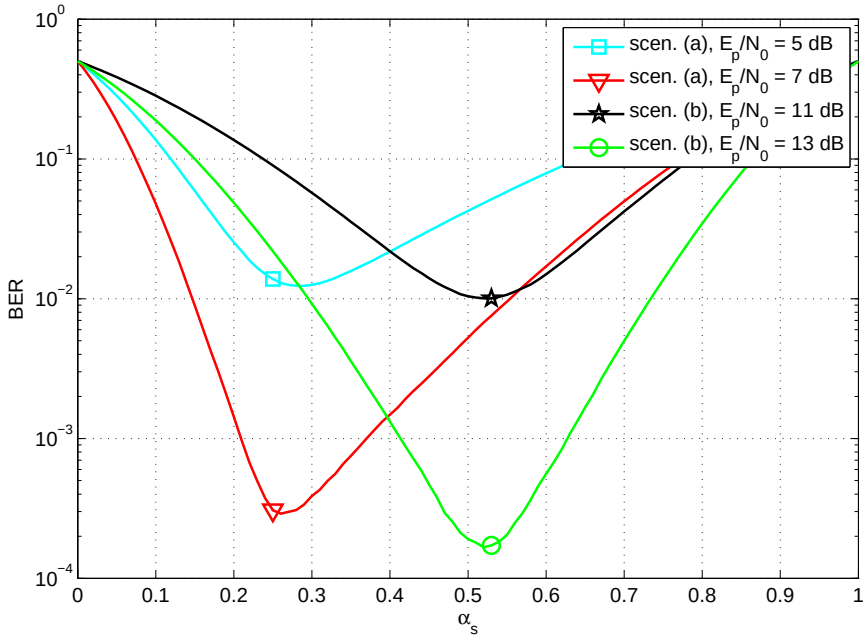

Figure 31: BER as a function of the power allocation coefficient of the source S for NC1 and NC2.

[3]The value of the $(N + 1)$-st power coefficient is obtained from the power constraint equation.

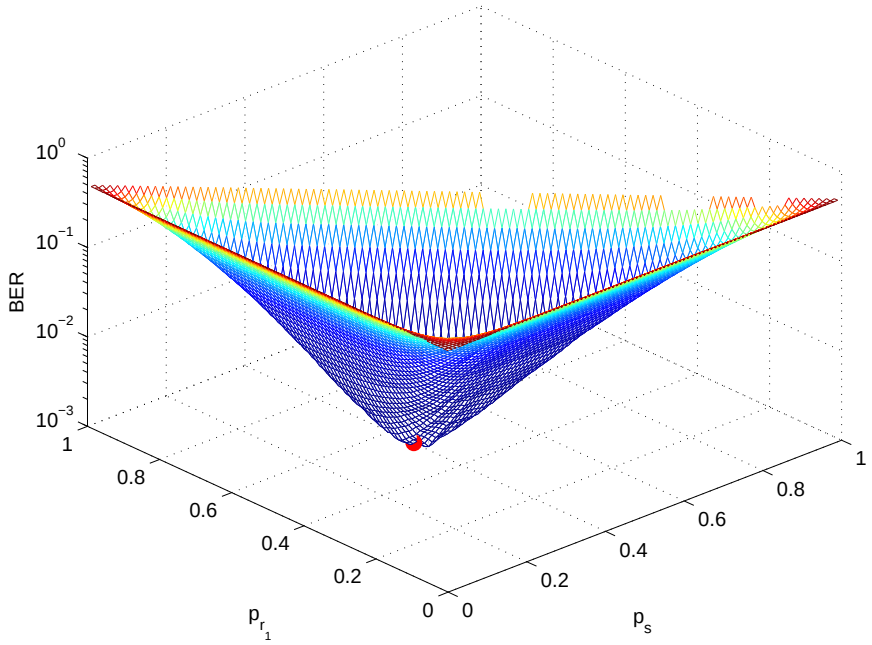

Figure 32: BER as a function of power allocation coefficients of the source S and relay R_1 for NC3.

7.5.4 BER Performance for Dual-Hop Configurations

Figures 33-34 compare the schemes listed in Sec. 7.5.1 for the single relay configurations NC1 and NC2, respectively. For a specific value of the E_g/N_0 ratio, 10^4 different bursts are transmitted, each conveying $M = 10^3$ information symbols and experiencing a different realization of the wireless propagation channels. In particular, for each realization of the transmission, independent channel gains are generated and the CIRs of the different links are selected randomly from a set of 100 sample channel responses given by [25].

In Figure 33, it can be noted that the DF-NCR-EP [54] offers a gain of about 4 dB at the target BER of 10^{-3} with respect to the conventional DT. In contrast, in Figure 34, the DT slightly outperforms the DF-NCR-EP by approximately 1 dB. The reason is simply that the scenario NC1 of Figure 33 favors the relayed path $\mathcal{P}(\mathrm{S},\mathrm{R},\mathrm{D})$, while for NC2 in Figure 34 $\mathcal{P}(\mathrm{S},\mathrm{R},\mathrm{D})$ turns out to be unfavorable. Anyway, it can be argued from both the figures that the proposed JPAPS scheme: *i*) coincides with the

approximated version AJPAPS, which, however, shows one less order of complexity; *ii*) yields a performance improvement of 3 dB with respect to the DF-NCR-EP and the DT in Figures 33 and 34, respectively, and *iii*) offers a gain of 1 dB with respect to the AF-CR-OP [58] for both NC1 and NC2, and of about 2 dB (4.5 dB) for NC1 (NC2) with respect to the AF-NCR-OP [34]. It has to be noted that, although the JPAPS requires a much lower computational load (and the AJPAPS even less), it outperforms the DF-CR-EP by 1.5 dB (1 dB) for NC1 (NC2), and it incurs in a negligible 0.4 dB loss compared to the DF-CR-OP in which the PA coefficients are found by an exhaustive search, i.e., performing the transmission for each possible couple of power coefficients (with a fixed step size) and then selecting the one that minimizes the BER.

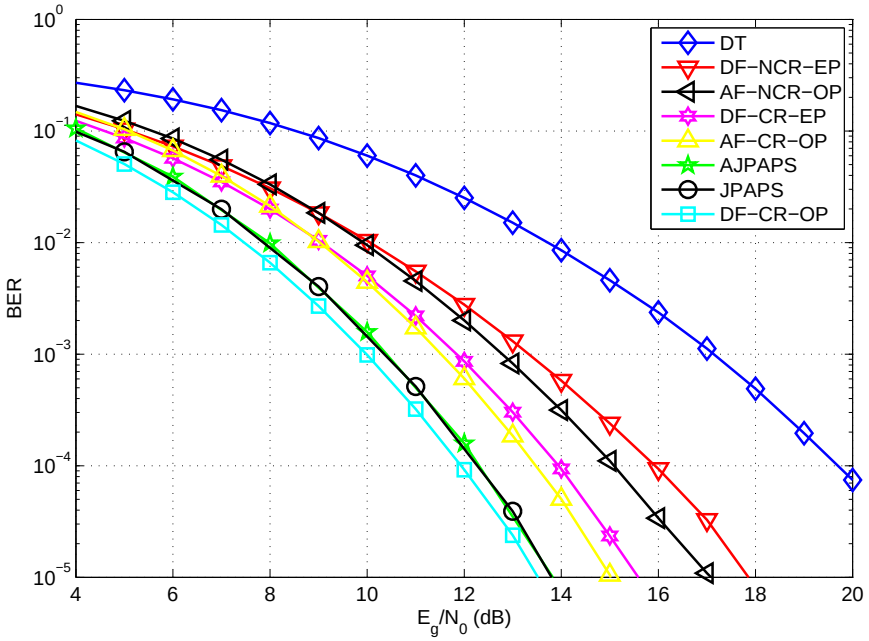

Figure 33: BER as a function of the SNR for various transmission schemes (NC1).

7.5.5 BER Performance for Multi-Hop Configurations

Figures 35-36 address two scenarios with $N = 2$ relays corresponding to NC3 and NC4, respectively. As in NC1, in the multi-hop line configuration NC3 of Figure 35,

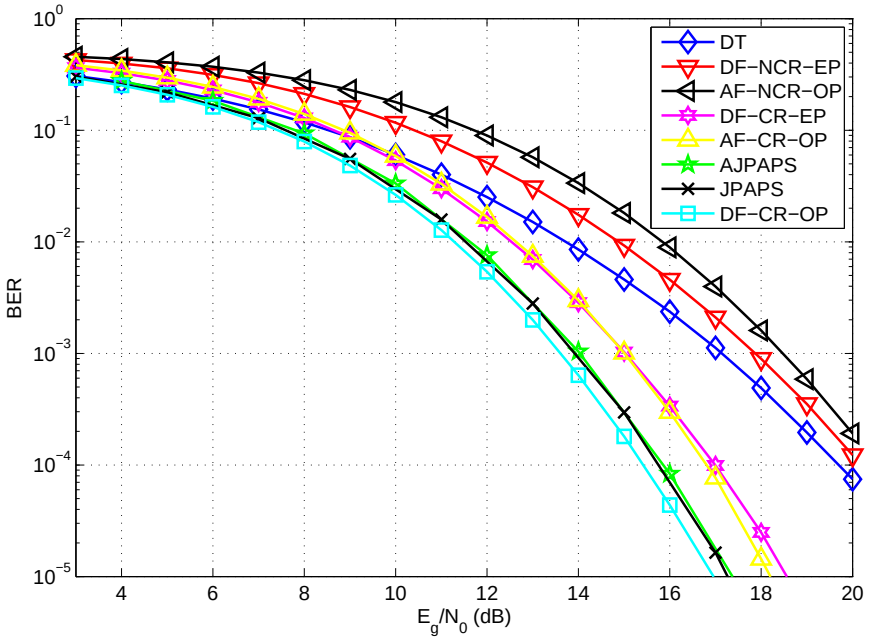

Figure 34: BER as a function of the SNR for various transmission schemes (NC2).

a more favorable path exists as well, i.e., the relayed path $\mathcal{P}(\mathrm{S}, \mathrm{R}_1, \mathrm{R}_2, \mathrm{D})$. Thus, the DF-NCR-EP based on $\mathcal{P}(\mathrm{S}, \mathrm{R}_1, \mathrm{R}_2, \mathrm{D})$ shows a performance gain of 4 dB over the DF-NCR-EP based on $\mathcal{P}(\mathrm{S}, \mathrm{R}_1, \mathrm{D})$ and even of 7 dB with respect to the DT. On the other hand, for the square configuration NC4 of Figure 36, $\mathcal{P}(\mathrm{S}, \mathrm{R}_1, \mathrm{R}_2, \mathrm{D})$ is no longer the most convenient path, and the DF-NCR-EP that employs that route is outperformed by the DT and the DF-NRC-EP based on $\mathcal{P}(\mathrm{S}, \mathrm{R}_1, \mathrm{D})$, which come out to be almost equivalent. By applying the proposed JPAPS (or the AJPAPS, which again yields the same error performance), a considerable gain of about 4 dB is enabled on the DF-NCR-EP for NC3, which goes up to 5 dB for NC4. Interestingly, the JPAPS keeps on having an advantage of 2 dB for both NC3 and NC4 also against the cooperative DF-CR-EP, in spite of requiring a much lower complexity.

As the last test case, Figure 37 refers to the configuration NC5 in which up to $N = 10$ relays can be adopted by the transmission schemes. To be specific, the DF-NCR-OP scheme that employs the path $\mathcal{P}(\mathrm{S}, \mathrm{R}_\mathrm{c}, \mathrm{D})$, where R_c is the relay located at the center of the square, exhibits a gain of more than 6 dB compared to

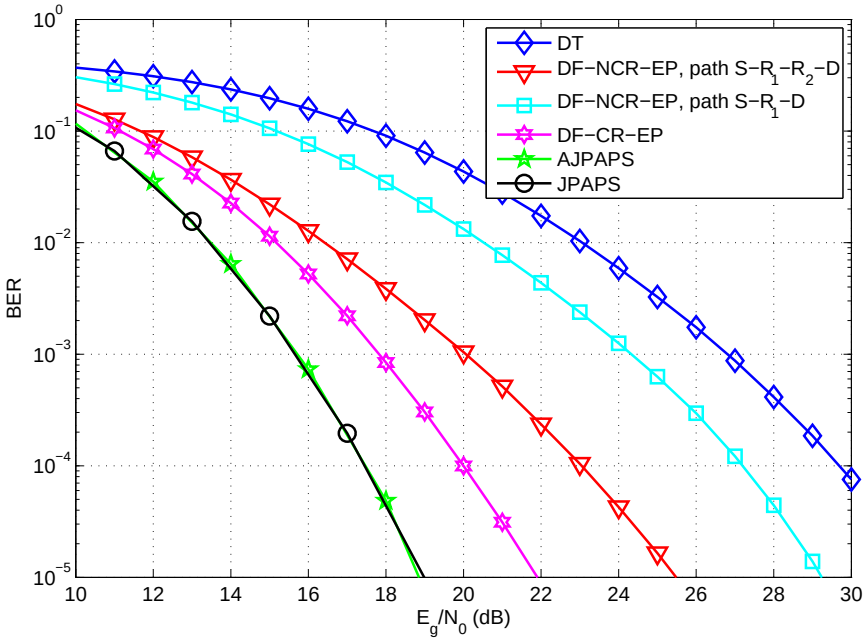

Figure 35: BER as a function of the SNR for various transmission schemes (NC3).

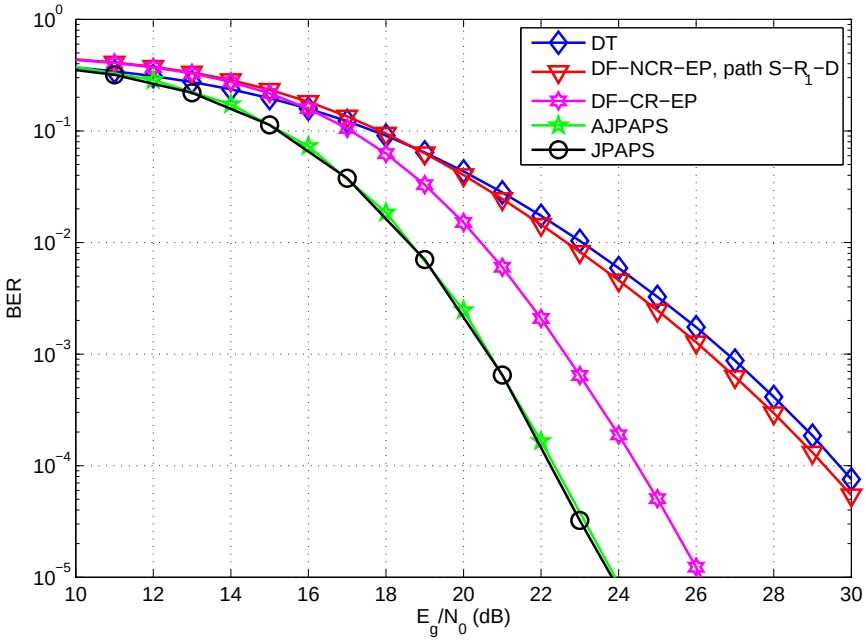

Figure 36: BER as a function of the SNR for various transmission schemes (NC4).

the DT, while, without optimizing the PA coefficients, the advantage on the direct transmission reduces to 5 dB. Notice that the proposed JPAPS, even when only one relay can be used, brings an additional performance gain of 4.5 dB relative to the DF-NCR-OP, which always adopts the relay R_c. Then, if all the relays are available for transmission, the multi-hop JPAPS (and also its approximated version) considerably outperforms the dual-hop JPAPS scheme by more than 6 dB.

Hence, the results obtained for the multi-hop scenarios corroborate the effectiveness of the proposed JPAPS and AJPAPS techniques, which show remarkable gains compared to the benchmark schemes specified in Sec. 7.5.1.

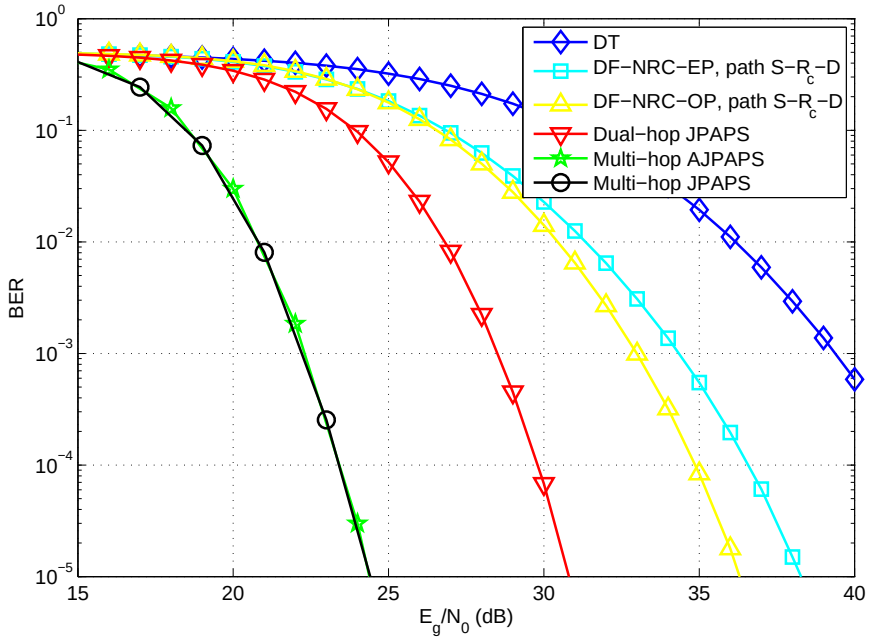

Figure 37: BER as a function of the SNR for various transmission schemes (NC5).

CHAPTER VIII

GENERALIZED CODE-MULTIPLEXING FOR UWB SYSTEMS

8.1 Introduction

The differential UWB receivers enable simple receiver structures, but the delay component required by the correlation unit, amounting to tens or even hundreds of nanoseconds, presents a non negligible drawback in terms of hardware implementation. In both cases, the delay component is built via either analog circuitry or digital sampling [83, 24, 12]. However, they still suffer from the need for accurate delay lines on the order of multiples of symbol intervals.

To overcome the implementation issue posed by the delay components, the frequency-shifted reference (FSR) system has been proposed to separate the reference and data-modulated signals in the frequency domain at the price of requiring an analog carrier [30]. The FSR is further simplified by the code-multiplexed TR (CM-TR) [18] and code-shifted reference (CSR) [61] schemes based on orthogonal code sequence design. Noteworthy, both systems are promising schemes as they require neither delay elements nor analog carriers, while even exhibiting better bit error rate (BER) performance compared to the FSR solution.

The aim of this section is to generalize the CM-TR and CSR concepts through a novel design we refer to as "generalized code-multiplexing," or GCM [102, 103] for short in the following. The rationale of the proposed transmitter and receiver structure relies on the formulation of a constrained optimization problem (OP), which maximizes the BER performance metric under a given set of constraints mainly adopted to keep complexity at affordable levels. Several features differentiate the

proposed approach from previous work and define our contributions.

1. The GCM inherits the basic structure of the CM-TR and CSR systems based on a simple energy detector without any delay line components. As a further step, however, after solving offline a joint OP on the transmitted and decoding codes for a given frame size N_f and number of information symbols M conveyed within each block, improved BER link performance and higher spectral efficiency are enabled.

2. When the frame size $N_f > 2^M$, the non-deterministic polynomial hard (NP-hard) nature of the original constrained OP can circumvented by deriving the closed-form optimal solution from an equivalent system with $N_f = 2^M$.

3. To take account of the emission power restriction imposed by the Federal Communications Commission (FCC) for UWB communications, we develop the GCM systems with peak power constraint, which can maintain the same error performance as the existing designs while enjoying lower peak power levels.

4. The GCM framework is then extended to the more general case when inter-frame interference (IFI) arises, as typically occurs in high data rate transmissions. Through the formulation of an OP based on a properly modified signal model, the IFI effects can be mitigated, and thus obtaining a considerable performance improvement compared to some existing codes.

8.2 System Model

Consider the GCM system depicted in Fig. 38. A sequence of M information symbols $\mathbf{a} \triangleq [a_1, \cdots, a_M]^T, a_i \in \{\pm 1\}$ are encoded at the transmitter into a block of N_f frame symbols $\mathbf{b} \triangleq \left[b_0, \cdots, b_{N_f-1}\right]^T$ according to the rule $\mathbf{b} = \boldsymbol{\chi}(\mathbf{a})$, $\boldsymbol{\chi} \triangleq [\chi_0, \chi_1, \cdots, \chi_{N_f-1}]^T$. Thus, the transmitted signal corresponding to the data block $\mathbf{a}$

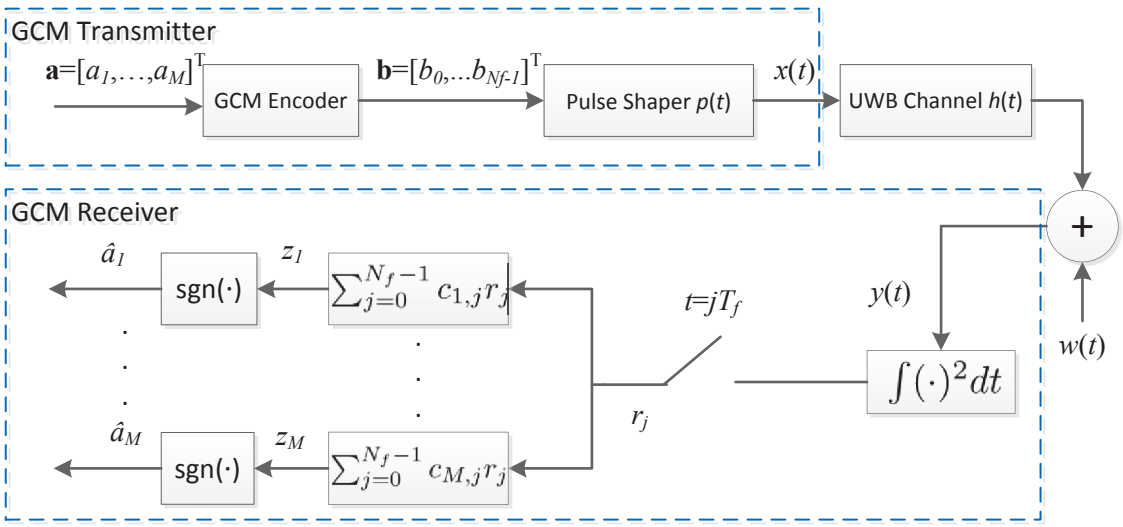

Figure 38: System diagram of a block transmission for GCM systems.

can be written as

$$x(t) = \sum_{j=0}^{N_f-1} b_j p(t - jT_f), \tag{141}$$

where $p(t)$ is the Gaussian monocycle pulse with duration T_p, N_f is the number of frames in the block, and T_f is the frame interval. Note that, for the time being, inter-frame interference (IFI) is avoided by choosing $T_f > T_m + T_p$, where T_m is defined as the maximum excess delay of the channel; however this assumption will be dropped in Sec. 8.4. For the sake of notational simplicity, we do not explicitly consider the typical frame structure for time hopping (TH) in that it can be removed at the receiver prior to further signal processing without incurring IFI under the condition of sufficiently long T_f.

The UWB propagation channel is assumed to be highly frequency-selective with the channel impulse response (CIR) modeled as

$$h(t) = \sum_{n=0}^{N_p-1} \alpha_n \delta(t - \tau_n), \tag{142}$$

where N_p is the total number of paths with amplitude α_n and delay τ_n. The channel coherence time, wherein the CIR stays approximately constant, is assumed to be longer than the block transmission interval $T_b = T_f N_f$.

After processing the received signal with a low-pass filter[1] having impulse response $f_{\rm rx}(t)$, which eliminates the out-of-band (OOB) interference and noise, in correspondence of (141), we obtain

$$x(t) = \sum_{j=0}^{N_f-1} b_j g(t - jT_f) + w(t), \tag{143}$$

where $w(t)$ is a band-limited AWGN component with two-sided power spectrum density $N_0/2$, and the channel template $g(t) \triangleq p(t) * h(t) * f_{\rm rx}(t)$ has frame energy $E_f \triangleq \int_0^{T_m+T_p} g^2(t)dt$.

Under the assumption that timing has been acquired, energy integration is performed on the received signal

$$r_j = \int_{jT_f}^{(j+1)T_f} x^2(t)dt, \quad j \in \mathcal{J}, \tag{144}$$

with $\mathcal{J} \triangleq \{0, \cdots, N_f-1\}$. Then, the decision variable for the kth information symbol is obtained as

$$z_k = \mathbf{c}_k^T \mathbf{r}, \quad k \in \mathcal{K}, \tag{145}$$

where $\mathbf{c}_k \triangleq [c_{k,0}, c_{k,1}, \cdots, c_{k,N_f-1}]^T$ is the decoding vector, $\mathbf{r} \triangleq [r_0, r_1, \cdots, r_{N_f-1}]^T$ includes the outputs in (144), and $\mathcal{K} \triangleq \{1, \cdots, M\}$. As a final step, the estimate of the information symbol is given by

$$\hat{a}_k = \text{sgn}(z_k), \quad k \in \mathcal{K}. \tag{146}$$

The system model in Eqs. (141), (143)-(146) subsumes some existing code-multiplexed (CM) designs.

1. *Code-Multiplexed Transmitted Reference (CM-TR)* The CM-TR system transmits the reference and the data-modulated signals together with $M = 1$[18]. The CM-TR encoder is specified by

$$b_j = \chi_j(a_1) = d_j + a_1 u_j, \quad j \in \mathcal{J}, \tag{147}$$

[1] A quite similar system model holds in the case of employing a bandpass filter.

where the codewords $\mathbf{d} \triangleq [d_0, d_1, \cdots, d_{N_f-1}]^T$ and $\mathbf{u} \triangleq [u_0, u_1, \cdots, u_{N_f-1}]^T$ used for the reference and the data-modulated signals, respectively, have the properties: *i*) $d_j, u_j \in \{\pm 1\}$, $j \in \mathcal{J}$; and *ii*) they are orthogonal, i.e., $\mathbf{d}^T\mathbf{u} = 0$. At the receiver, the integrator output $\mathbf{r}$, after being correlated by the decoding vector $\mathbf{c}_1 = \mathbf{d} \odot \mathbf{u}$, yields the decision variable for the information symbol transmitted at each block. Note that, in fact, the CM-TR system can be considered as a generalized binary pulse position modulation (B-PPM) [81].

2. *Code-Shifted Reference (CSR)* In the CSR system, $M \geq 1$ information symbols $\mathbf{a}$ are transmitted into N_f frames according to the encoding rule [61]

$$b_j = \chi_j(\mathbf{a}) = \sqrt{M} v_{0,j} + \sum_{k=1}^{M} a_k v_{k,j}, \quad j \in \mathcal{J}, \tag{148}$$

where among the transmitted codewords $\mathbf{v}_k \triangleq [v_{k,0}, v_{k,1}, \cdots, v_{k,N_f-1}]^T, k \in \{0\} \cup \mathcal{K}$, the codeword with $k = 0$ ($\mathbf{v}_0$) is for the reference signal, whereas those for $k \in \mathcal{K}$ are used for the M information symbols. For data detection, the transmitted codewords $\mathbf{v}_k$ and decoding vectors $\mathbf{c}_k$ are chosen such that the following conditions are satisfied:

C1) $c_{k,j}, v_{i,j} \in \{\pm 1\}, k \in \mathcal{K}, j \in \mathcal{J}, i \in \{0\} \cup \mathcal{K}$;

C2) $\sum_{j=0}^{N_f-1} c_{k,j} = 0, k \in \mathcal{K}$;

C3) $\mathbf{c}_k^T(\mathbf{v}_0 \odot \mathbf{v}_i) = \begin{cases} N_f, & i = k, k \in \mathcal{K} \\ 0, & i \neq k, i \in \{0\} \cup \mathcal{K}, k \in \mathcal{K} \end{cases}$;

C4) $\mathbf{c}_k^T(\mathbf{v}_i \odot \mathbf{v}_j) = 0, \forall i, j, k \in \mathcal{K}$.

The following comments are worth emphasizing.

(a) To comply with C1)-C4), Walsh codes are employed for $\mathbf{v}_k$ and $\mathbf{c}_k$ in [61, Table 1].

(b) At most, $M = N_f/2$ information symbols can be encoded into N_f frames. This is because, for the Walsh codes with length 2^N, there exist, at most, $2^{N-1}+1$ transmitted codewords and 2^{N-1} decoding vectors that satisfy conditions C1)-C4).

8.3 GCM Optimal Design

In this section, we formulate a constrained OP to design the GCM encoder $\mathbf{b} = \boldsymbol{\chi}(\mathbf{a})$ and decoding matrix $\mathbf{C} \triangleq [\mathbf{c}_1, \cdots, \mathbf{c}_M]$ so that the link performance in terms of the BER metric is optimized under a given set of assumptions.

8.3.1 Formulation of GCM Systems

Let us first define the GCM system we are dealing with, which subsumes CM-TR and CSR as special cases.

Definition 1. *A transmitter with encoder* $\mathbf{b} = \boldsymbol{\chi}(\mathbf{a})$ *and a receiver with decoding matrix* $\mathbf{C}$ *form a GCM system if the following assumptions are satisfied:*

A1) $c_{k,j} \in \{\pm 1\}, k \in \mathcal{K}, j \in \mathcal{J}$*;*

A2) $\sum_{j=0}^{N_f-1} c_{k,j} = 0, k \in \mathcal{K}$*;*

A3) The error probabilities on $a_k, k \in \mathcal{K}$ *are equal.*

Then, we derive an equivalent definition of the GCM system that will be particularly useful to formulate the GCM OP. To be specific, we take the conditions of both the absence of IFI and sufficiently large product BT_f, B being the bandwidth of the receiver low-pass filter $f_{\text{rx}}(t)$.

Proposition 6. *A GCM system with encoder* $\mathbf{b} = \boldsymbol{\chi}(\mathbf{a})$ *and decoding matrix* $\mathbf{C}$ *holds if assumption A3) is replaced by A3a)-A3b) as:*

A1) $c_{k,j} \in \{\pm 1\}, k \in \mathcal{K}, j \in \mathcal{J}$*;*

A2) $\sum_{j=0}^{N_f-1} c_{k,j} = 0, k \in \mathcal{K}$;

A3a) $\mathbf{c}_k^T(\mathbf{b}_i \odot \mathbf{b}_i) = \Psi\, a_{i,k},\ i \in \mathcal{I},\ k \in \mathcal{K}$;

A3b) $\|\mathbf{b}_i\|_2^2 = E_{\mathbf{b}},\ i \in \mathcal{I}$,

where $\mathbf{a}_i \triangleq [a_{i,1}, \cdots, a_{i,M}]^T$ *and* $\mathbf{b}_i \triangleq \left[b_{i,0}, \cdots, b_{i,N_f-1}\right]^T$, *with* $i \in \mathcal{I} \triangleq \{1, \cdots, 2^M\}$, *denote the realizations of the information symbol* $\mathbf{a}$ *and the transmitted symbol* $\mathbf{b}$, *respectively, with* $\mathbf{b}_i = \boldsymbol{\chi}(\mathbf{a}_i)$; $E_{\mathbf{b}}$ *is the energy of the transmitted symbol* $\mathbf{b}_i$, *assumed to be constant* $\forall i \in \mathcal{I}$; *and* Ψ *is a parameter that strictly depends on both the encoding rule* $\mathbf{b} = \boldsymbol{\chi}(\mathbf{a})$ *and the decoding matrix* $\mathbf{C}$.

Proof. See Appendix C. □

Now, a key result about the GCM system is ready to be derived, as stated in the sequel.

Proposition 7. *Assuming a GCM system with encoder* $\boldsymbol{\chi}(\mathbf{a})$ *and decoding matrix* $\mathbf{C}$ *satisfying Proposition 6, the BER performance is asymptotically approximated in terms of the twice time-bandwidth product* $L \triangleq \lceil 2BT_f \rceil$ *when* L *is large as*

$$\mathrm{BER}_{\mathrm{GCM}}(\Omega) = Q\left[\Omega\left(\frac{2M}{\gamma} + \frac{N_f L}{2\gamma^2}\right)^{-1/2}\right], \tag{149}$$

where $\Omega \triangleq M\Psi/E_{\mathbf{b}}$, $\gamma \triangleq E_{bit}/N_0$ *is the received-bit-energy-to-noise-spectral-density ratio, and* $Q(x) \triangleq \frac{1}{\sqrt{2\pi}} \int_x^\infty \exp(-t^2/2)dt$.

Proof. See Appendix D. □

Given Propositions 6-7, we are now ready to establish the relationship between our GCM systems and existing systems.

Corollary 2. *The CM-TR system is a GCM system with* $M = 1$ *and* $\Omega = 1$.

Proof. First, it can be shown that assumptions A1)-A2) hold for the CM-TR system as well. The entries of the decoding vector $\mathbf{c}_1 = \mathbf{d} \odot \mathbf{u}$ take values in $\{\pm 1\}$, while

$$\sum_{j=0}^{N_f-1} c_{1,j} = \mathbf{d}^T \mathbf{u} = 0. \tag{150}$$

Then, the signal component in the decision variable $z_1 = \mathbf{c}_1^T \mathbf{r}$ can be rearranged as

$$\begin{aligned} \mathbf{c}_1^T(\mathbf{b} \odot \mathbf{b}) &= (\mathbf{d} \odot \mathbf{u})^T \left[(\mathbf{d} + a_1\mathbf{u}) \odot (\mathbf{d} + a_1\mathbf{u})\right] \\ &= 2(\mathbf{d} \odot \mathbf{u})^T \left[\mathbf{1}_{N_f \times 1} + a_1(\mathbf{d} \odot \mathbf{u})\right] = 2N_f a_1, \end{aligned} \tag{151}$$

and the energy of the transmitted symbols $\mathbf{b}_1$ (corresponding to a_1) becomes

$$E_{\mathbf{b}} = \|\mathbf{b}_1\|_2^2 = (\mathbf{d} + a_1\mathbf{u})^T(\mathbf{d} + a_1\mathbf{u}) = 2N_f, \tag{152}$$

which indicates that assumptions A3a)-A3b) hold. Therefore, by exploiting the results derived in the proof of Propositions 1-7, we conclude that the CM-TR system is a special case of GCM systems with $\Omega = 1$. □

Corollary 3. *The CSR system is equivalent to a GCM system with* $\Omega = \sqrt{M}$.

Proof. In order to prove the equivalence between the CSR under C1)-C4) and the GCM under A1)-A3b) for a particular objective value Ω, let us start by replacing the expression obtained from (148) for a generic realization of the transmitted symbols $\mathbf{b} = \sqrt{M}\mathbf{v}_0 + \sum_{i=1}^{M} a_i \mathbf{v}_i$ into the signal component at the integrator output given by A3a). Thus, applying conditions C3)-C4) yields

$$\begin{aligned} \mathbf{c}_k^T(\mathbf{b} \odot \mathbf{b}) = M\mathbf{c}_k^T(\mathbf{v}_0 \odot \mathbf{v}_0) + 2\sqrt{M}\sum_{i=1}^{M} a_i \mathbf{c}_k^T(\mathbf{v}_0 \odot \mathbf{v}_i) \\ + \sum_{i=1}^{M}\sum_{j=1}^{M} a_i a_j \mathbf{c}_k^T(\mathbf{v}_i \odot \mathbf{v}_j) = 2\sqrt{M} N_f a_k, \quad k \in \mathcal{K}, \end{aligned} \tag{153}$$

which indicates that assumption A3a) holds for the CSR as well, with $\Psi = 2\sqrt{M}N_f$. Furthermore, due to the property $\mathbf{v}_i^T \mathbf{v}_j = 0$, $i \neq j$, exhibited by the Walsh codes, we

obtain

$$E_{\mathbf{b}} = \|\mathbf{b}\|_2^2 = \left(\sqrt{M}\mathbf{v}_0 + \sum_{j=1}^{M} a_j \mathbf{v}_j\right)^T \left(\sqrt{M}\mathbf{v}_0 + \sum_{i=1}^{M} a_i \mathbf{v}_i\right) = 2MN_f, \tag{154}$$

which proves that the CSR also satisfies A3b). As a result, in view of the proof of Propositions 1-7, the CSR system is a special case of GCM systems with $\Omega = \sqrt{M}$. $\square$

8.3.2 Optimization Problem for GCM Systems

According to Proposition 7, it can be recognized that given N_f, M, and L the BER performance metric is optimized whenever the encoder $\mathbf{b} = \boldsymbol{\chi}(\mathbf{a})$ and the decoding matrix $\mathbf{C}$ are designed so that Ω in (149) is maximized under assumptions A1)-A3b). Hence, Ω is just the objective function of the OP we are addressing. As such, in light of A3a), it will be denoted in the sequel as $\Omega(\mathbf{C}, \mathbf{X})$, namely depending on both the decoding matrix $\mathbf{C}$ and the $N_f \times 2^M$ matrix $\mathbf{X} \triangleq [\mathbf{x}_1, \cdots, \mathbf{x}_{2^M}]$ with $\mathbf{x}_i \triangleq \mathbf{b}_i \odot \mathbf{b}_i \triangleq [x_{i,0}, \cdots, x_{i,N_f-1}]^T, i \in \mathcal{I}$. Hence, after designating the $M \times 2^M$ matrix as $\mathbf{A} \triangleq [\mathbf{a}_1, \cdots, \mathbf{a}_{2^M}]$, we formulate the GCM joint constrained OP over $\mathbf{C}$ and $\mathbf{X}$, or joint OP (J-OP) for short, as

$$\begin{cases} (\mathbf{C}_{\mathrm{o}}, \mathbf{X}_{\mathrm{o}}) = \arg\max\limits_{\mathbf{C},\mathbf{X}} \{\Omega(\mathbf{C}, \mathbf{X})\} \\ \text{s.t.} \qquad \mathbf{C}^T\mathbf{X} = \Omega(\mathbf{C}, \mathbf{X})\mathbf{A} \\ \qquad\quad \mathbf{1}_{N_f \times 1}^T \mathbf{X} = M\mathbf{1}_{2^M \times 1}^T \\ \qquad\quad \mathbf{X} \geq \mathbf{0}_{N_f \times 2^M} \\ \qquad\quad \mathbf{C}^T\mathbf{1}_{N_f \times 1} = \mathbf{0}_{M \times 1} \\ \qquad\quad \mathbf{C} \odot \mathbf{C} = \mathbf{1}_{N_f \times M} \end{cases}, \tag{155}$$

where for convenience, we set $E_{\mathbf{b}} = M$; $\mathbf{X} \geq \mathbf{0}_{N_f \times 2^M}$ means that all entries of $\mathbf{X}$ are greater than or equal to 0; $\mathbf{C} \odot \mathbf{C} = \mathbf{1}_{N_f \times M}$ means that the entries of $\mathbf{C}$ take values in $\{\pm 1\}$; and the objective function is given by

$$\Omega(\mathbf{C}, \mathbf{X}) = \frac{1}{M2^M} \cdot \mathbf{1}_{M \times 1}^T \left[(\mathbf{C}^T\mathbf{X}) \odot \mathbf{A}\right] \mathbf{1}_{2^M \times 1}, \tag{156}$$

which can be obtained from the first constraint of (155) originating from A3a). If the decoding matrix $\mathbf{C}$ is given, the J-OP in (155) is simplified to

$$\begin{cases} \mathbf{X}_{\text{o}} = \arg\max\limits_{\mathbf{X}} \{\Omega(\mathbf{X})\} \\ \text{s.t.} \quad \mathbf{C}^T\mathbf{X} = \Omega(\mathbf{X})\mathbf{A} \\ \qquad\quad \mathbf{1}_{N_f\times 1}^T\mathbf{X} = M\mathbf{1}_{2^M\times 1}^T \\ \qquad\quad \mathbf{X} \geq \mathbf{0}_{N_f\times 2^M} \end{cases}, \tag{157}$$

labeled as GCM encoder-based OP, or E-OP for short.

Now, the following remarks about the OPs (155)-(157) are of interest.

1. The J-OP in (155) is a mixed integer programming (MIP) problem since the optimization has to be performed over the matrices $\mathbf{C}$ and $\mathbf{X}$, whose entries take integer and real values, respectively. As a result, it is generally NP-hard, and its computational complexity is really demanding even for small N_f and M. As will be shown in Sec. 8.3.3, however, the optimal transmitted and decoding code matrices for $N_f \geq 2^M$ can be found by solving an equivalent problem for $N_f = 2^M$ with a closed-form optimal solution. In contrast, the (sub-optimal) E-OP in (157), which belongs to the class of linear programming (LP) OPs, can be solved by applying some well-known polynomial-complexity algorithms (see e.g., [43, 9]).

2. The optimal GCM design offers several advantages over the existing CM-TR and CSR: *i*) BER performance can be improved; *ii*) the system design does not rely on the properties of any codeword set, such as the Walsh codes; *iii*) the E-OP allows the optimization on any given decoding matrix satisfying A1)-A2) only; *iv*) the frame length N_f is not restricted to the form 2^N, with N being some integers, as required by the CSR; and *v*) the number of symbols M that can be embedded into a single data block, can be greater than those of the CM-TR ($M = 1$) and the CSR ($M \leq N_f/2$), which results in a higher spectral

efficiency.

3. The solutions to the J-OP or E-OP aim at optimizing the BER performance. The GCM framework gives the freedom to consider alternative optimization criteria as well. A viable option is to minimize the peak power of the transmitted signal (141) [3] under a predefined BER level determined by a value of Ω, say Ω_{c}, with $\Omega_{\mathrm{c}} \leq \Omega_{\mathrm{o}}$, Ω_{o} denoting the optimal objective value of J-OP in (155). This means to constrain the entries of the matrix $\mathbf{X}$ to be below a threshold Υ, or more formally $[\mathbf{X}]_{i,j} \leq \Upsilon$, $\forall j \in \mathcal{J}$, $\forall i \in \mathcal{I}$, and to modify the first constraint of (155) into $\mathbf{C}^T\mathbf{X} = \Omega_{\mathrm{c}}\mathbf{A}$. Hence, the corresponding OP is to minimize the peak power Υ while keeping the average power as $\mathbf{1}_{N_f\times 1}^T\mathbf{X} = M\mathbf{1}_{2^M\times 1}^T$. Thus, this peak power based OP, or PP-OP for short, can be formulated as

$$\begin{cases} (\mathbf{C}_{\mathrm{o}}, \mathbf{X}_{\mathrm{o}}) = \arg\min\limits_{\mathbf{C},\mathbf{X}} \{\Upsilon(\mathbf{C}, \mathbf{X})\} \\ \text{s.t.} \quad \mathbf{X} \leq \Upsilon(\mathbf{C}, \mathbf{X})\mathbf{1}_{N_f\times 2^M} \\ \qquad \mathbf{C}^T\mathbf{X} = \Omega_{\mathrm{c}}\mathbf{A} \\ \qquad \mathbf{1}_{N_f\times 1}^T\mathbf{X} = M\mathbf{1}_{2^M\times 1}^T \\ \qquad \mathbf{X} \geq \mathbf{0}_{N_f\times 2^M} \\ \qquad \mathbf{C}^T\mathbf{1}_{N_f\times 1} = \mathbf{0}_{M\times 1} \\ \qquad \mathbf{C} \odot \mathbf{C} = \mathbf{1}_{N_f\times M} \end{cases} . \tag{158}$$

4. For practical UWB communications with predetermined system parameters, i.e., N_f and M, the J-OP can be solved offline, and the optimized encoder $\boldsymbol{\chi}(\mathbf{a})$ and decoding matrix $\mathbf{C} \triangleq [\mathbf{c}_1, \cdots, \mathbf{c}_M]$ can be stored locally as look-up tables at the transmitter and the receiver. When the system parameters are determined in the real-time communications, the transmitter can solve J-OP and then send the optimized decoding matrix to the receiver as preamble, or a central unit can optimize the J-OP and send the optimized results to both the transmitter and the receiver.

8.3.3 Optimal Codes for Large Frame Size N_f

The considerable complexity of the MIP constrained J-OP in (155) when $N_f > 2^M$ can be avoided by analytically solving an equivalent problem with $N_f = 2^M$. For the sake of convenience, the following two lemmas can help, where we designate the original J-OP in (155) with frame length $N_f > 2^M$ as "larger problem," or LJ-OP, and the corresponding equivalent J-OP with $N_f = 2^M$ as "smaller problem," or SJ-OP.

Lemma 1. *For any feasible solution to the LJ-OP, there exists a feasible solution to the SJ-OP such that the solutions provide the same objective value* Ω.

Proof. See Appendix E. □

Lemma 2. *Assume that the mappings* $\Gamma : \mathbf{A}_{2^M \times M} \rightarrow \mathbf{B}_{N_f \times M}$ *and* $\Lambda : \mathbf{A}_{2^M \times 2^M} \rightarrow \mathbf{B}_{N_f \times 2^M}$ *exist such that for any feasible solution* $(\mathbf{C}, \mathbf{X})$ *to the SJ-OP,* $[\Gamma(\mathbf{C}), \Lambda(\mathbf{X})]$ *is the feasible solution corresponding to the LJ-OP, both with the same objective value, i.e.,* $\Omega(\mathbf{C}, \mathbf{X}) = \Omega\left[\Gamma(\mathbf{C}), \Lambda(\mathbf{X})\right]$. *Then,* $[\Gamma(\mathbf{C}_\mathrm{o}), \Lambda(\mathbf{X}_\mathrm{o})]$ *is the optimal solution to the LJ-OP, when* $(\mathbf{C}_\mathrm{o}, \mathbf{X}_\mathrm{o})$ *is the optimal solution of the SJ-OP.*

Proof. Corresponding to the optimal solution $(\mathbf{C}_\mathrm{o}, \mathbf{X}_\mathrm{o})$ for the SJ-OP, there exists a feasible solution $[\Gamma(\mathbf{C}_\mathrm{o}), \Lambda(\mathbf{X}_\mathrm{o})]$ for the LJ-OP such that $\Omega(\mathbf{C}_\mathrm{o}, \mathbf{X}_\mathrm{o}) = \Omega\left[\Gamma(\mathbf{C}_\mathrm{o}), \Lambda(\mathbf{X}_\mathrm{o})\right] = \Omega_\mathrm{o}$. Then, $[\Gamma(\mathbf{C}_\mathrm{o}), \Lambda(\mathbf{X}_\mathrm{o})]$ must also be optimal since if there exists a solution $(\mathbf{C}', \mathbf{X}')$ to the LJ-OP which is better than $[\Gamma(\mathbf{C}_\mathrm{o}), \Lambda(\mathbf{X}_\mathrm{o})]$, i.e., with $\Omega(\mathbf{C}', \mathbf{X}') > \Omega\left[\Gamma(\mathbf{C}_\mathrm{o}), \Lambda(\mathbf{X}_\mathrm{o})\right]$, according to Lemma 1, there would exist a feasible solution for the SJ-OP with objective value equal to $\Omega(\mathbf{C}', \mathbf{X}')$ greater than $\Omega(\mathbf{C}_\mathrm{o}, \mathbf{X}_\mathrm{o})$, which results in a contradiction. □

Lemmas 1 and 2 allow us to establish a one-to-one relationship between the optimal solutions of the GCM J-OPs with $N_f > 2^M$ and those with $N_f = 2^M$. Thus, the problem is how to find the mappings Γ and Λ. A simple option is to apply the zero

padding method, which gives

$$\mathbf{C}_{N_f\times M}=\Gamma_{\rm zp}(\mathbf{C}'_{2^M\times M})=\begin{bmatrix}\mathbf{C}'_{2^M\times M}\\ \mathbf{1}_{((N_f-2^M)/2)\times M}\\ -\mathbf{1}_{((N_f-2^M)/2)\times M}\end{bmatrix}, \tag{159}$$

$$\mathbf{X}_{N_f\times 2^M}=\Lambda_{\rm zp}(\mathbf{X}'_{2^M\times 2^M})=\begin{bmatrix}\mathbf{X}'_{2^M\times 2^M}\\ \mathbf{0}_{(N_f-2^M)\times 2^M}\end{bmatrix}, \tag{160}$$

or alternatively, the repetition codes with $N_f=P2^N$, P being a positive integer, as

$$\mathbf{C}_{N_f\times M}=\Gamma_{\rm rc}(\mathbf{C}'_{2^M\times M})=\mathbf{1}_{P\times 1}\otimes\mathbf{C}'_{2^M\times M}, \tag{161}$$

$$\mathbf{X}_{N_f\times 2^M}=\Lambda_{\rm rc}(\mathbf{X}'_{2^M\times 2^M})=\frac{1}{P}\mathbf{1}_{P\times 1}\otimes\mathbf{X}'_{2^M\times 2^M}. \tag{162}$$

It can be easily verified that $[\Gamma(\mathbf{C}),\Lambda(\mathbf{X})]$ in (159)-(162) is the feasible solution for LJ-OP, given the feasible solution $(\mathbf{C},\mathbf{X})$ for the SJ-OP, and the solutions provide the same objective value Ω.

Now, the next step is to show that the optimal encoding and decoding matrices solving the SJ-OP can be analytically found, as stated in the sequel.

Proposition 8. *Considering the GCM system with $N_f=2^M$, the optimal decoding matrix $\mathbf{C}_{\rm o}$ is the $2^M\times M$ matrix*

$$\mathbf{C}_{\rm o}=[\mathbf{z}_1,\cdots,\mathbf{z}_{2^M}]^T, \tag{163}$$

where the vectors $\mathbf{z}_i$, $i\in\mathcal{I}$, are all the 2^M realizations of length M with entries ±1. In addition, the optimal encoder for the information symbols $\mathbf{a}$ is given by

$$b_j=\chi_j(\mathbf{a})=\begin{cases}\pm\sqrt{M}, & \mathbf{z}_j=\mathbf{a}\\ 0, & \text{otherwise}\end{cases},\quad j\in\mathcal{J}, \tag{164}$$

with the optimal objective value $\Omega_{\rm o}=M$.

Proof. See Appendix F. □

As a further result, Lemmas 1-2 can be exploited together with Proposition 8 to derive the optimal performance of the GCM system with $N_f \geq 2^M$, as summarized in the following proposition.

Proposition 9. *For a GCM system with $N_f \geq 2^M$, the optimal BER performance can be asymptotically approximated as a function of the received-bit-energy-to-noise-spectral-density ratio γ (defined after Eq. (149)) by*

$$\mathrm{BER}_{\mathrm{GCM}}|_{N_f \geq 2^M} = Q\left[\left(\frac{2}{\gamma M} + \frac{N_f L}{2\gamma^2 M^2}\right)^{-1/2}\right]. \tag{165}$$

Proof. This follows from Lemmas 1-2 and Proposition 8 by plugging $\Omega_{\mathrm{o}} = M$ into (149). □

The following remark about the optimal codes of GCM systems is now of interest.

- When $N_f = 2^M$, the optimal GCM system derived in Proposition 8 is essentially an M-PPM, and when $N_f > 2^M$, the optimal GCM system can be treated as a generalized M-PPM (e.g., PPM with zero padding or repetition in Eqs. (159)-(162)). However, different from the conventional PPM, where data symbols are carried via different delays of the transmitted pulse, the GCM systems convey the data symbols via the amplitude values of frame symbols $\mathbf{b}$, thus allowing higher data rate communications by embedding more symbols in one block, i.e., $M > \log_2(N_f)$, than the M-PPM, and enabling the system optimization with emission power constraint.

8.4 Code Design for Transmissions with IFI

This section extends the GCM framework to the case of high-rate transmissions where IFI arises when the frame interval T_f is shorter than the channel delay spread. To maintain a reasonable complexity, we will avoid an overall (constrained) optimization of the codeword matrices $\mathbf{C}$ and $\mathbf{X}$ as made in the J-OP (155) in the case of the absence of IFI. Instead, a sub-optimal yet effective IFI-mitigation method will be

pursued based on a two-step procedure with a simple rationale. The basic result we will exploit can be summarized in the following lemma.

Lemma 3. *Any permutation of the feasible solution* $(\mathbf{C}, \mathbf{X})$ *to J-OP (155), namely* $(\bar{\mathbf{C}}, \bar{\mathbf{X}}) = (\mathbf{PC}, \mathbf{PX})$ *with* $\mathbf{P}$ *being an* $N_f \times N_f$ *permutation matrix, is still a feasible solution satisfying all the constraints with the same objective value* Ω*.*

Proof. From (155), it can be obtained that: *i)* $\bar{\mathbf{C}}^T\bar{\mathbf{X}} = \mathbf{C}^T\mathbf{P}^T\mathbf{PX} = \mathbf{C}^T\mathbf{X} = \Omega\mathbf{A}$; *ii)* $\mathbf{1}_{N_f\times 1}^T\bar{\mathbf{X}} = \mathbf{1}_{N_f\times 1}^T\mathbf{PX} = \mathbf{1}_{N_f\times 1}^T\mathbf{X} = M\mathbf{1}_{2^M\times 1}^T$; *iii)* $\bar{\mathbf{C}}^T\mathbf{1}_{N_f\times 1} = \mathbf{C}^T\mathbf{P}^T\mathbf{1}_{N_f\times 1} = \mathbf{C}^T\mathbf{1}_{N_f\times 1} = \mathbf{0}_{M\times 1}$; and *iv)* $\bar{\mathbf{C}} \odot \bar{\mathbf{C}} = \mathbf{C} \odot \mathbf{C} = \mathbf{1}_{N_f\times M}$. Since all the constraints are satisfied, it can be concluded that both $(\mathbf{X}, \mathbf{C})$ and $(\bar{\mathbf{C}}, \bar{\mathbf{X}}) = (\mathbf{PC}, \mathbf{PX})$ are feasible solutions to the J-OP with the same objective value Ω. □

Hence, in the first step of the proposed code design for transmissions with IFI, we solve J-OP (155) assuming that IFI does not exist and thus obtaining the sub-optimal solution $(\mathbf{C}_\mathrm{o}, \mathbf{X}_\mathrm{o})$. Then given $(\mathbf{C}_\mathrm{o}, \mathbf{X}_\mathrm{o})$, the second step consists of finding the permutation matrix $\mathbf{P}_\mathrm{o}$ such that $(\mathbf{P}_\mathrm{o}\mathbf{C}_\mathrm{o}, \mathbf{P}_\mathrm{o}\mathbf{X}_\mathrm{o})$ still solves J-OP (155), but at the same time, conveniently reduces the IFI contribution. Different from the J-OP, however, the optimization of the matrix $\mathbf{P}$ is now based on the reformulation of the mean value and the variance of the decision variable of Appendix A in order to account for the IFI effect as well. The aforementioned approach leads to a modified constrained OP, as stated in the following proposition.

Proposition 10. *Assuming the channel template has support* $[0, 2T_f]$*, given the solution to J-OP (155)* $(\mathbf{C}_\mathrm{o}, \mathbf{X}_\mathrm{o})$*, the permutation matrix* $\mathbf{P}_\mathrm{o}$*, which mitigates the IFI effect in terms of BER performance, is found through the GCM IFI-based constrained*

OP, or I-OP for short, formulated as

$$\begin{cases} \mathbf{P}_{\mathrm{o}} = \arg\max\limits_{\mathbf{P}} \{\Phi(\mathbf{P})\} \\ \text{s.t.} \quad \mathbf{C}_{\mathrm{o}}^{T}\mathbf{P}^{T}\mathbf{J}_{N_f}\mathbf{P}\mathbf{X}_{\mathrm{o}} = \mathbf{A}\boldsymbol{\Phi} \\ \qquad\quad \boldsymbol{\Phi} > \Phi(\mathbf{P})\mathbf{I}_{2^M} \\ \qquad\quad \mathbf{P} \in \mathcal{P} \end{cases}, \tag{166}$$

where $\boldsymbol{\Phi} \triangleq \mathrm{diag}\{\Phi_1, \Phi_2, \cdots, \Phi_{2^M}\}$ *and* $\mathcal{P}$ *is the set of all the permutation matrices with size* $N_f \times N_f$*. According to (166), the codeword matrices to be employed for IFI mitigation become* $(\mathbf{P}_{\mathrm{o}}\mathbf{C}_{\mathrm{o}}, \mathbf{P}_{\mathrm{o}}\mathbf{X}_{\mathrm{o}})$*.*

Proof. See Appendix G. □

A few remarks about Proposition 10 can be made as follows.

1. As shown in Appendix 10, the OP (166) relies on maximizing a part of the mean value of the decision variable that corresponds to the contribution of interfering symbols. Therefore, the optimal permutation matrix $\mathbf{P}_{\mathrm{o}}$ can be interpreted as an "equalization" matrix such that the frame energy from the previous symbol can be properly exploited within the current frame.

2. Unlike J-OP (155) where the constraint $\mathbf{C}^{T}\mathbf{X} = \Omega(\mathbf{C}, \mathbf{X})\mathbf{A}$ holds with the scalar Ω, in I-OP (166), this restriction is circumvented by adopting the diagonal matrix $\boldsymbol{\Phi}$ and adding the constraint $\boldsymbol{\Phi} > \Phi(\mathbf{P})\mathbf{I}_{2^M}$. After all, with only a scalar as in (155), there may not exist a feasible $\mathbf{P}$ given $(\mathbf{C}_{\mathrm{o}}, \mathbf{X}_{\mathrm{o}})$ such that all 2^M equalities can hold. Furthermore, although the aforementioned choice yields better performance, as demonstrated in Sec. 8.5, the BER for different realization $\mathbf{a}_i$ of the information symbols may differ.

8.5 Numerical Results

In this section, we illustrate the optimal solutions of the proposed OPs for some values of the number of frames N_f and the number of symbols M per block. Then, the

performance of the proposed optimal GCM systems is quantified through numerical simulations, taking as benchmark the existing CSR design in [61] using Walsh codes. We do not consider the FSR system, which shows identical performance to the CM-TR systems in the absence of IFI and inferior performance in the presence of IFI [18, 61]. The transmitted pulse $p(t)$ is the second derivative of a Gaussian function with width $T_p = 1.0$ ns. We use the channel models described in [25] for random channel realizations. The one-sided bandwidth of the low-pass filter at the receiver is $B = 2.5$ GHz. In this section, all OPs are solved using the general solver in [1].

8.5.1 Optimal Codes for GCM Systems

Table 3 summarizes the optimization results of J-OP (155) corresponding to the number of frames $N_f = 2, 4, 6, 8$ and a few values of the number of symbols M conveyed by each block. When ($N_f = 2$, $M = 1$), ($N_f = 4, M = 1$), ($N_f = 8$, $M = 1$), and ($N_f = 8$, $M = 4$), the proposed codes offer the same performance as the CSR systems using Walsh codes, which means that Walsh codes are optimal for these cases. On the other hand, when ($N_f = 4$, $M = 2$), ($N_f = 8$, $M = 2$), and ($N_f = 8$, $M = 3$), since the CSR systems using Walsh codes yield sub-optimal solutions to the OP in (155), i.e., the CSR systems are not optimized in the view of power efficiency, the proposed codes achieve significant improvement compared to the CSR systems. Additionally, the optimization performed on ($N_f = 4, M = 3$) and $N_f = 6$, where Walsh codes do not exist, gives us the flexibility to design GCM systems with different N_f and M. Finally, the results for $N_f \geq 2^M$ corroborate Proposition 9, where $\Omega_{\text{o}} = M$.

8.5.2 Performance of Optimal Codes for GCM Systems

Fig. 39 displays the BER performance of the proposed GCM systems for $N_f = 4, 8$ and different numbers of information symbols per block M. We adopt CM1 channel model with $T_f = 80$ ns to avoid IFI and $L = 2BT_f = 400$. Given N_f and M, it is

Frame length	Number of symbols	Walsh codes	Optimal codes
$N_f = 2$	$M = 1$	1	1
$N_f = 4$	$M = 1$	1	1
	$M = 2$	$\sqrt{2}$	2
	$M = 3$	N/A	1
$N_f = 6$	$M = 1$	N/A	1
	$M = 2$	N/A	2
	$M = 3$	N/A	1
$N_f = 8$	$M = 1$	1	1
	$M = 2$	$\sqrt{2}$	2
	$M = 3$	$\sqrt{3}$	3
	$M = 4$	2	2

Table 3: Objective value Ω for the CSR with Walsh codes and the GCM with optimal codes.

worth noting that the theoretical BERs in (149) overlap with the simulated curves. This result validates the accuracy of the Gaussian approximation whenever L is large which we assumed in the proof of Proposition 1. In all, the system with ($N_f = 8$, $M = 3$) achieves the best BER performance and gains about 1.8 dB over the ($N_f = 8$, $M = 2$) one at BER = 10^{-5}. When $N_f = 4$, the optimal system with $M = 2$ is close to that with ($N_f = 8$, $M = 3$), while outperforms the ($N_f = 4$, $M = 1$) one by about 3 dB at BER= 10^{-5}.

8.5.3 Performance Comparisons of Optimal GCM Systems with Existing Design

In this subsection, we compare the performance of the GCM systems with optimal codes to the CSR system in [61] and simple TR (STR) system in [14] with CM1 channel model and $T_f = 80$ ns. Fig. 40 verifies the BER improvement of the proposed GCM over the existing designs. At BER= 10^{-5}, indeed, for the cases of ($N_f = 4, M = 2$) and ($N_f = 8, M = 2$) the proposed GCM design outperforms the CSR by about 1.8 dB, whereas for ($N_f = 8, M = 3$) case, the advantage of the optimal system increases to about 2.7 dB.

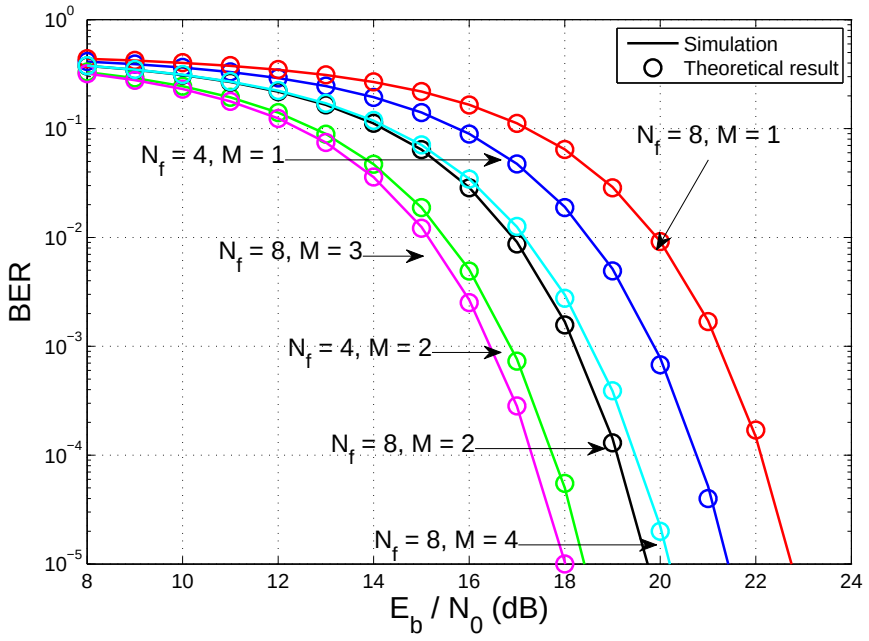

Figure 39: BER performance of the optimal GCM with different frame sizes N_f and number of symbols M.

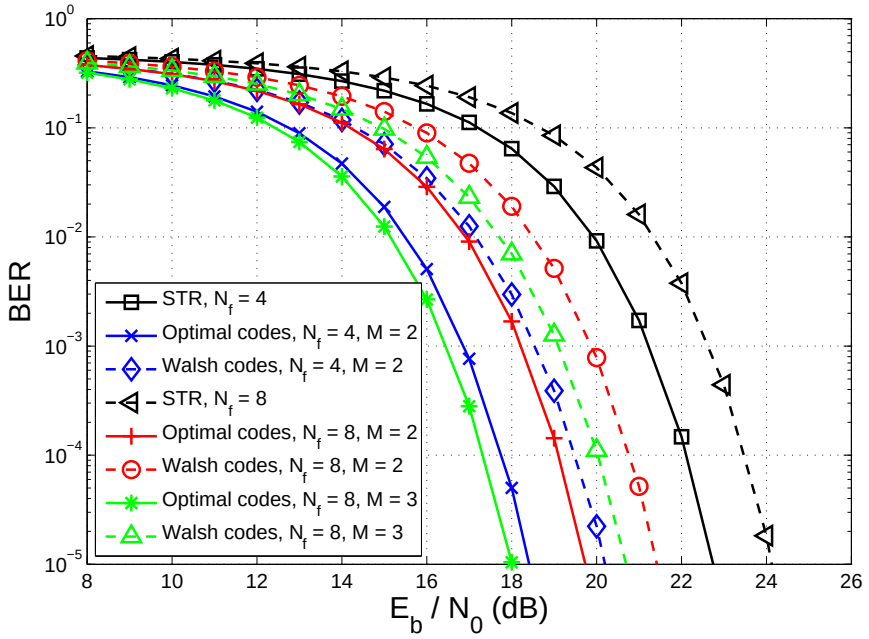

Figure 40: BER comparisons for the GCM using optimal codes, the design in [61] using Walsh codes, and the STR.

8.5.4 GCM Systems with Peak-to-Average Power Ratio Constraint

Fig. 41 depicts the relationship between the peak-to-average power ratio (PAPR) which is defined as

$$\text{PAPR} = \frac{\max X_{j,i}}{(\sum_{i=1}^{2^M}\sum_{j=0}^{N_f-1} X_{j,i}/2^M/N_f)}, \tag{167}$$

and Ω_{c} of the GCM systems with $N_f = 8$ and different M. Here, we compare PAPRs of the GCM systems optimized by PP-OP (158) for different levels of $\Omega_{\text{c}}, \Omega_{\text{c}} \leq \Omega_{\text{o}}$ and the Walsh code. Note that, for $M = 2, 4$, since $\Omega_{\text{o}} = 2$, we only have the results for $\Omega_{\text{c}} \leq 2$. For GCM system in J-OP (155), PAPR becomes $\max X_{j,i} N_f/M$ since we assumed that $\mathbf{1}_{N_f\times 1}^T \mathbf{X} = M\mathbf{1}_{2^M\times 1}^T$. From Fig. 41, first of all, as Ω_{c} increases (therefore, with better error performance), the minimum PAPR increases monotonically, thus providing the trade-off between the system error performance and the PAPR value. Secondly, the PAPRs of $M = 2$ and $M = 4$ are the same when $\Omega_{\text{c}} = 0.5, 1, 1.5, 2$ and their PAPRs are higher than those of $M = 3$ when $\Omega_{\text{c}} = 0.5, 1, 1.5$. Thus, unlike the case of Ω_{c}, the PAPR is not a monotonically increasing or decreasing function depending on M. Thirdly, the GCM system optimized by PP-OP (158) yields smaller PAPR than the CSR system with the Walsh code thus confirming effectiveness of our GCM code design.

8.5.5 Performance Comparisons of GCM with IFI

Fig. 42 illustrates the BER comparisons with CM1 channel model and the following code-multiplexing systems: *i*) GCM system with optimal solution from J-OP (155) and optimal code sequence design from I-OP (166), *ii*) GCM system with optimal solution from J-OP (155) but with non-optimal code sequence design, and *iii*) CSR with Walsh code. $N_f = 8$ and $M = 2$. For *i*) and *ii*), we firstly obtain the transmitted

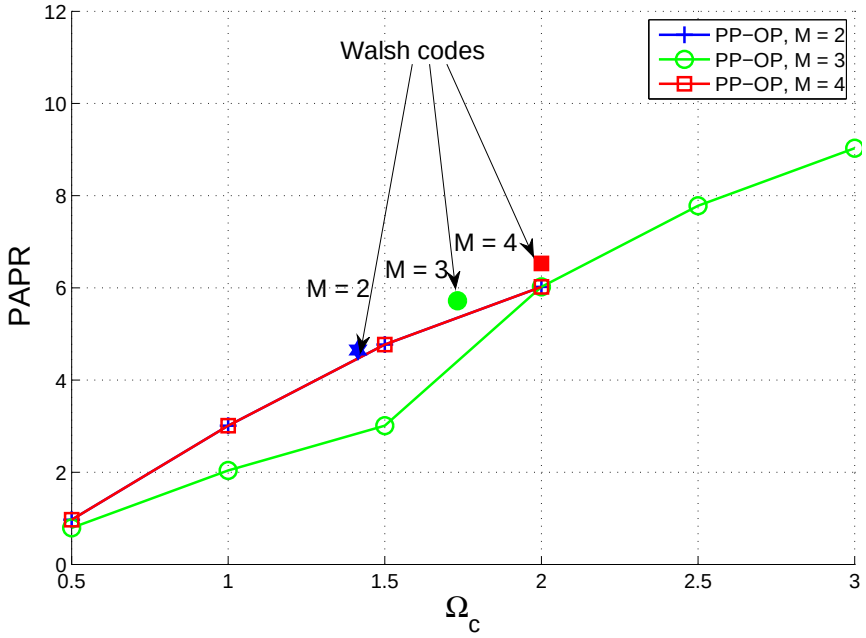

Figure 41: Peak-to-average power ratio for different GCM systems with $N_f = 8$.

symbols matrix and decoding matrix from J-OP (155) as:

$$\mathbf{X}_{\mathrm{o}} = \begin{bmatrix} 1 & 0 & 1 & 0 & 0 & 0 & 0 & 0 \\ 0 & 1 & 0 & 1 & 0 & 0 & 0 & 0 \\ 0 & 0 & 0 & 0 & 1 & 0 & 1 & 0 \\ 0 & 0 & 0 & 0 & 0 & 1 & 0 & 1 \end{bmatrix}^T, \tag{168}$$

$$\mathbf{C}_{\mathrm{o}} = \begin{bmatrix} +1 & +1 & +1 & +1 & -1 & -1 & -1 & -1 \\ +1 & -1 & +1 & -1 & +1 & -1 & +1 & -1 \end{bmatrix}^T, \tag{169}$$

with $\Omega_{\mathrm{o}} = 2$. Next, we solve I-OP (166) with $(\mathbf{C}_{\mathrm{o}}, \mathbf{X}_{\mathrm{o}})$ in Eqs. (168) and (169) and the optimal permutation matrix is

$$\mathbf{P}_{\mathrm{o}} = \begin{bmatrix} \mathbf{e}_1 & \mathbf{e}_3 & \mathbf{e}_2 & \mathbf{e}_4 & \mathbf{e}_5 & \mathbf{e}_7 & \mathbf{e}_6 & \mathbf{e}_8 \end{bmatrix}, \tag{170}$$

where $\mathbf{e}_j$ denotes the jth column of an identity matrix $\mathbf{I}_{N_f}$. Therefore, the corresponding codewords for *i)* are $\bar{\mathbf{X}}_{\mathrm{o}} = \mathbf{P}_{\mathrm{o}}\mathbf{X}_{\mathrm{o}}, \bar{\mathbf{C}}_{\mathrm{o}} = \mathbf{P}_{\mathrm{o}}\mathbf{C}_{\mathrm{o}}$ with $\Phi_{\mathrm{o}} = 0$ and we adopt $(\mathbf{C}_{\mathrm{o}}, \mathbf{X}_{\mathrm{o}})$ in Eqs. (168) and (169) for *ii)* with $\Phi = -1$.

To simulate a high-rate UWB communication in a stringent channel environment, we set $T_f = 6, 8$ ns to include IFI and data rate 41.67 Mbit/s and 31.25 Mbit/s, respectively. As shown in Fig. 42, when $T_f = 8$ ns, the GCM with optimal code sequence design achieves 1 dB gain over the one with non-optimal sequence design and 4 dB gain over the CSR system with Walsh code at BER $= 10^{-5}$. When the data rate increases ($T_f = 6$ ns), the advantage of the optimal code sequence design is clear and the gap between optimal sequence and non-optimal code sequence increases to around 10 dB at BER $= 2 \times 10^{-2}$.

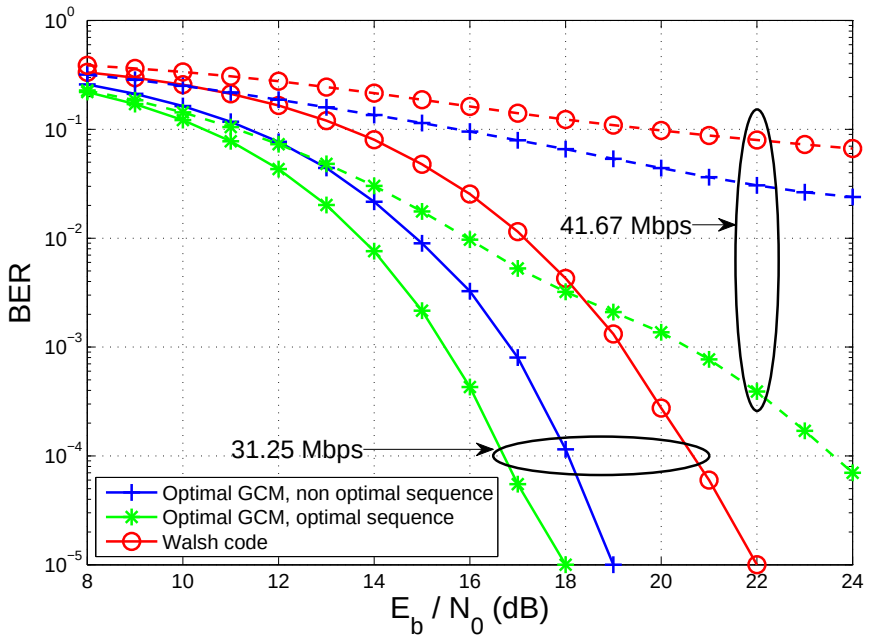

Figure 42: BER comparisons for different GCM systems with and without optimal code sequence design in the presence of IFI with CM1 channel.

In addition, we compare the BER performance of different code-multiplexing systems with CM4 channel model, whose maximum excess delay T_m is about 360 ns. Due to the long excess delay, the frame duration T_f is increased to 30 or 40 ns in order to obtain affordable system performance. From Fig. 43, similar conclusions about the results for the CM1 channel model can be drawn for the CM4 one as well. In fact, the optimal GCM system with optimal code sequence design obtains the best

error performance among the three systems and the gains relative to non-optimal code sequence design become around 1.5 dB and 5 dB for $T_f = 30, 40$ ns, respectively, at BER $= 10^{-5}$.

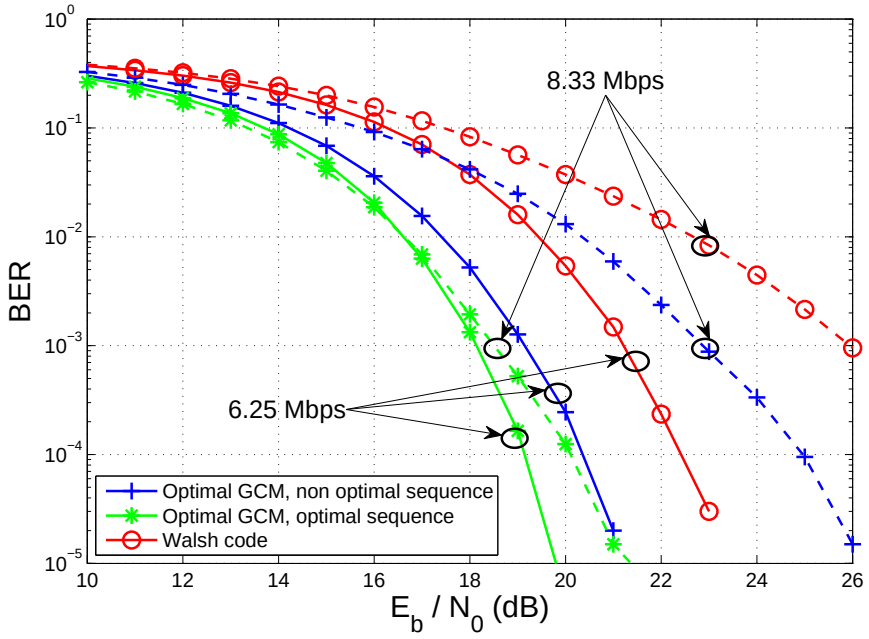

Figure 43: BER comparisons for different GCM systems with and without optimal code sequence design in the presence of IFI with CM4 channel.

CHAPTER IX

PERFORMANCE IMPACTS OF NON-IDEAL ANTENNAS

Previous chapters assume that the UWB antennas are ideal, i.e., they have perfect delta response. However, in practice, the UWB antennas are not ideal and can introduce significant linear and/or nonlinear distortion [48]. Without proper handling, the linear and/or nonlinear distortion can result in significant performance degradation, which should be mitigated.

In this chapter, we investigate the performance impacts of the non-ideal antennas for non-coherent UWB systems regulated by IEEE 802.15.4a-2007. Fig. 44 illustrates the non-ideal frequency response of UWB antennas measured by experimental data considered. From Fig. 44, the antennas exhibit almost ideal frequency response from 2 GHz to 5.5 GHz.

On the other hand, the antennas present significant distortion when the frequency is greater than 5.5 GHz, which includes the spectrum of the mandatory channel in high band in IEEE 802.15.4a-2007 [40] (now a part of IEEE 802.15.4-2011 [39]) with center frequency 7.9872 GHz and bandwidth 499.2 MHz channel number 9 (see Fig. 45

Fig. 46 displays the error performance of optimal GCM transmissions with $M = 2$, $N_f = 8$, IEEE 802.15.4a channel numbers $3, 5, 9$, and non-ideal channel frequency response in Fig. 45. We adopt CM1 channel model and $T_f = 50$ns. We observe that, for mandatory channel number 3 (center frequency $f_c = 4.4928$ GHz), the error performance with non-ideal antennas exhibits almost the same as that with ideal antennas for low SNR, and the loss is about 0.5 dB at BER= 10^{-5}. When comes

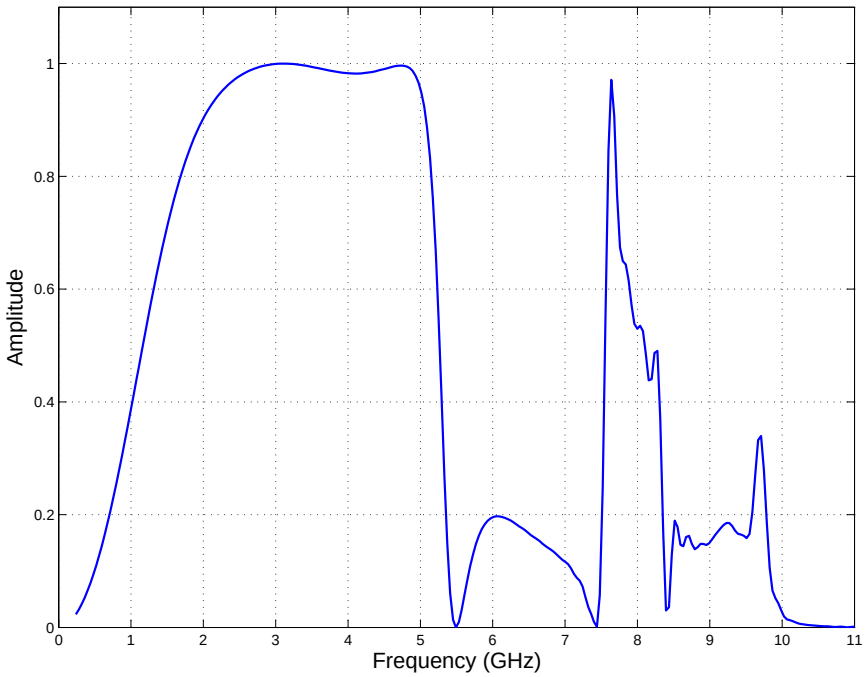

Figure 44: An illustration of the non-ideal frequency response of UWB antennas.

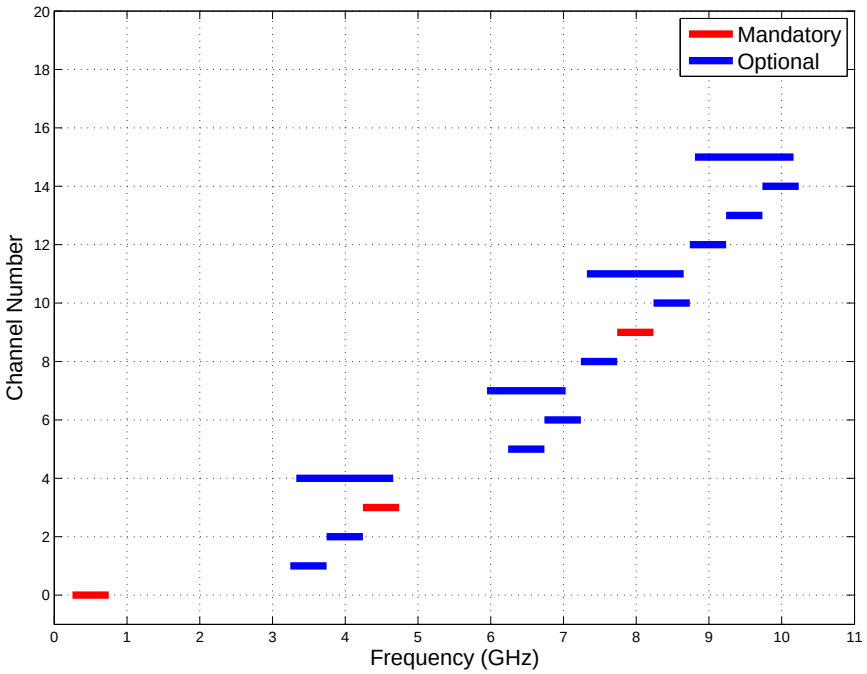

Figure 45: Channel assignments of IEEE 802.15.4a-2007 UWB physical layer.

to mandatory channel number 9 ($f_c = 7.9872$ GHz), the performance loss increases to around 3 dB at BER$= 10^{-5}$ because antenna distortion. We also consider the optional channel number 5, where significant distortion caused by antennas can be found. The performance degradation under channel number 5 ($f_c = 6.4896$ GHz) becomes 8 dB at BER$= 10^{-5}$.

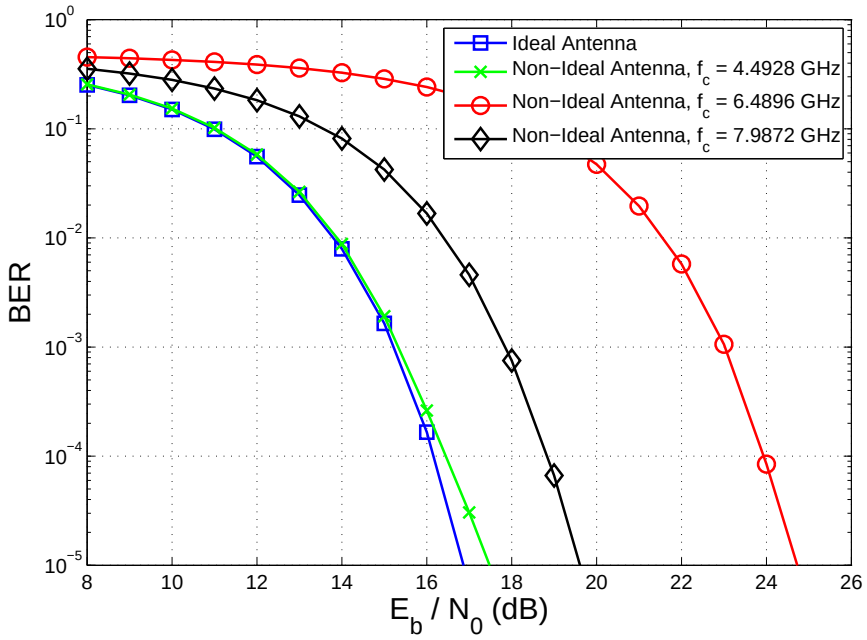

Figure 46: Performance of optimal GCM transmissions with IEEE 802.15.4a channel numbers $3, 5, 9$ and non-ideal antennas.

CHAPTER X

CONCLUDING REMARKS

The objective of the proposed research is to design low-complexity high-performance UWB systems that *i)* avoid the stringent channel estimation and maintain the simple hardware structure of the noncoherent receivers; *ii)* lower the computational complexity of the existing receivers with the aid of advanced digital signal processing techniques; and *iii)* improve the error performance of the noncoherent receivers by taking account of practical imperfections.

The main contributions of the thesis are listed as follows:

- Proposed low-complexity iterative multi-symbol detectors;
- Revealed the fundamental problem - rank-1 perturbation problem for multi-symbol detection;
- Proposed low-complexity modified unconstrained relaxation multi-symbol detectors;
- Proposed low-complexity semidefinite programming multi-symbol detectors;
- Studied the log-likelihood metric of multi-symbol detectors;
- Developed list sphere decoding for soft-input soft-output multi-symbol detectors;
- Investigated the distribution of correlation noise when the number of concurrent users is small;
- Proposed improved differential receivers in the presence of impulsive correlation noise;

- Proposed joint power allocation and path selection for differential transmitted reference relaying systems;
- Proposed generalized code-multiplexing systems and formulated the optimization problem for generalized code-multiplexing systems in terms of error performance;
- Analyzed some optimal codes and their performance for code-multiplexing systems;
- Optimized the codes for code-multiplexing systems in the presence of inter-frame interference; and
- Examined the performance impacts of non-ideal antennas.

10.1 Future Topics

In the following, we summarize a list of interesting research topics that can be pursued along the line of this dissertation:

- Improved generalized code-multiplexing designs, including maximum-likelihood detectors, code designs for relaying GCM systems, and multi-access interference suppression. Despite the simplicity of GCM systems, the existing GCM receiver is generally not an MLD given the integration outputs. The MLD for GCM and its performance are unknown. In addition, in the presence of MAI, the performance degradation and mitigation methods are not investigated for GCM systems.
- Improved noncoherent systems with finite-bit (e.g., 1-bit)-resolution analog-to-digital converters (ADCs). Most of noncoherent receivers assumes full-resolution ADCs. However, because of the very high sampling rate of UWB signals, full-resolution ADCs pose significant burden on hardware, and thus finite-resolution

(e.g., 1-bit or 2-bit) ADCs for UWB systems are of great interest.

- Detection and synchronization for noncoherent UWB signals in the presence of strong narrow-band interference (NBI). Because of the low power of UWB signals and relative strong power of narrow-band signals, NBI could cause performance degradation in UWB detection and synchronization. Hence, a future extension is to study the impact of NBI to the work in this thesis and to propose new methods of improvements.

10.2 Publications

10.2.1 Journal Publications (in press/published)

[J1] **Q. Zhou**, X. Ma, and V. Lottici, "Generalized code-multiplexing transmissions for UWB systems," *IEEE Trans. Wireless Commun.*, 2013, accepted.

[J2] **Q. Zhou** and X. Ma, "Shot interference detection and mitigation for heterogeneous networks," *IEEE Trans. Veh. Technol.*, 2013, accepted.

[J3] **Q. Zhou** and X. Ma, "Element-based lattice reduction algorithms for large MIMO detection," *IEEE J. Sel. Areas Commun.*, vol. 31, no 2, pp. 274-286, Feb. 2013.

[J4] **Q. Zhou** and X. Ma, "Soft-input soft-output multiple symbol differential detection for UWB communications," *IEEE Commun. Lett.*, vol. 16, no. 8, pp. 1296–1299, Aug. 2012.

[J5] **Q. Zhou** and X. Ma, "Designing low-complexity near-optimal multiple-symbol detectors for impulse radio UWB systems," *IEEE Trans. Signal Process.*, vol. 60, no. 5, pp. 2460–2469, May 2012.

[J6] **Q. Zhou**, X. Ma, and V. Lottici, "Fast multi-symbol based iterative detectors for UWB communications," *EURASIP J. Appl. Signal Process.*, vol. 2010, May

2010.

10.2.2 Journal Publications (submitted/in preparation)

[J1] **Q. Zhou** and X. Ma, "Improved element-based lattice reduction algorithms for wireless communications," *IEEE Trans. Wireless Commun.*, Oct., 2012, submitted.

[J2] **Q. Zhou** and X. Ma, "Receiver designs for differential UWB systems with multiple access interference," *IEEE Trans. Commun.*, Jan., 2013, submitted.

[J3] M. Mondelli, **Q. Zhou**, X. Ma, and V. Lottici, "Joint power allocation and path selection for decode-and-forward differential transmitted reference IR-UWB multi-hop relay systems," *IEEE Trans. Commun.*, Apr., 2013, submitted.

10.2.3 Conference Publications

[C1] **Q. Zhou**, and X. Ma, "Joint transceiver designs using lattice reduction algorithms," in *Proc. IEEE China Summit and Int. Conf. on Signal and Info. Process. (ChinaSIP)*, Beijing, China, July 2013, submitted.

[C2] Q. Wen, **Q. Zhou**, and X. Ma, "Fixed-point realization of lattice-reduction aided MIMO receivers with complex K-best algorithm," in *Proc. Int. Conf. on Acoustic, Speech, and Signal Proc. (ICASSP)*, Vancouver, Canada, May 2013, accepted.

[C3] **Q. Zhou** and X. Ma, "An improved LR-aided K-best algorithm for MIMO detection," in *Proc. IEEE Int. Conf. on Wireless Commun. and Signal Process. (WCSP)*, Huangshan, China, Oct. 2012, accepted.

[C4] **Q. Zhou**, J. Pan, X. Ma, and S. E. Ralph, "Lattice-reduction-aided Wiener filtering for communications over ISI channels," in *Proc. IEEE Int. Conf. on Signal Process. (ICSP)*, Beijing, China, Oct. 2012, pp. 1477–1481.

[C5] M. Mondelli, **Q. Zhou**, X. Ma, and V. Lottici, "A cooperative approach for amplify-and-forward differential transmitted reference IR-UWB relay systems," in *Proc. Int. Conf. on Acoustic, Speech, and Signal Proc. (ICASSP)*, Kyoto, Japan, Mar. 2012, pp. 2905–2908.

[C6] **Q. Zhou** and X. Ma, "Receiver designs for UWB differential transmitted reference systems with multiple access interference," in *Proc. Int. Conf. Ultra-wideband Commun. (ICUWB)*, Bologna, Italy, Sept. 2011, pp. 205–209.

[C7] **Q. Zhou** and X. Ma, "Robust designs for femtocell networks with interference from macrocell users," in *Proc. IEEE Global Commu. Conf. Workshop on Femtocell Networks*, Houston, TX, Dec. 2011, pp. 214–218.

[C8] **Q. Zhou**, X. Ma, and V. Lottici, "Generalized code-multiplexing transmissions for UWB systems," in *45th Annual Conf. on Info. Sci. and Systems (CISS)*, Baltimore, MD, Mar. 2011, pp. 1–6.

[C9] **Q. Zhou** and X. Ma, "Designing low-complexity detectors for generalized SC-FDMA systems," in *45th Annual Conf. on Info. Sci. and Systems (CISS)*, Baltimore, MD, Mar. 2011, pp. 1–6.

[C10] **Q. Zhou**, J. Chen, and X. Ma, "Extended multi-symbol differential detection for IR-UWB communications," in *Proc. Military Commu. Conf. (MILCOM)*, San Jose, CA, Oct. 2010, pp. 2387–2392.

[C11] **Q. Zhou**, X. Ma, and R. Rice, "A near-optimal multi-symbol based detector for UWB communications," in *Proc. IEEE Int. Conf. Ultra-Wideband, (ICUWB)*, vol. 1, Nanjing, China, Sept. 2010, pp. 1–4.

[C12] **Q. Zhou**, X. Ma, and R. Rice, "Near-ML detection based on semi-definite programming for UWB communications," in *Proc. IEEE Int. Symp. Inf. Theory (ISIT)*, Austin, TX, June 2010, pp. 2253–2257.

[C13] **Q. Zhou**, L. Zhang, and L. Ma, "Learning topographic sparse coding through similarity function," in *Proc. Int. Conf. on Natural Computation*, vol. 3, Jinan, China, Oct. 2008, pp. 241–245.

10.2.4 Patents

[P1] **Q. Zhou** and X. Ma, "Enhanced lattice reduction systems and methods," Sept. 20 2012, US Patent 20,120,236,968.

[P2] **Q. Zhou** and X. Ma, "An improved lattice-reduction-aided K-best algorithm for low complexity and high performance communications," disclosure submitted on Sept. 23, 2012.

[P3] **Q. Zhou** and X. Ma, "An improved complex lattice-reduction-aided K-best algorithm for low complexity and high performance communications," disclosure submitted on Sept. 23, 2012.

[P4] **Q. Zhou** and X. Ma, "Interference Detection and Mitigation for Heterogeneous Networks," disclosure submitted on Sept. 25, 2012.

[P5] **Q. Zhou** and X. Ma, "Element-based lattice reduction+ (ELR+) algorithms for wireless communications," disclosure submitted on Sept. 28, 2012.

APPENDIX A

PROOF OF PROPOSITION 1

From the Karush-Kuhn-Tucker (KKT) conditions, the sufficient and necessary condition for the optimal solution $\mathbf{X}^*$ of the SDP problem (36) is (cf. [95, Ch. 4.2])

$$\begin{aligned} \mathbf{F} &\succeq 0, \\ \mathbf{X}^* &\succeq 0, \\ X^*_{i,i} &= 1, \\ \mathbf{F} + \mathrm{Diag}(\mathbf{f}) &= -\mathbf{P}, \\ \mathbf{X}^*\mathbf{F} &= \mathbf{0}, \end{aligned} \tag{171}$$

where $\mathbf{F}$ and $\mathbf{f}$ are the dual variables of the SDP problem in (36).

Assuming that the SDP problem (36) yields a rank-1 solution $\mathbf{X}^* = \mathbf{b}\mathbf{b}^T$, from the last two equations in (171), we have (cf. [41, Eq. (10)])

$$\mathbf{f} = -\mathrm{Diag}(\mathbf{b})^{-1}\mathbf{P}\mathbf{b}. \tag{172}$$

Now the problem is to find the necessary and sufficient condition that $\mathbf{F}$ is positive semi-definite (PSD), where matrix $\mathbf{F}$ can be represented as

$$\begin{aligned} \mathbf{F} &= -\mathbf{P} - \mathrm{Diag}(\mathbf{f}) \\ &= -\mathbf{P} + \mathrm{Diag}(\mathbf{b})^{-1}\mathrm{Diag}(\mathbf{P}\mathbf{b}) \\ &= (M+1)\mathbf{I} - \mathbf{b}\mathbf{b}^T - \sigma\mathbf{u}_1\mathbf{b}^T - \sigma\mathbf{b}\mathbf{u}_1^T - \sigma^2\sum_{l=1}^{L}\mathbf{u}_l\mathbf{u}_l^T \\ &\quad + \mathrm{Diag}(\mathbf{b})^{-1}\mathrm{Diag}\left(\left(\sigma\mathbf{u}_1\mathbf{b}^T + \sigma\mathbf{b}\mathbf{u}_1^T + \sigma^2\sum_{l=1}^{L}\mathbf{u}_l\mathbf{u}_l^T\right)\mathbf{b}\right) \\ &= (M+1)\mathbf{I} - \mathbf{b}\mathbf{b}^T - \sigma\mathbf{A}. \end{aligned} \tag{173}$$

Note that from the last equation in (171), $\mathbf{b}$ is the eigenvector of $\mathbf{F}$ with eigenvalue 0 and $(M+1)\mathbf{I}-\mathbf{b}\mathbf{b}^T$ is a rank-M matrix with non-zero eigenvalues $(M+1)$. Therefore, matrix $\mathbf{F}$ is PSD if

$$\lambda_{\mathbf{A},\max} \leq \frac{M+1}{\sigma}. \tag{174}$$

On the other hand, if (174) holds true and $\mathbf{X} = \mathbf{b}\mathbf{b}^T$, then $\mathbf{F}$ is PSD. Thus, $\mathbf{X}$ is an optimal solution. This concludes the proof. A similar proof for binary least squares problem can be found in [41].

APPENDIX B

PROOF OF PROPERTY 4

Suppose the $M+1$ eigenvalues of matrix $\mathbf{Q}$ are $\lambda_j, j = 0, \cdots, M$. Since $\mathbf{Q}$ is a random matrix with zeros on the diagonal,

$$\sum_{j=0}^{M} \lambda_j = \text{Trace}(\mathbf{Q}) = 0, \tag{175}$$

and λ_j's are distinct with probability one. Thus,

$$\min_j \lambda_j < 0 < \max_j \lambda_j \tag{176}$$

with probability one.

APPENDIX C

PROOF OF PROPOSITION 6

We prove that assumption A3) is equivalent to A3a)-A3b), assuming the absence of IFI and a sufficiently large product BT_f, i.e., between the bandwidth B of the receiver low-pass filter $f_{\rm rxp}(t)$ and the frame interval T_f. First, let us focus on the statistics of the samples at the integrator output r_j, $j \in \mathcal{J}$, given by (144). Exploiting the IFI-free condition, i.e., that the support of the channel template $g(t)$ is less than the frame interval T_f, and keeping in mind the expression of the received signal in (143), we obtain

$$r_j = b_j^2 \int_0^{T_f} g^2(t)dt + \underbrace{2b_j \int_0^{T_f} g(t)w_j(t)dt + \int_0^{T_f} w_j^2(t)\,dt}_{\varphi_j}, \tag{177}$$

where $w_j(t) \triangleq w(t + jT_f)$.

Applying the sampling theorem to the (177) yields (c.f., [82])

$$r_j = b_j^2 E_f + \underbrace{2b_j \sum_{n=0}^{L-1} w_{j,n} g_n}_{\varphi_{j,1}} + \underbrace{\sum_{n=0}^{L-1} w_{j,n}^2}_{\varphi_{j,2}}, \tag{178}$$

where $L \triangleq \lceil 2BT_f \rceil$, $g_n \triangleq \sqrt{T_s} g(nT_s)$, $w_{j,n} \triangleq \sqrt{T_s} w_j(nT_s)$ are independent and identically distributed (i.i.d.) Gaussian random variables with zero mean and variance $N_0/2$, $T_s \triangleq \dfrac{1}{2B}$ is the sampling interval, and $E_f = \sum_{n=0}^{L-1} g_n^2$. If L is sufficiently large, in view of the central limit theorem, $\varphi_{j,2}$ can be approximated as a Gaussian random variable. Since $\mathrm{E}\{\varphi_{j,1}\varphi_{j,2}\} = \mathrm{E}\{\sum_{n=0}^{L-1} g_n w_{j,n}^3\} = 0$, we can treat $\varphi_{j,1}$ and $\varphi_{j,2}$ as independent Gaussian-distributed variables. Therefore, the mean and the variance of r_j for a given realization of the symbols $\mathbf{a}$ are given, respectively, by [82, 18, 61]

$$\mathrm{E}\{r_j|\mathbf{a}\} = b_j^2 E_f + \frac{LN_0}{2}, \tag{179}$$

$$\begin{aligned}\mathrm{Var}\{r_j|\mathbf{a}\} &= \mathrm{Var}\{\varphi_j|\mathbf{a}\} \\ &= \mathrm{Var}\{\varphi_{j,1}|\mathbf{a}\} + \mathrm{Var}\{\varphi_{j,2}|\mathbf{a}\} \\ &= 4b_j^2 \sum_{n=0}^{L-1} g_n^2 \mathrm{Var}\{w_{j,n}\} + \sum_{n=0}^{L-1} \left(\mathrm{E}\{w_{j,n}^4\} - \mathrm{E}\{w_{j,n}^2\}^2\right) \\ &= 2b_j^2 E_f N_0 + \frac{LN_0^2}{2}. \end{aligned} \tag{180}$$

Therefore, the decision variable z_k, $k \in \mathcal{K}$, in (145) can be rearranged as

$$z_k = \mathbf{c}_k^T \mathbf{r} = E_f \mathbf{c}_k^T (\mathbf{b} \odot \mathbf{b}) + \xi_k, \tag{181}$$

where, under assumptions A1)-A2) of Definition 6, $\xi_k \triangleq \mathbf{c}_k^T \boldsymbol{\varphi}$, with $\boldsymbol{\varphi} \triangleq \left[\varphi_0, \cdots, \varphi_{N_f-1}\right]^T$, has mean

$$\mathrm{E}\{\xi_k|\mathbf{a}\} = \frac{LN_0}{2} \sum_{j=0}^{N_f-1} c_{k,j} = 0, \tag{182}$$

and variance

$$\mathrm{Var}\{\xi_k|\mathbf{a}\} = 2E_f N_0 \sum_{j=0}^{N_f-1} b_j^2 + \frac{N_f L N_0^2}{2}. \tag{183}$$

Hence, z_k in (181) can be modeled for a given vector $\mathbf{a}$ as a Gaussian-distributed random variable, whose mean and variance after imposing assumptions A3a)-A3b) and (181)-(182) are given by

$$\mathrm{E}\{z_k|\mathbf{a}\} = E_f \mathbf{c}_k^T (\mathbf{b} \odot \mathbf{b}) = E_f \Psi\, a_{i,k}, i \in \mathcal{I}, k \in \mathcal{K}, \tag{184}$$

and

$$\mathrm{Var}\{z_k|\mathbf{a}\} = 2E_f N_0 E_{\mathbf{b}} + \frac{N_f L N_0^2}{2}, \tag{185}$$

respectively. Therefore, we deduce from (184)-(185) that the error probabilities on $a_k, k \in \mathcal{K}$, are all the same. Similarly, it can be shown that assumption A3) induces A3a)-A3b), which concludes the proof about the necessary and sufficient condition of assumption A3).

APPENDIX D

PROOF OF PROPOSITION 7

Due to assumption A3b), i.e., $\|\mathbf{b}_i\|_2^2 = E_{\mathbf{b}}$, $i \in \mathcal{I}$, the received bit energy results in

$$E_{bit} = \frac{E_f}{M} \sum_{j=0}^{N_f-1} b_j^2 = \frac{E_f}{M} E_{\mathbf{b}}. \tag{186}$$

Hence, from (184)-(185), the error probabilities on the information symbols a_k become identical over k and are expressed by

$$\begin{aligned}
\mathrm{BER}_{\mathrm{GCM}}(\Omega) &= Q\left[\left(\frac{\mathrm{E}\{z_k|\mathbf{a}\}^2}{\mathrm{Var}\{z_k|\mathbf{a}\}}\right)^{1/2}\right] \\
&= Q\left[\left(\frac{E_f^2\Psi^2}{2E_fN_0E_{\mathbf{b}} + N_fLN_0^2/2}\right)^{1/2}\right] \\
&= Q\left[\left(\frac{2E_fN_0E_{\mathbf{b}} + N_fLN_0^2/2}{E_f^2\Psi^2}\right)^{-1/2}\right] \\
&= Q\left[\left(\frac{E_{\mathbf{b}}^2}{\Psi^2M^2}\left(\frac{2MN_0}{E_{bit}} + \frac{N_fLN_0^2}{2E_{bit}^2}\right)\right)^{-1/2}\right] \\
&= Q\left[\Omega\left(\frac{2M}{\gamma} + \frac{N_fL}{2\gamma^2}\right)^{-1/2}\right],
\end{aligned} \tag{187}$$

where $\gamma \triangleq E_{bit}/N_0$ and $\Omega \triangleq M\Psi/E_{\mathbf{b}}$.

APPENDIX E

PROOF OF LEMMA 1

The feasible solution $\mathbf{C}$ for the J-OP (155) is an $N_f \times M$ matrix, which has, at most, 2^M distinct rows due to assumption A1). Hence, a $2^M \times M$ decoding matrix $\bar{\mathbf{C}}$ can be constructed whose rows are all the 2^M realizations with entries $\{\pm 1\}$ such that

$$\mathbf{C} = \mathbf{T}\bar{\mathbf{C}}, \tag{188}$$

where $\mathbf{T}$ is an $N_f \times 2^M$ mapping matrix having in each row only one element equal to 1 and all the others equal to 0. It can be obtained

$$\mathbf{1}_{2^M \times 1}^T \mathbf{T}^T \mathbf{X} = \mathbf{1}_{N_f \times 1}^T \mathbf{X} = M \mathbf{1}_{2^M \times 1}^T, \tag{189}$$

$$\bar{\mathbf{C}}^T \bar{\mathbf{X}} = \bar{\mathbf{C}}^T \mathbf{T}^T \mathbf{X} = (\mathbf{T}\bar{\mathbf{C}})^T \mathbf{X} = \mathbf{C}^T \mathbf{X}, \tag{190}$$

i.e., the matrices $\bar{\mathbf{C}}$ and $\bar{\mathbf{X}} \triangleq \mathbf{T}^T \mathbf{X}$ satisfy both the first and second constraints of the J-OP as well. Since $\bar{\mathbf{C}}^T \mathbf{1}_{2^M \times 1} = \mathbf{0}_{M \times 1}$ and $\bar{\mathbf{C}} \odot \bar{\mathbf{C}} = \mathbf{1}_{2^M \times M}$, we conclude that $(\bar{\mathbf{C}}, \bar{\mathbf{X}}) = (\bar{\mathbf{C}}, \mathbf{T}^T \mathbf{X})$ is a feasible solution to the J-OP (155) with $N_f = 2^M$ (SJ-OP) and the value of the objective function is the same as that given by the feasible solution $(\mathbf{C}, \mathbf{X})$ with $N_f > 2^M$ (LJ-OP).

APPENDIX F

PROOF OF PROPOSITION 8

Bearing in mind the proof of Lemma 1, the optimal decoding matrix $\mathbf{C}_{\mathrm{o}}$ for the GCM system with frame length $N_f = 2^M$ is known to be the $2^M \times M$ matrix given by (163), with the rows being all the realizations of length M with entries ± 1. Hence, the J-OP in (155) can be relaxed to the set of 2^M decoupled OPs

$$\begin{cases} \mathbf{x}_i^{(\mathrm{o})} = \arg\max\limits_{\mathbf{x}_i} \{\Omega_i(\mathbf{x}_i)\} \\ \text{s.t.} \quad \mathbf{a}_i^T \mathbf{a}_i \Omega_i(\mathbf{x}_i) = (\mathbf{C}_{\mathrm{o}} \mathbf{a}_i)^T \mathbf{x}_i \\ \qquad \mathbf{1}_{2^M \times 1}^T \mathbf{x}_i = M \\ \qquad \mathbf{x}_i \geq \mathbf{0}_{2^M \times 1} \end{cases} . \tag{191}$$

each corresponding to a different realization $\mathbf{a}_i$ of the information symbols.

It is readily shown that, the optimal solution of the OP (191) is

$$x_{i,j}^{(\mathrm{o})} = \begin{cases} M, & j = \bar{k} \\ 0, & \text{otherwise} \end{cases}, \quad i, j \in \mathcal{I}, \tag{192}$$

where $\bar{k} = \arg\max_k [\mathbf{C}_{\mathrm{o}} \mathbf{a}_i]_k$, i.e., $\mathbf{z}_{\bar{k}} = \mathbf{a}_i$. Now, we note that: *i*) since $\mathbf{x}_i^{(\mathrm{o})}$ in (192) is the feasible solution of OP (191), then it optimally solves also (191); *ii*) the optimal values of Ω_i concerning the 2^M OPs in (191) are all equal to M. Therefore, it can be concluded that $\mathbf{X}_{\mathrm{o}} \triangleq [\mathbf{x}_1^{(\mathrm{o})}, \cdots, \mathbf{x}_{2^M}^{(\mathrm{o})}]$ is the optimal solution of the J-OP (155).

APPENDIX G

PROOF OF PROPOSITION 10

Assume that the channel template can be written as $g(t) = g_0(t) + g_1(t - T_f)$, with both $g_0(t)$ and $g_1(t)$ having support $[0, T_f]$. Similar to the approach used in Appendix A, in view of large $L = \lceil 2BT_f \rceil$, the mean value and the variance of r_j for a given realization of the information symbols $\mathbf{a}$ can be written as

$$\mathrm{E}\{r_j|\mathbf{a}\} = b_j^2 E_f^{(0)} + b_{j-1}^2 E_f^{(1)} + 2b_j b_{j-1} E_f^{(0,1)} + \frac{LN_0}{2}, \tag{193}$$

$$\mathrm{Var}\{r_j|\mathbf{a}\} = 2\left(b_j^2 E_f^{(0)} + b_{j-1}^2 E_f^{(1)} + 2b_j b_{j-1} E_f^{(0,1)}\right) N_0 + \frac{LN_0^2}{2}, \tag{194}$$

where $E_f^{(0)} = \int_0^{T_f} g_0^2(t)dt$, $E_f^{(1)} = \int_0^{T_f} g_1^2(t)dt$, and $E_f^{(0,1)} = \int_0^{T_f} g_1(t)g_2(t)dt$. Then, assuming $E_f^{(0,1)} \ll E_f^{(0)}$ and $E_f^{(0,1)} \ll E_f^{(1)}$ [18], (193)-(194) can be approximated as

$$\mathrm{E}\{r_j|\mathbf{a}\} \approx b_j^2 E_f^{(0)} + b_{j-1}^2 E_f^{(1)} + \frac{LN_0}{2}, \tag{195}$$

$$\mathrm{Var}\{r_j|\mathbf{a}\} \approx 2\left(b_j^2 E_f^{(0)} + b_{j-1}^2 E_f^{(1)}\right) N_0 + \frac{LN_0^2}{2}. \tag{196}$$

Now, by applying the $N_f \times N_f$ permutation matrix $\mathbf{P}$ on the solution $(\mathbf{C}_\mathrm{o}, \mathbf{X}_\mathrm{o})$ to J-OP (155), one obtains the feasible solution $(\bar{\mathbf{C}}, \bar{\mathbf{X}}) = (\mathbf{P}\mathbf{C}_\mathrm{o}, \mathbf{P}\mathbf{X}_\mathrm{o})$. Accordingly, the mean value and the variance of the decision variable $z_k = \sum_{j=0}^{N_f-1} \bar{c}_{j,k} r_j$, for a given $\mathbf{a}_i$, result as

$$\mathrm{E}\{z_k|\mathbf{a}_i\} \approx \sum_{j=0}^{N_f-1} \bar{c}_{j,k}\left[E_f^{(0)}\bar{b}_{j,i}^2 + E_f^{(1)}\bar{b}_{j-1,i}^2\right], \tag{197}$$

$$\mathrm{Var}\{z_k|\mathbf{a}_i\} \approx 2N_0 E_f \sum_{j=0}^{N_f-1} \bar{b}_{j,i}^2, + \frac{N_f LN_0^2}{2}, \tag{198}$$

where $\bar{c}_{j,k} \triangleq \left[\bar{\mathbf{C}}\right]_{j,k}$ and $\bar{b}_{j,i}^2 \triangleq \left[\bar{\mathbf{X}}\right]_{j,i}$, $j \in \mathcal{J}$, $i \in \mathcal{I}$, $1 \le k \le M$. Since Lemma 3 shows that both $(\mathbf{C}_\mathrm{o}, \mathbf{X}_\mathrm{o})$ and $(\bar{\mathbf{C}}, \bar{\mathbf{X}})$ satisfy all constraints of the J-OP (155) with the same

objective Ω, we have: *i*) $\sum_{j=0}^{N_f-1} \bar{c}_{j,k}\bar{b}_{j,i}^2 = \Omega a_{i,k}$, and *ii*) $\sum_{j=0}^{N_f-1} \bar{b}_{j,i}^2 = M$, $\forall i \in \mathcal{I}$. This means that (197)-(198) turn into

$$\mathrm{E}\{z_k|\mathbf{a}_i\}] \approx E_f^{(0)}\Omega a_{i,k} + E_f^{(1)} \sum_{j=0}^{N_f-1} \bar{c}_{j,k}\bar{b}_{j-1,i}^2, \tag{199}$$

$$\mathrm{Var}\{z_k|\mathbf{a}_i\} \approx 2N_0E_fM + \frac{N_fLN_0^2}{2}, \tag{200}$$

respectively. Bearing in mind that the variance in (200) is independent of both $\bar{\mathbf{C}}$ and $\bar{\mathbf{X}}$, we can argue from (199) that a possible criterion to mitigate IFI in terms of BER performance is to choose the permutation matrix $\mathbf{P}$ such that the constraints

$$\sum_{j=0}^{N_f-1} \bar{c}_{j,k}\bar{b}_{j-1,i}^2 = \Phi_i a_{i,k}, \quad i \in \mathcal{I}, \tag{201}$$

hold. After dropping the terms $\bar{b}_{-1,i}^2$ caused by inter-block interference (IBI), (201) can be equivalently put in matrix notation as

$$\mathbf{C}_{\mathrm{o}}^T\mathbf{P}^T\mathbf{J}_{N_f}\mathbf{P}\mathbf{X}_{\mathrm{o}} = \mathbf{A}\mathbf{\Phi}, \tag{202}$$

where $\mathbf{\Phi} \triangleq \mathrm{diag}\{\Phi_1, \Phi_2, \cdots, \Phi_{2^M}\}$ and $\mathbf{A}$ is the $M \times 2^M$ matrix containing all the realizations $\mathbf{a}_i$. Then, we add the constraints

$$\mathbf{\Phi} > \Phi\mathbf{I}_{2^M}, \tag{203}$$

and maximize Φ to have a scalar-valued objective function.

In summary, the matrices for IFI mitigation will result as $(\mathbf{P}_{\mathrm{o}}\mathbf{C}_{\mathrm{o}}, \mathbf{P}_{\mathrm{o}}\mathbf{X}_{\mathrm{o}})$, where the optimal permutation matrix $\mathbf{P}_{\mathrm{o}}$ is found by maximizing the scalar objective Φ under the constraints (202)-(203).

REFERENCES

[1] "LINGO - Optimization Modeling Software for Linear, Nonlinear, and Integer Programming."

[2] "PulsON 410: The Worlds Best Ranging Radio."

[3] Abou-Rjeily, C., Daniele, N., and Belfiore, J.-C., "On the amplify-and-forward cooperative diversity with time-hopping ultra-wideband communications," *IEEE Trans. Commun.*, vol. 56, pp. 630–641, Apr. 2008.

[4] Analui, B. and Hajimiri, A., "Statistical analysis of integrated passive delay lines," in *Proc. IEEE Custom Integrated Circuits Conf.*, (San Jose, CA), pp. 107–110, Sept. 2003.

[5] Beaulieu, N. C. and Hu, B., "Soft-limiting receiver structures for time-hopping UWB in multiple-access interference," *IEEE Trans. Veh. Technol.*, vol. 57, pp. 810–818, Mar. 2008.

[6] Beaulieu, N. C., Shao, H., and Fiorina, J., "P-order metric UWB receiver structures with superior performance," *IEEE Trans. Commun.*, vol. 56, pp. 1666–1676, Oct. 2008.

[7] Berrou, C., Glavieux, A., and Thitimajshima, P., "Near Shannon limit error-correcting coding and decoding: Turbo-codes," in *Proc. IEEE Int. Conf. Commu.*, vol. 2, (Geneva, Swizerland), pp. 1064–1070, May 1993.

[8] Bletsas, A., Khisti, A., Reed, D. P., and Lippman, A., "A simple cooperative diversity method based on network path selection," *IEEE J. Sel. Areas Commun.*, vol. 24, pp. 659–672, Mar. 2006.

[9] Boyd, S. and Vandenberghe, L., *Convex optimization*. Cambridge university press, 2004.

[10] Cassioli, D., Vatalaro, F., Win, M. Z., and Molisch, A. F., "Performance of low-complexity Rake reception in a realistic UWB channel," in *Proc. IEEE Int. Conf. Commun.*, vol. 2, (New York, NY), pp. 763–767, May 2002.

[11] Cassioli, D., Win, M. Z., and Molisch, A. F., "The ultra-wide bandwidth indoor channel: from statistical model to simulations," *IEEE J. Sel. Areas Commun.*, vol. 20, pp. 1247–1257, Aug. 2002.

[12] Casu, M. R. and Durisi, G., "Implementation aspects of a transmitted-reference UWB receiver," *Wireless Commun. and Mobile Comput.*, vol. 5, pp. 537–549, May 2005.

[13] Casu, M. and Durisi, G., "Implementation aspects of a transmitted-reference UWB receiver," *Wireless Commun. and Mobile Comput.*, vol. 5, pp. 537–549, May 2005.

[14] Chao, Y.-L. and Scholtz, R. A., "Optimal and suboptimal receivers for ultra-wideband transmitted reference systems," in *Proc. IEEE Globecom*, vol. 2, (San Francisco, CA), pp. 759–763, Dec. 2003.

[15] Chao, Y.-L. and Scholtz, R. A., "Multiple access performance of ultra-wideband transmitted reference systems in multipath environments," in *Proc. Wireless Commu. and Networking Conf. (WCNC)*, vol. 3, (Atlanta, GA), pp. 1788–1793, 2004.

[16] Choi, J. D. and Stark, W. E., "Performance of ultra-wideband communications with suboptimal receivers in multipath channels," *IEEE J. Sel. Areas Commun.*, vol. 20, pp. 1754–1766, Dec. 2002.

[17] Cramer, R. J. M., Scholtz, R. A., and Win, M. Z., "Evaluation of an ultra-wide-band propagation channel," *IEEE Trans. Antennas Propag.*, vol. 50, pp. 561–570, May 2002.

[18] D'amico, A. A. and Mengali, U., "Code-multiplexed UWB transmitted-reference radio," *IEEE Trans. Commun.*, vol. 56, pp. 2125–2132, Dec. 2008.

[19] D'Amico, A. A. and Taponecco, L., "A differential receiver for UWB systems," *IEEE Trans. Wireless Commun.*, vol. 5, pp. 1601–1605, July 2006.

[20] Digham, F. F., Alouini, M.-S., and Simon, M. K., "On the energy detection of unknown signals over fading channels," *IEEE Trans. Commun.*, vol. 55, pp. 21–24, Jan. 2007.

[21] Do, M. N. and Vetterli, M., "Wavelet-based texture retrieval using generalized Gaussian density and kullback-leibler distance," *IEEE Trans. Image Process.*, vol. 11, pp. 146–158, Feb. 2002.

[22] (FCC), F. C. C., "First report and order in the matter of revision of part 15 of the commissions rules regarding ultra-wideband transmission systems," *Tech. Rep. ET Docket 98-153*, Apr. 2002.

[23] FCC 02–48, "FFC First Report and Order: In the matter of Revision of Part 15 of the Commission's Rules Regarding Ultra-Wideband Tranmission Systems," Apr. 2002.

[24] Feng, L. and Namgoong, W., "An oversampled channelized UWB receiver with transmitted reference modulation," *IEEE Trans. Wireless Commun.*, vol. 5, pp. 1497–1505, June 2006.

[25] Foerster, J. R., "Channel modeling sub-committee report final," 2002.

[26] Franz, S. and Mitra, U., "Generalized UWB transmitted reference systems," *IEEE J. Sel. Areas Commun.*, vol. 24, pp. 780–786, Apr. 2006.

[27] Fredman, M. L. and Tarjan, R. E., "Fibonacci heaps and their uses in improved network optimization algorithms," *Journal of the ACM*, vol. 34, pp. 596–615, Jul. 1987.

[28] Gallager, R. G., *Low-Density Parity-Check Codes*. Cambridge, MA: MIT Press, 1963.

[29] Gezici, S., Tian, Z., Giannakis, G. B., Kobayashi, H., Molisch, A. F., Poor, H. V., and Sahinoglu, Z., "Localization via ultra-wideband radios: a look at positioning aspects for future sensor networks," *IEEE Signal Process. Mag.*, vol. 22, pp. 70–84, July 2005.

[30] Goeckel, D. L. and Zhang, Q., "Slightly frequency-shifted reference ultra-wideband (UWB) radio," *IEEE Trans. Commun.*, vol. 55, pp. 508–519, Mar. 2007.

[31] Goemans, M. X. and Williamson, D. P., "Improved approximation algorithms for maximum cut and satisfiability problems using semidefinite programming," *J. ACM*, vol. 42, no. 6, pp. 1115–1145, 1995.

[32] Guérin, R. and Orda, A., "Computing shortest paths for any number of hops," *IEEE/ACM Trans. on Networking*, vol. 10, pp. 613–620, Oct. 2002.

[33] Guo, N. and Qiu, R. C., "Improved autocorrelation demodulation receivers based on multiple-symbol detection for UWB communications," *IEEE Trans. Wireless Commun.*, vol. 5, pp. 2026–2031, Aug. 2006.

[34] Hamdi, M., Mietzner, J., and Schober, R., "Multiple-differential encoding for multi-hop amplify-and-forward IR-UWB systems," *IEEE Trans. Wireless Commun.*, vol. 10, pp. 1–15, Aug. 2011.

[35] Helmberg, C., Rendl, F., Vanderbei, R. J., and Wolkowicz, H., "An interior-point method for semidefinite programming," *SIAM J. Optim.*, vol. 6, pp. 342–361, 1996.

[36] Hochwald, B. M. and ten Brink, S., "Achieving near-capacity on a multiple-antenna channel," *IEEE Trans. Commun.*, vol. 51, pp. 389–399, Mar. 2003.

[37] Hoctor, R. and Tomlinson, H., "Delay-hopped transmitted-reference RF communications," in *Proc. IEEE UWBST*, (Baltimore, MD), pp. 265–269, May 2002.

[38] Hussain, M. G., "Ultra-wideband impulse radar-an overview of the principles," *IEEE Aerosp. and Electron. Syst. Mag.*, vol. 13, no. 9, pp. 9–14, 1998.

[39] IEEE, "IEEE 802.15.4-2011, Part 15.4: Low-Rate Wireless Personal Area Networks (LR-WPANs)," Mar. 2007.

[40] IEEE, "IEEE 802.15.4a-2007, Part 15.4: Wireless Medium Access Control (MAC) and Physical Layer (PHY) Specications for Low-Rate Wireless Personal Area Networks (WPANs); Amendment 1: Add Alternate PHYs," Mar. 2007.

[41] Jaldén, J., Martin, C., and Ottersten, B., "Semidefinite programming for detection in linear systems - optimality conditions and space-time decoding," in *Proc. IEEE Int. Conf. Acoustics, Speech, and Signal Processing*, vol. 4, (Hong Kong, China), Apr. 2003.

[42] Jaldén, J. and Ottersten, B., "On the complexity of sphere decoding in digital communications," *IEEE Trans. Signal Process.*, vol. 53, pp. 1474–1484, Apr. 2005.

[43] Karmarkar, N., "A new polynomial-time algorithm for linear programming," in *Proc. 16th Annual ACM Symp. on Theory of Computing*, (New York, NY), pp. 302–311, ACM, 1984.

[44] Laneman, J. N., Tse, D. N. C., and Wornell, G. W., "Cooperative diversity in wireless networks: Efficient protocols and outage behavior," *IEEE Trans. Inform. Theory*, vol. 50, no. 12, pp. 3062–3080, 2004.

[45] Le, B., Rondeau, T. W., Reed, J. H., and Bostian, C. W., "Analog-to-digital converters," *IEEE Signal Process. Mag.*, vol. 22, pp. 69–77, Nov. 2005.

[46] Le, L. and Hossain, E., "Multihop cellular networks: potential gains, research challenges, and a resource allocation framework," *IEEE Commun. Mag.*, vol. 45, pp. 66–73, Sept. 2007.

[47] Li, G., Tousi, Y. M., Hassibi, A., and Afshari, E., "Delay-line-based analog-to-digital converters," *IEEE Trans. Circuits Syst. II*, vol. 56, pp. 464–468, June 2009.

[48] Liang, J., Chiau, C., Chen, X., and Parini, C., "Study of a printed circular disc monopole antenna for UWB systems," *IEEE Trans. Antennas Propag.*, vol. 53, pp. 3500–3504, Nov. 2005.

[49] Lottici, V., D'Andrea, A., and Mengali, U., "Channel estimation for ultra-wideband communications," *IEEE J. Sel. Areas Commun.*, vol. 20, pp. 1638–1645, Dec. 2002.

[50] Lottici, V. and Tian, Z., "Multiple symbol differential detection for UWB communications," *IEEE Trans. Wireless Commun.*, vol. 7, pp. 1656–1666, May 2008.

[51] Luo, X., Yang, L., and Giannakis, G. B., "Designing optimal pulse-shapers for ultra-wideband radios," in *IEEE Conf. on Ultra-Wideband Systems and Technologies*, pp. 349–353, Nov. 2003.

[52] Lupas, R. and Verdu, S., "Near-far resistance of multiuser detectors in asynchronous channels," *IEEE Trans. Commun.*, vol. 38, pp. 496–508, Apr. 1990.

[53] Ma, W.-K., Davidson, T. N., Wong, K. M., Luo, Z.-Q., and Ching, P.-C., "Quasi-maximum-likelihood multiuser detection using semi-definite relaxation with application to synchronous CDMA," *IEEE Trans. Signal Process.*, vol. 50, pp. 912–922, Apr. 2002.

[54] Maichalernnukul, K., Kaiser, T., and Zheng, F., "On the performance of coherent and noncoherent UWB detection systems using a relay with multiple antennas," *IEEE Trans. Wireless Commun.*, vol. 8, pp. 3407–3414, July 2009.

[55] Meher, P. K., Valls, J., Juang, T.-B., Sridharan, K., and Maharatna, K., "50 years of CORDIC: Algorithms, architectures, and applications," *IEEE Trans. Circuits Syst. I*, vol. 56, pp. 1893–1907, Sept. 2009.

[56] Mitra, J. and Lampe, L., "Design and analysis of robust detectors for TH IR-UWB systems with multiuser interference," *IEEE Trans. Commun.*, vol. 57, pp. 2210–2214, Aug. 2009.

[57] Molisch, A. F., "Ultra-wide-band propagation channels," *Proc. of IEEE*, vol. 97, pp. 353–371, Feb. 2009.

[58] Mondelli, M., Zhou, Q., Ma, X., and Lottici, V., "A cooperative approach for amplify-and-forward differential transmitted reference IR-UWB relay systems," in *IEEE Int. Conf. Acoust., Speech, and Signal Proc.*, no. 2979–2883, pp. 2905–2908, May 2012.

[59] Nesterov, Y., "Quality of semidefinite relaxation for nonconvex quadratic optimization," Tech. Rep. CORE Discussion Paper 9719, Belgium, Mar. 1997.

[60] Ng, T. C.-Y. and Yu, W., "Joint optimization of relay strategies and resource allocations in cooperative cellular networks," *IEEE J. Sel. Areas Commun.*, vol. 25, pp. 328–339, Feb. 2007.

[61] Nie, H. and Chen, Z., "Code-shifted reference transceiver for impulse radio ultra-wideband systems," *Phys. Commu.*, vol. 2, pp. 274–284, Dec. 2009.

[62] Parks, T. W. and McClellan, J. H., "Chebyshev approximation for nonrecursive digital filters with linear phase," *IEEE Trans. Circuit Theory*, vol. 19, pp. 189–194, Mar. 1972.

[63] Patwari, N., Ash, J. N., Kyperountas, S., Hero III, A. O., Moses, R. L., and Correal, N. S., "Locating the nodes: Cooperative localization in wireless sensor networks," *IEEE Signal Process. Mag.*, vol. 22, pp. 54–69, July 2005.

[64] Porcino, D. and Hirt, W., "Ultra-wideband radio technology: Potential and challenges ahead," *IEEE Commun. Mag.*, vol. 41, pp. 66–74, July 2003.

[65] Proakis, J. G., *Digital Communications*. New York: McGraw-Hill, Inc., 4th ed. ed., 2001.

[66] Quek, T. Q. S. and Win, M. Z., "Analysis of UWB transmitted-reference communication systems in dense multipath channels," *IEEE J. Sel. Areas Commun.*, vol. 23, pp. 1863–1874, Sept. 2005.

[67] Rendl, F., Vanderbei, R. J., and Wolkowicz, H., "Max-min eigenvalue problems, primal-dual interior point algorithms, and trust region subproblems," *Optimization Methods and Software*, vol. 5, pp. 1–16, 1995.

[68] Sahinoglu, Z., Gezici, S., and Guvenc, I., *Ultra-wideband positioning systems*, vol. 2. Cambridge university press Cambridge, UK, 2008.

[69] Saleh, A. A. M. and Valenzuela, R. A., "A statistical model for indoor multipath propagation," *IEEE J. Sel. Areas Commun.*, vol. 5, pp. 128–137, Feb. 1987.

[70] Schantz, H. G. and Fullerton, L., "The diamond dipole: A Gaussian impulse antenna," in *IEEE Int. Symp. Antennas and Propagation Society*, vol. 4, (Boston, MA), pp. 100–103, 2001.

[71] Schenk, A. and Fischer, R. F. H., "Soft-output sphere decoder for multiple-symbol differential detection of impulse-radio ultra-wideband," in *Proc. IEEE Int. Symp. on Info. Theory*, pp. 2258–2262, July 2010.

[72] Schenk, A. and Fischer, R. F. H., "Decision-feedback differential detection in impulse-radio ultra-wideband systems," *IEEE Trans. Commun.*, vol. 59, pp. 1604–1611, June 2011.

[73] Schenk, A. and Fischer, R. F. H., "Design rules for bit-interleaved coded impulse-radio ultra-wideband modulation with autocorrelation-based detection," in *Proc. IEEE Int. Symp. on Wireless Commu. Systems*, (Aachen, Germany), pp. 146–150, Nov. 2011.

[74] Schenk, A., Fischer, R. F. H., and Lampe, L., "A new stopping criterion for the sphere decoder in UWB impulse–radio multiple–symbol differential detection," in *Proc. of IEEE Int. Conf. on Ultra-Wideband (ICUWB)*, (Vancuver, Canda), pp. 589–594, Sept. 2009.

[75] Shao, H. and Beaulieu, N. C., "A novel zonal UWB receiver with superior performance," *IEEE Trans. Commun.*, vol. 57, pp. 1197–1206, Apr. 2009.

[76] Shiwei Zhao, S., Orlik, P., Molisch, A. F., Huaping Liu, H., and Jinyun Zhang, J., "Hybrid ultrawideband modulations compatible for both coherent and transmit-reference receivers," *IEEE Trans. Wireless Commun.*, vol. 6, pp. 2551–2559, July 2007.

[77] Stojmenovic, I., "Position-based routing in ad hoc networks," *IEEE Commun. Mag.*, vol. 40, pp. 128–134, Jul. 2002.

[78] Tan, P. H. and Rasmussen, L. K., "Multiuser detection in CDMA - a comparison of relaxations, exact, and heuristic search methods," *IEEE Trans. Wireless Commun.*, vol. 3, pp. 1802–1809, Sept. 2004.

[79] Tan, P. H., Rasmussen, L. K., and Lim, T. J., "Constrained maximum-likelihood detection in CDMA," *IEEE Trans. Commun.*, vol. 49, pp. 142–153, Jan. 2001.

[80] Taylor, J. D., *Introduction to ultra-wideband radar systems*. CRC Press LLC, 1995.

[81] Tutay, M. E. and Gezici, S., "Optimal and suboptimal receivers for code-multiplexed transmitted-reference ultra-wideband systems," *Wireless Commun. and Mobile Comput.*., Sept. 2011.

[82] Urkowitz, H., "Energy detection of unknown deterministic signals," *Proc. IEEE*, vol. 55, pp. 523–531, Apr. 1967.

[83] van Stralen, N., Dentinger, A., Welles, K., I., Gaus, R., J., Hoctor, R., and Tomlinson, H., "Delay hopped transmitted reference experimental results," in *Proc. IEEE UWBST*, pp. 93–98, May 2002.

[84] Varanasi, M. and Aazhang, B., "Parametric generalized Gaussian density estimation," *J. of the Acoust. Soc. of Am.*, vol. 86, p. 1404, 1989.

[85] Wang, Z. and Giannakis, G. B., "Wireless multicarrier communications," *IEEE Signal Process. Mag.*, vol. 17, pp. 29–48, May 2000.

[86] Wang, Z., Lv, T., Gao, H., and Li, Y., "A novel two-way relay UWB network with joint non-coherent detection in multipath," in *IEEE Veh. Tech. Conf.*, pp. 1–5, May 2011.

[87] WiMedia, "WiMedia PHY Specification 1.5," Aug. 2009.

[88] Win, M. Z., Chrisikos, G., and Sollenberger, N. R., "Performance of RAKE reception in dense multipath channels: implications of spreading bandwidth and selection diversity order," *IEEE J. Sel. Areas Commun.*, vol. 18, pp. 1516–1525, Aug. 2000.

[89] Win, M. Z. and Scholtz, R. A., "Impulse radio: How it works," *IEEE Commun. Lett.*, vol. 2, pp. 36–38, Feb. 1998.

[90] Win, M. Z. and Scholtz, R. A., "On the energy capture of ultrawide bandwidth signals in dense multipath environments," *IEEE Commun. Lett.*, vol. 2, pp. 245–247, Sept. 1998.

[91] Win, M. Z. and Scholtz, R. A., "Ultra-wide bandwidth time-hopping spread-spectrum impulse radio for wireless multiple-access communications," *IEEE Trans. Commun.*, vol. 48, pp. 679–691, Apr. 2000.

[92] Win, M. Z. and Scholtz, R. A., "Characterization of ultra-wide bandwidth wireless indoor channels: a communication-theoretic view," *IEEE J. Sel. Areas Commun.*, vol. 20, pp. 1613–1627, Dec. 2002.

[93] Witrisal, K., Leus, G., Janssen, G., Pausini, M., Troesch, F., Zasowski, T., and Romme, J., "Noncoherent ultra-wideband systems," *IEEE Signal Process. Mag.*, vol. 26, pp. 48–66, July 2009.

[94] Witrisal, K., Pausini, M., and Trindade, A., "Multiuser interference and inter-frame interference in UWB transmitted reference systems," in *Proc. Joint Int. Workshop on UWBS with Conf. on UWBST*, (Kyoto, Japan), pp. 96–100, May 2004.

[95] Wolkowicz, H., Saigal, R., and Vandenberghe, L., *Handbook of semidefinite programming: theory, algorithms, and applications*. Springer Netherlands, 2000.

[96] Worm, A., Hoeher, P., and Wehn, N., "Turbo-decoding without SNR estimation," *IEEE Commun. Lett.*, vol. 4, pp. 193–195, June 2000.

[97] Yang, L. and Giannakis, G. B., "Optimal pilot waveform assisted modulation for ultrawideband communications," *IEEE Trans. Wireless Commun.*, vol. 3, pp. 1236–1249, July 2004.

[98] Yang, L. and Giannakis, G. B., "Ultra-wideband communications: An idea whose time has come," *IEEE Signal Process. Mag.*, vol. 21, pp. 26–54, Nov. 2004.

[99] Yener, A., Yates, R. D., and Ulukus, S., "CDMA multiuser detection: a nonlinear programming approach," *IEEE Trans. Commun.*, vol. 50, pp. 1016–1024, June 2002.

[100] Zhou, Q. and Ma, X., "Receiver designs for UWB differential transmitted reference systems with multiple access interference," in *Proc. Int. Conf. Ultra-wideband Commun. (ICUWB)*, (Bologna, Italy), pp. 205–209, 2011.

[101] Zhou, Q. and Ma, X., "Designing low-complexity near-optimal multiple-symbol detectors for impulse radio UWB systems," *IEEE Trans. Signal Process.*, vol. 60, pp. 2460–2469, May 2012.

[102] Zhou, Q., Ma, X., and Lottici, V., "Generalized code-multiplexing transmissions for UWB systems," in *45th Annual Conf. on Info. Sci. and Systems (CISS)*, (Baltimore, MD), pp. 1–6, Mar. 2011.

[103] Zhou, Q., Ma, X., and Lottici, V., "Generalized code-multiplexing transmissions for UWB systems," *IEEE Trans. Wireless Commun.*, 2012. accepted.

[104] Zhou, Q., Ma, X., and Rice, R., "A near-optimal multi-symbol based detector for UWB communications," in *Proc. IEEE Int. Conf. Ultra-Wideband, (ICUWB)*, vol. 1, (Nanjing, China), pp. 1–4, Sept. 2010.

[105] Zhu, S., Leung, K. K., and Constantinides, A. G., "Distributed cooperative data relaying for diversity in impulse-based UWB ad-hoc networks," *IEEE Trans. Wireless Commun.*, vol. 8, pp. 4037–4047, Aug. 2009.

VITA

Qi Zhou was born on January 2, 1985 in Hengyang, Hunan, China. He received the B.S. degree in Mathematics and Applied Mathematics from the Beijing University of Posts and Telecommunications, Beijing, P. R. China, in 2006, the M.S. degree in Computer Science from Shanghai Jiaotong University, Shanghai, P. R. China, in 2009, and the M.S. degree in Electrical and Computer Engineering from the Georgia Institute of Technology, Atlanta, GA, in 2009. He is now working towards the Ph.D. degree in the School of Electrical and Computer Engineering, Georgia Institute of Technology. His current research interests include transceiver designs for ultra-wideband communications, interference mitigation for femtocell/macrocell networks, equalizations for large multiple-input multiple-output systems, and VLSI implementation of energy-efficient high-throughput detectors.